

Supporting Information for:

**Electrostatic vs. Inductive Effects in Phosphine Ligand Donor
Properties and Reactivity**

Margaret L. Kelty, Andrew J. McNeece, Josh W. Kurutz, Alexander S. Filatov, John S.
Anderson*

Department of Chemistry, The University of Chicago, Chicago, IL, USA.

*Correspondence to: jsanderson@uchicago.edu

Table of Contents

Experimental Procedures	8
General Considerations	8
X-ray structure determination	8
Synthesis of reported compounds	9
Procedure for oxidative addition of C ₆ F ₆	11
Procedures for catalytic C-F borylation	13
NMR Characterization Spectra	15
Ph ₂ PCH ₂ BF ₃ K (K1)	15
Figure S1. ¹ H NMR spectrum of K1 in DMSO- <i>d</i> ₆	15
Figure S2. ³¹ P{ ¹ H} NMR spectrum of K1 in DMSO- <i>d</i> ₆	15
Figure S3. ¹⁹ F{ ¹ H} NMR spectrum of K1 in DMSO- <i>d</i> ₆	16
Figure S4. ¹³ C{ ¹ H} NMR spectrum of K1 collected in DMSO- <i>d</i> ₆	16
Figure S5. ¹¹ B{ ¹ H} NMR spectrum of K1 in DMSO- <i>d</i> ₆	17
[PPh ₄][Rh(acac)(CO)(PPh ₂ (CH ₂ BF ₃))] (2)	17
Figure S6. ¹ H NMR spectrum of 2 collected in CDCl ₃	17
Figure S7. ³¹ P{ ¹ H} NMR spectrum of 2 collected in CDCl ₃	18
Figure S8. ¹⁹ F{ ¹ H} NMR spectrum of 2 collected in CDCl ₃	18
Figure S9. ¹³ C{ ¹ H} NMR spectrum of 2 collected in CDCl ₃	19
Figure S10. ¹¹ B{ ¹ H} NMR spectrum of 2 in CDCl ₃	19
[PPh ₄][SePPh ₂ (CH ₂ BF ₃)] ([PPh ₄][1 ^{Se}])	20
Figure S11. ¹ H NMR spectrum of [PPh ₄][1 ^{Se}] in CDCl ₃	20
Figure S12. ³¹ P{ ¹ H} NMR spectrum of [PPh ₄][1 ^{Se}] in CDCl ₃	20
Figure S13. ¹⁹ F{ ¹ H} NMR spectrum of [PPh ₄][1 ^{Se}] in CDCl ₃	21
Figure S14. ¹³ C{ ¹ H} NMR spectrum of [PPh ₄][1 ^{Se}] in CDCl ₃	21
Figure S15. ¹¹ B{ ¹ H} NMR spectrum of [PPh ₄][1 ^{Se}] in CDCl ₃	22
Figure S16. DOSY NMR spectrum of [PPh ₄][1 ^{Se}] in CDCl ₃	22
[TEA][SePPh ₂ (CH ₂ BF ₃)] ([TEA][1 ^{Se}])	23
Figure S17. ¹ H NMR spectrum of [TEA][1 ^{Se}] in CDCl ₃	23
Figure S18. ³¹ P{ ¹ H} NMR spectrum of [TEA][1 ^{Se}] in CDCl ₃	23
Figure S19. ¹⁹ F{ ¹ H} NMR spectrum of [TEA][1 ^{Se}] in CDCl ₃	24
Figure S20. ¹³ C{ ¹ H} NMR spectrum of [TEA][1 ^{Se}] in CDCl ₃	24

Figure S21. $^{11}\text{B}\{^1\text{H}\}$ NMR spectrum of $[\text{TEA}][\mathbf{1}^{\text{Se}}]$	25
$[\text{PPh}_4][\text{SePPh}_2(2\text{-BF}_3\text{Ph})]$ ($[\text{PPh}_4][\mathbf{3}^{\text{Se}}]$).....	26
Figure S22. ^1H NMR spectrum of $[\text{PPh}_4][\mathbf{3}^{\text{Se}}]$ in CD_3CN	26
Figure S23. $^{31}\text{P}\{^1\text{H}\}$ NMR spectrum of $[\text{PPh}_4][\mathbf{3}^{\text{Se}}]$ in CD_2Cl_2	26
Figure S24. $^{19}\text{F}\{^1\text{H}\}$ NMR spectrum of $[\text{PPh}_4][\mathbf{3}^{\text{Se}}]$ in CD_3CN	27
Figure S25. $^{13}\text{C}\{^1\text{H}\}$ NMR spectrum of $[\text{PPh}_4][\mathbf{3}^{\text{Se}}]$ in CD_3CN	27
Figure S26. $^{11}\text{B}\{^1\text{H}\}$ NMR spectrum of $[\text{PPh}_4][\mathbf{3}^{\text{Se}}]$ in CD_3CN	28
Variable solvent ^{31}P NMR spectra of $[\text{PPh}_4][\mathbf{1}^{\text{Se}}]$, $[\text{TEA}][\mathbf{1}^{\text{Se}}]$ and $[\text{PPh}_4][\mathbf{3}^{\text{Se}}]$	29
Figure S27. $^{31}\text{P}\{^1\text{H}\}$ NMR spectra of $[\text{PPh}_4][\mathbf{1}^{\text{Se}}]$ in CD_3CN and $\text{DMSO-}d_6$	29
Figure S28. $^{31}\text{P}\{^1\text{H}\}$ NMR spectra of $[\text{PPh}_4][\mathbf{1}^{\text{Se}}]$ in CDCl_3 and CD_2Cl_2	29
Figure S29. $^{31}\text{P}\{^1\text{H}\}$ NMR spectrum of $[\text{PPh}_4][\mathbf{1}^{\text{Se}}]$ in $(\text{CD}_3)_2\text{CO}$	30
Figure S30. $^{31}\text{P}\{^1\text{H}\}$ NMR spectra of $[\text{PPh}_4][\mathbf{1}^{\text{Se}}]$ in solvent mixtures.....	30
Figure S31. $^{31}\text{P}\{^1\text{H}\}$ NMR spectra of $[\text{PPh}_4][\mathbf{1}^{\text{Se}}]$ with PPh_4Br	31
Figure S32. $^{31}\text{P}\{^1\text{H}\}$ NMR spectra of $[\text{PPh}_4][\mathbf{1}^{\text{Se}}]$ in with (TBA) salts	31
Figure S34. $^{31}\text{P}\{^1\text{H}\}$ NMR spectrum of $[\text{TEA}][\mathbf{1}^{\text{Se}}]$ in various solvents	32
Figure S35. $^{31}\text{P}\{^1\text{H}\}$ NMR spectrum of $[\text{TEA}][\mathbf{1}^{\text{Se}}]$ in various solvents.....	33
Figure S36. $^{31}\text{P}\{^1\text{H}\}$ NMR spectra of $[\text{PPh}_4][\mathbf{3}^{\text{Se}}]$ in various solvents	33
Figure S37. $^{31}\text{P}\{^1\text{H}\}$ NMR spectra of SePPh_2Et in various solvents.....	34
Figure S38. $^{31}\text{P}\{^1\text{H}\}$ NMR spectra of SePPh_3 in various solvents.	34
Figure S39. ^1H NMR spectra of $[\text{TEA}][\mathbf{1}^{\text{Se}}]$ and $[\text{PPh}_4][\mathbf{1}^{\text{Se}}]$ in CD_2Cl_2	35
Figure S40. ^1H NMR spectra of $[\text{TEA}][\mathbf{1}^{\text{Se}}]$ and $[\text{PPh}_4][\mathbf{1}^{\text{Se}}]$ in $\text{DMSO-}d_6$	35
Figure S41. ^1H NMR spectra showing methylene resonance of $[\text{TEA}][\mathbf{1}^{\text{Se}}]$ and $[\text{PPh}_4][\mathbf{1}^{\text{Se}}]$ in CD_2Cl_2 and $\text{DMSO-}d_6$	36
Figure S42. ^{19}F NMR spectra showing the BF_3 resonance of $[\text{TEA}][\mathbf{1}^{\text{Se}}]$ and $[\text{PPh}_4][\mathbf{1}^{\text{Se}}]$ in CD_2Cl_2 and $\text{DMSO-}d_6$	36
NMR spectra of the reaction kinetics of C_6F_6 oxidative addition.....	37
K1 with $\text{Ni}(\text{COD})_2$	37
Figure S43. $^{31}\text{P}\{^1\text{H}\}$ NMR spectrum of the reaction of K1 and $\text{Ni}(\text{COD})_2$ in THF.....	37
Figure S44. $^{19}\text{F}\{^1\text{H}\}$ NMR spectrum of the reaction of K1, $\text{Ni}(\text{COD})_2$, and C_6F_6	37
Figure S45. $^{19}\text{F}\{^1\text{H}\}$ NMR spectrum of the reaction of K1, $\text{Ni}(\text{COD})_2$, and C_6F_6	38
Figure S46. ^{19}F NMR spectrum of the reaction between K1, $\text{Ni}(\text{COD})_2$ and C_6F_6 in THF with CF_3Ph and OPPh_3	38

Figure S47. Time course monitoring of the ^{19}F NMR spectrum of the reaction between K1 , $\text{Ni}(\text{COD})_2$ and C_6F_6 in THF with CF_3Ph and OPPh_3	39
Figure S48. $^{31}\text{P}\{^1\text{H}\}$ NMR spectrum of the reaction between K1 , $\text{Ni}(\text{COD})_2$ and C_6F_6 in THF with CF_3Ph and OPPh_3	40
Figure S49. Time course monitoring of the $^{31}\text{P}\{^1\text{H}\}$ NMR spectrum of the reaction between K1 , $\text{Ni}(\text{COD})_2$ and C_6F_6 in THF with CF_3Ph and OPPh_3	41
PCy_3 with $\text{Ni}(\text{COD})_2$	42
Figure S50. ^{19}F NMR spectrum of the reaction between PCy_3 , $\text{Ni}(\text{COD})_2$ and C_6F_6 in THF with CF_3Ph and OPPh_3	42
Figure S51. Time course monitoring of the ^{19}F NMR spectrum of the reaction between PCy_3 , $\text{Ni}(\text{COD})_2$ and C_6F_6 in THF with CF_3Ph and OPPh_3	43
Figure S52. $^{31}\text{P}\{^1\text{H}\}$ NMR spectrum of the reaction between PCy_3 , $\text{Ni}(\text{COD})_2$ and C_6F_6 in THF with CF_3Ph and OPPh_3	44
Figure S53. Time course monitoring of the $^{31}\text{P}\{^1\text{H}\}$ NMR spectrum of the reaction between PCy_3 , $\text{Ni}(\text{COD})_2$ and C_6F_6 in THF with CF_3Ph and OPPh_3	45
PEt_3 with $\text{Ni}(\text{COD})_2$	46
Figure S54. ^{19}F NMR spectrum of the reaction between PEt_3 , $\text{Ni}(\text{COD})_2$ and C_6F_6 in THF with CF_3Ph and OPPh_3	46
Figure S55. Time course monitoring of the ^{19}F NMR spectrum of the reaction between PEt_3 , $\text{Ni}(\text{COD})_2$ and C_6F_6 in THF with CF_3Ph and OPPh_3	47
Figure S56. $^{31}\text{P}\{^1\text{H}\}$ NMR spectrum of the reaction between PEt_3 , $\text{Ni}(\text{COD})_2$ and C_6F_6 in THF with CF_3Ph and OPPh_3	48
Figure S57. Time course monitoring of the $^{31}\text{P}\{^1\text{H}\}$ NMR spectrum of the reaction between PEt_3 , $\text{Ni}(\text{COD})_2$ and C_6F_6 in THF with CF_3Ph and OPPh_3	49
Table S1. Summary of observed rates from NMR monitoring experiments.....	50
Figure S58. $^{31}\text{P}\{^1\text{H}\}$ NMR spectrum of the reaction of PEt_3 , $\text{Ni}(\text{COD})_2$, and C_6F_6 in THF	50
NMR spectra of the catalytic C-F borylation reactions.....	51
Figure S59. $^{19}\text{F}\{^1\text{H}\}$ NMR spectrum of the 1,2-difluorobenzene reaction mixture.....	51
Figure S60. $^{19}\text{F}\{^1\text{H}\}$ NMR spectrum of the 1,3-difluorobenzene reaction mixture.....	52
Figure S61. $^{19}\text{F}\{^1\text{H}\}$ NMR spectrum of the 1,4-difluorobenzene reaction mixture.....	53
Figure S62. $^{19}\text{F}\{^1\text{H}\}$ NMR spectrum of the 1,2,4-trifluorobenzene reaction mixture.....	54
Figure S63. $^{19}\text{F}\{^1\text{H}\}$ NMR spectrum of the 1,3,5-trifluorobenzene reaction mixture.....	55
GC/MS characterization of $\text{C}_6\text{H}_5\text{Bpin}$	56
Figure S64. GC trace of the $\text{C}_6\text{H}_5\text{F}$ reaction mixture.....	56
Figure S65. Mass spectrum of the $\text{C}_6\text{H}_5\text{Bpin}$ peak from the $\text{C}_6\text{H}_5\text{F}$ reaction mixture.....	57

Infrared Spectra.....	58
Figure S66. IR spectrum (KBr Pellet) of K1	58
Figure S67. IR spectrum (DCM Solution) of 2	58
Figure S68. IR spectrum (KBr pellet) of 2	59
Figure S69. IR spectrum (CDCl ₃ solution) of [PPh ₄][1 ^{Se}].....	59
Figure S70. IR spectrum (KBr pellet) of [TEA][1 ^{Se}].....	60
Figure S71. IR spectrum (KBr pellet) of [PPh ₄][3 ^{Se}].....	60
Figure S72. IR spectra of 2 in different solvents	61
Figure S73. IR spectra of Rh(CO) ₂ acac in different solvents.....	61
UV-visible spectra	62
Figure S74. Reaction between Ni(COD) ₂ , 1 equivalent of K1 , and C ₆ F ₆ in THF	62
Figure S75. Reaction between Ni(COD) ₂ , 2 equivalents of K1 , and C ₆ F ₆ in THF	63
Figure S76. Reaction between Ni(COD) ₂ , 3 equivalents of K1 , and C ₆ F ₆ in THF	64
Figure S77. Reaction between Ni(COD) ₂ , 4 equivalents of K1 , and C ₆ F ₆ in THF	65
Figure S78. Reaction between Ni(COD) ₂ , 8 equivalents of K1 , and C ₆ F ₆ in THF	66
Figure S79. Reaction of Ni(COD) ₂ and 2 equivalents of K1 in THF	67
Calculations.....	67
General considerations.....	67
Figure S80. Calculated structure of 1 ^{Se} (cisoid structure).....	70
Table S2. Coordinates of optimized structure of 1 ^{Se} (cisoid structure)	70
Figure S81. Calculated structure of 1 ^{Se} (transoid structure)	71
Table S3. Coordinates of calculated structure of edited 1 ^{Se} (transoid structure).	71
Table S4. Calculated electric field and <i>J</i> _{P-Se} for calculated structures of 1 ^{Se}	72
Figure S82. Optimized structure of SePPh ₂ Et	73
Table S5. Coordinates of calculated structure of SePPh ₂ Et.....	73
Figure S83. Optimized structure of 2	74
Table S6. Coordinates of calculated structure of 2	74
Figure S84. Optimized structure of 1 ^{Se} with explicit MeCN solvation.	76
Table S7. Coordinates of calculated structure of 1 ^{Se} with explicit MeCN solvation.....	76
Figure S85. Optimized structure of 1 ^{Se} with explicit DCM solvation.	79
Table S8. Coordinates of calculated structure of 1 ^{Se} with explicit DCM solvation	79
Figure S86. Optimized structure of 1 ^{Se} with explicit CHCl ₃ solvation.....	82

Table S9. Coordinates of calculated structure of 1 ^{Se} with explicit CHCl ₃ solvation.....	82
NBO Analysis.....	84
Correlation between J_{P-Se} and TEP	85
Figure S87. Plot of experimental J_{P-Se} reported in CDCl ₃ vs. TEP.....	85
Table S10. Additional data points added to main text Figure 2.....	85
Table S11. Phosphines used in the J_{P-Se} vs. TEP fit.....	86
Further analysis of solvent dependence	87
Figure S88. Plots of J_{P-Se} as a function of solvent dielectric.....	87
Table S12. J_{P-Se} (Hz) for [PPh ₄][1 ^{Se}], [PPh ₄][3 ^{Se}], SePPh ₂ Et and SePPh ₃	88
Table S13. Fit parameters for the linear fits of J_{P-Se} to $1/(4\pi\epsilon)$	88
Table S14. J_{P-Se} (Hz) for [PPh ₄][1 ^{Se}] with additional salts	88
Discussion of the slopes of J_{P-Se} versus $1/(4\pi\epsilon)$ for [PPh ₄][1 ^{Se}] and [PPh ₄][3 ^{Se}].....	89
Single crystal X-ray crystallography	90
Figure S89. SXR structure of K1 with K ⁺ counterion shown.....	90
Figure S90. SXR structure of 2 with PPh ₄ ⁺ counterion shown.....	90
Figure S91. SXR structure of [PPh ₄][1 ^{Se}] with PPh ₄ ⁺ counterion shown	91
Figure S92. Space filling model of the SXR structure of [PPh ₄][1 ^{Se}].....	91
Figure S93. SXR structure of [TEA][1 ^{Se}] with TEA ⁺ counterion shown.....	92
Figure S94. Space filling model of the SXR structure of [TEA][1 ^{Se}].....	92
Figure S95. SXR structure of [PPh ₄][3 ^{Se}] with PPh ₄ ⁺ counterion shown	93
Table S15. Selected average bond lengths for SXR structures.....	93
Discussion of van der Waals radii in 2	93
Table S16. Refinement data for crystal structures of K1 , 2 , [PPh ₄][1 ^{Se}], [TEA][1 ^{Se}], and [PPh ₄][3 ^{Se}].....	94
Catalytic C-F borylation trial reactions.....	96
Table S17. Initial scan of additives for C-F borylation of 1,3 difluorobenzene.	96
Table S18. Variation of reaction conditions with H ₂ O as an additive.....	97
Table S19. Variation of reaction conditions with alcohols as additives.....	98
Table S20. Variation of reaction conditions with MeOH as an additive	99
Table S21. Variation of reaction time with MeOH and CsOH and control reactions	100
Table S22. Variation of addition order and additives	101
Table S23. Variation of cations.	102
Table S24. Variation of reaction solvent.	103

References..... 104

Experimental Procedures

General Considerations

All reagents were purchased from commercial suppliers and used without further purification unless otherwise specified. $\text{K}[\text{ICH}_2\text{BF}_3]$,¹ $\text{K}[\text{PPh}_2(o\text{-BF}_3\text{Ph})]$,^{2,3,4} SePPh_3 and SePPh_2Et ^{5,6} were synthesized according to literature procedures. All manipulations were carried out under an atmosphere of N_2 using standard Schlenk and glovebox techniques. Glassware was dried at 180 °C for a minimum of two hours and cooled under vacuum prior to use. All reactions were carried out in 20 mL scintillation vials unless otherwise specified. Catalytic reactions were carried out in 4 mL screw thread borosilicate glass vials. All volumes below 1 mL were measured using Hamilton 100 or 250 μL syringes. Solvents were dried on a solvent purification system from Pure Process Technology and stored over 4 Å molecular sieves under N_2 . Tetrahydrofuran was stirred over NaK alloy and run through an additional activated alumina plug prior to use to ensure dryness. Solvents were tested for H_2O and O_2 using a standard solution of sodium-benzophenone ketyl radical anion. C_6D_6 , CDCl_3 , acetone-*d*₆, CD_3CN , and $\text{DMSO-}d_6$ were dried by passage over a column of activated alumina and stored over 4 Å molecular sieves in the glovebox. ^1H , $^{13}\text{C}\{^1\text{H}\}$, $^{19}\text{F}\{^1\text{H}\}$, $^{11}\text{B}\{^1\text{H}\}$, and $^{31}\text{P}\{^1\text{H}\}$ data were acquired on a combination of two three spectrometers: a 400 MHz Bruker DRX spectrometer equipped with a BBO probe; a 500 MHz Bruker Avance-II+ spectrometer equipped with a $^1\text{H}\{^{19}\text{F}, ^{13}\text{C}, ^{31}\text{P}\}$ QNP probe; and a 500 MHz Bruker Avance III HD spectrometer equipped with a Bruker BBFO “Smart” probe. All spectrometers use Topspin. Chemical shifts are reported in ppm units referenced to residual solvent resonances for ^1H and $^{13}\text{C}\{^1\text{H}\}$ spectra, and external standards for $^{31}\text{P}\{^1\text{H}\}$, $^{11}\text{B}\{^1\text{H}\}$, $^{19}\text{F}\{^1\text{H}\}$ and ^{19}F . Assignments for ^{13}C NMR resonances were made based on previously reported (PPh_4) and related compounds ($\text{Rh}(\text{acac})(\text{CO})\text{PPh}_3$, PPh_2Et , $\text{PPh}_2(2\text{-BF}_3\text{-Ph})$).^{2,3,7-10} Unless otherwise indicated, multipoint baseline corrections were applied to ^{19}F NMR spectra in Mnova to remove broad peaks in the baseline around 150 – 220 ppm resulting from Teflon within the probe. NMR samples were prepared by dissolving approximately 10-20 mg of the sample in about 0.5 mL of the appropriate deuterated solvent. No change in signal position or coupling was observed as a function of concentration. IR spectra were recorded on a Bruker Tensor II. Solution IR were recorded in a solution cell using CaF_2 windows, and then the solvent signal was subtracted out. Solid IR were recorded using a KBr pellet. Elemental analysis was performed by Midwest Microlabs.

X-ray structure determination

The diffraction data were measured at 100 K on a Bruker D8 VENTURE with PHOTON 100 CMOS detector system equipped with a Mo-target micro-focus X-ray tube ($\lambda = 0.71073$ Å). Data reduction and integration were performed with the Bruker APEX3 software package (Bruker AXS, version 2015.5-2, 2015). Data were scaled and corrected for absorption effects using the multi-scan procedure as implemented in SADABS (Bruker AXS, version 2014/5, 2015, part of Bruker APEX3 software package). The structure was solved by the dual method implemented in SHELXT¹¹ and refined by a full-matrix least-squares procedure using OLEX2¹² software package (XL refinement program version 2014/7¹³). Suitable crystals were mounted on a cryo-

loop and transferred into the cold nitrogen stream of the Bruker D8 Venture diffractometer. Most of the hydrogen atoms were generated by geometrical considerations and constrained to idealized geometries and allowed to ride on their carrier atoms with an isotropic displacement parameter related to the equivalent displacement parameter of their carrier atoms. The co-crystallized THF and phenyl rings of the phosphine were modeled for disorder in **K1**. For [PPh₄][**1**^{Se}], after fully solving and refining the structure, a relatively large residual peak was observed suggesting a possible co-crystallized submixture. The peak was located close to the CH₂-BF₃ bond, and the distance correlated well with a P-I bond length. Thus, this component was refined as a (Ph)₂P-I (refined occupancy about 4%). While it is hard to concretely assign the identity of such a small submixture, we note that several examples of (R)₂P-I molecules have been previously reported with P-I bond lengths between 2.45-2.55 Å.¹⁴

Synthesis of reported compounds

Synthesis of Ph₂PCH₂BF₃K (K1). To a stirring solution of PPh₂ (0.368 g, 1.97 mmol) in THF (5 mL) was added a solution of KHMDS (0.398 g, 1.99 mmol, 1 eq) in THF (5 mL), resulting in a bright red homogeneous solution. This was added dropwise over 20 minutes to a stirring slurry of K[ICH₂BF₃] (0.541 g, 2.18 mmol, 1.1 eq) in THF (5 mL). After addition, the resulting slurry was stirred for 1 hour, placed in the freezer at -40 °C to settle for 1 hour and then filtered through Celite. The filtrate was dried under vacuum, and the resulting sticky white solid was washed with Et₂O (2 x 10 mL), leaving behind Ph₂PCH₂BF₃K as a white powder (0.301 g, 0.98 mmol, 50%). ¹H NMR (400 MHz, 25 °C, DMSO-*d*₆) δ = 7.33 (t, *J* = 8 Hz, 4H, *o*-Ph-H), 7.24-7.14 (m, 6H, *m*- and *p*-Ph-H), 0.8 (dq, *J*_{P-H} = 14 Hz, *J*_{F-H} = 4 Hz, 2H, CH₂BF₃). ³¹P{¹H} NMR (162 MHz, 25 °C, DMSO-*d*₆) δ = -15.9 (q, *J*_{P-F} = 13 Hz, PPh₂(CH₂BF₃)). ¹⁹F{¹H} NMR (376 MHz, 25 °C, DMSO-*d*₆) δ = -133.9 (broad s, 3F, BF₃). ¹³C{¹H} NMR (126 MHz, 25 °C, DMSO-*d*₆) δ = 144.4 (d, *J*_{C-P} = 25 Hz, C_{ipso}), 132.0 (d, *J*_{C-P} = 50 Hz, C_{ortho}), 127.6 (s, C_{para}), 126.9 (s, C_{meta}), 17.0 (broad s, CH₂BF₃). ¹¹B{¹H} NMR (160 MHz, 25 °C, DMSO-*d*₆) δ = 4.0 (broad s). IR (KBr pellet): 3419 (w), 3053 (m), 2916 (w), 2885 (w), 1954 (w), 1881 (w), 1807 (w), 1584 (m), 1480 (m), 1433 (s), 1386 (m), 1168 (s), 1093 (m), 1046 (s), 931 (s), 742 (s), 697 (s). **K1** was too air sensitive for reliable elemental analysis, and instead was consistent with full oxidation of the phosphine sample despite multiple attempts. Elem. Anal: Calc'd (Ph₂PCH₂BF₃K+O): C 48.5 H 3.8 N 0 Found: C 48.1 H 4.0 N 0.

Synthesis of [PPh₄][Rh(acac)(CO)(PPh₂(CH₂BF₃))] (2). To a stirring THF solution (3 mL) of Rh(acac)(CO)₂ (67 mg, 0.26 mmol) was added a THF solution (5 mL) of **K1** (80 mg, 0.26 mmol, 1 eq) and a DCM solution (4 mL) of PPh₄Br (109 mg, 0.26 mmol, 1 eq), resulting in a color change from light yellow to brown. The reaction was stirred at room temperature for 1 hour, then filtered, evacuated to dryness, and washed with petroleum ether leaving [PPh₄][Rh(acac)(CO)(PPh₂(CH₂BF₃))] as a brown oil, which was crystallized by vapor diffusion of Et₂O into a CHCl₃ or DCM solution at room temperature to yield yellow crystals (146 mg, 0.17 mmol, 67%). ¹H NMR (400 MHz, 25 °C, CDCl₃) δ = 7.85 (m, 8H, Ph and PPh₄) 7.73 (m, 8H, PPh₄), 7.57 (m, 8H, PPh₄) 7.19 (m, 6H, Ph) 5.30 (s, 1 H, CH_{acac}), 1.92 (s, 3H, CH_{3acac}), 1.62 (m, 2H, CH₂BF₃), 1.56 (s, 3H, CH_{3acac}). ³¹P{¹H} NMR (162 MHz, 25 °C, CDCl₃) δ = 40.4 (dq, *J*_{P-Rh} = 166 Hz, *J*_{P-F} = 10 Hz, 1P, PPh₂(CH₂BF₃)), 25.6 (s, 1P, PPh₄). ¹⁹F{¹H} NMR (376 MHz, 25 °C, CDCl₃) δ = -131.6 (broad s, 3F, BF₃). ¹³C{¹H} NMR (126 MHz, 25 °C, CDCl₃) δ = 190.5 (dd, *J*_{C-Rh} = 79 Hz, *J*_{C-P} = 25 Hz, Rh-CO), 186.6 (s, CO_{acac}), 185.6 (s, CO_{acac}), 137.7 (d, *J*_{C-P} = 49 Hz, C_{ipso}),

135.9 (d, $J_{C-P} = 4$ Hz, PPh₄ C_{para}), 134.5 (d, $J_{C-P} = 10$ Hz, PPh₄ C_{meta}), 134.0 (d, $J_{C-P} = 11$ Hz, C_{ortho}), 130.9 (d, $J_{C-P} = 13$ Hz, PPh₄ C_{ortho}), 128.5 (d, $J_{C-P} = 3$ Hz, C_{para}), 127.0 (d, $J_{C-P} = 10$ Hz, C_{meta}), 117.6 (d, $J_{C-P} = 89$ Hz, PPh₄ C_{ipso}), 100.3 (s, CH_{acac}), 27.7 (d, $J_{C-P} = 5$ Hz, CH_{3acac}), 27.0 (s, CH_{3acac}), 19.1 (br s, CH₂BF₃). ¹¹B{¹H} NMR (160 MHz, 25 °C, CDCl₃) $\delta = 3.6$ (broad s). IR (DCM solution, CaF₂ windows, cm⁻¹): 3068 (m), 2969 (s), 2859 (m), 1962 (s, Rh-C≡O), 1574 (s, acac C=O), 1514 (s), 1487 (m), 1434 (m), 1383 (m), 1167 (m), 1104 (s). Elem. Anal: Calc'd ([PPh₄][Rh(acac)(CO)(PPh₂(CH₂BF₃))] C 61.8 H 4.7 N 0. Found: C 61.5 H 4.9 N 0.

Synthesis of [PPh₄][SePPh₂(CH₂BF₃)] ([PPh₄][¹Se]). To a stirring solution of K1 (50 mg, 0.16 mmol) in THF (5 mL) was added a 10-fold excess of solid selenium powder (129 mg, 1.6 mmol, 10 eq), followed by PPh₄Br (75 mg, 0.17 mmol, 1.1 eq) in DCM (3 mL). This mixture was stirred overnight, then filtered through Celite and all volatiles were removed in vacuo. Crystallization by vapor diffusion of Et₂O into a CDCl₃ or DCM solution of [PPh₄][¹Se] gave the product as clear crystals (60 mg, 0.087 mmol, 55%). Analytically pure samples were obtained by crystallizing [PPh₄][¹Se] from a mixture of hot MeCN and THF. ¹H NMR (400 MHz, 25 °C, CDCl₃) $\delta = 7.98$ -7.92 (m, 4H, Ph-H), 7.88-7.82 (m, 4H, *p*-Ph-H PPh₄), 7.77-7.70 (m, 8H, PPh₄), 7.65-7.57 (m, 8H, PPh₄), 7.30-7.24 (m, 6H, Ph-H) 1.89 (dq, $J_{P-H} = 10$ Hz, $J_{F-H} = 4$ Hz, 2H, CH₂BF₃). ³¹P{¹H} NMR (162 MHz, 25 °C, CDCl₃) $\delta = 33.59$ (q, $J_{P-F} = 10$ Hz, $J_{P-Se} = 656$ Hz, 1P, SePPh₂(CH₂BF₃)), 22.08 (s, 1P, PPh₄). ¹⁹F{¹H} NMR (376 MHz, 25 °C, CDCl₃) $\delta = -132.93$ (broad s, 3F, BF₃). ¹³C{¹H} NMR (126 MHz, 25 °C, CDCl₃) $\delta = 135.9$ (d, $J_{C-P} = 88.2$ Hz, C_{ipso}), 135.9 (s, PPh₄ C_{para}), 134.4 (d, $J_{C-P} = 12.6$ Hz, PPh₄ C_{meta}), 132.3 (d, $J_{C-P} = 12.6$ Hz, C_{ortho}), 130.9 (d, $J_{C-P} = 25.2$ Hz, PPh₄ C_{ortho}), 129.8 (s, C_{para}), 127.5 (d, $J_{C-P} = 25.2$ Hz, C_{meta}), 117.5 (d, $J_{C-P} = 113.4$ Hz, PPh₄ C_{ipso}), 26.7 (broad s, CH₂BF₃). ¹¹B{¹H} NMR (160 MHz, 25 °C, CDCl₃) $\delta = 3.1$ (broad s). IR (CDCl₃ solution): 3058 (m), 1978 (w), 1907 (w), 1814 (w), 1590 (m), 1487 (m), 1438 (s), 1310 (w), 1144 (m), 1103 (s), 1023 (s). Elem. Anal: Calc'd ([PPh₄][SePPh₂(CH₂BF₃))] C 64.8 H 4.7 N 0. Found: C 65.0 H 4.7 N 0.3.

Synthesis of [TEA][SePPh₂(CH₂BF₃)] ([TEA][¹Se]). To a stirring solution of K1 (50 mg, 0.16 mmol) in THF (5 mL) was added a 10-fold excess of solid selenium powder (129 mg, 1.6 mmol, 10 eq), followed by TEABr (36 mg, 0.17 mmol, 1.05 eq) in DCM (3 mL). This mixture was stirred overnight, then filtered through Celite and all volatiles were removed in vacuo. Crystallization by vapor diffusion or layering of Et₂O into a DCM solution of [TEA][¹Se] at -35 °C gave the product as clear colorless needle shaped crystals (49 mg, 0.103 mmol, 63%). ¹H NMR (400 MHz, 25 °C, CDCl₃) $\delta = 7.93$ -7.84 (m, 4H, Ph-H), 7.36-7.3 (m, 6H, Ph-H), 3.18 (q, $J_{H-H} = 5$ Hz, 8 H, N(CH₂CH₃)₄), 1.94 (dq, $J_{P-H} = 16$ Hz, $J_{F-H} = 4$ Hz, 2H, CH₂BF₃), 1.20 (t, $J_{H-H} = 4$ Hz, 12 H, N(CH₂CH₃)₄). ³¹P{¹H} NMR (162 MHz, 25 °C, CDCl₃) $\delta = 32.2$ (q, $J_{P-F} = 10$ Hz, $J_{P-Se} = 678$ Hz, 1P, SePPh₂(CH₂BF₃)). ¹⁹F{¹H} NMR (376 MHz, 25 °C, CDCl₃) $\delta = -131.4$ (broad s, 3F, BF₃). ¹³C{¹H} NMR (101 MHz, 25 °C, CDCl₃) $\delta = 136.4$ (d, $J_{C-P} = 70$ Hz, C_{ipso}), 131.5 (d, $J_{C-P} = 11$ Hz, C_{ortho}), 130.0 (d, $J_{C-P} = 2$, C_{para}), 127.8 (d, $J_{C-P} = 12$ Hz, C_{meta}), 52.5 (t, $J_{C-N} = 2$ Hz, N(CH₂CH₃)₄), 23.3 (broad s, CH₂BF₃), 7.6 (s, N(CH₂CH₃)₄). ¹¹B{¹H} NMR (160 MHz, 25 °C, CDCl₃) $\delta = 2.9$ (broad s). IR (KBr pellet): 2981 (w), 2948(w), 1486, (m), 1436 (m), 1393 (w), 1370(w), 1310 (w), 1262 (w), 1139 (s), 1099 (s), 1023 (s), 969 (s), 953 (s), 808 (m), 762 (m), 732 (m), 698 (s). Elem. Anal: Calc'd ([TEA][SePPh₂(CH₂BF₃))] C 53.0 H 6.8 N 2.9. Found: C 52.8 H 7.0 N 3.1.

Synthesis of [PPh₄][SePPh₂(2-BF₃Ph)] ([PPh₄][3^{Se}]). To a stirring acetonitrile solution (10 mL) of K[PPh₂(2-BF₃Ph)] (50 mg, 0.14 mmol) was added an excess of elemental selenium (109 mg, 1.4 mmol, 10 eq) and this mixture was stirred for 6 hours at room temperature. The solution was filtered, and PPh₄Br (62 mg, 0.14 mmol, 1 eq) was added as a solid, the resulting slurry was stirred for 10 min, then all volatiles were removed under vacuum. The white powder was washed with 2 mL CHCl₃ to remove excess PPh₄Br, and then extracted into MeCN. Crystallization by diffusion of Et₂O into the filtered MeCN solution afforded [PPh₄][SePPh₂(2-BF₃Ph)] as clear crystals (Yield: 10 mg, 0.014 mmol, 10%). ¹H NMR (400 MHz, 25 °C, CD₃CN) δ = 8.04 (dd, 1H, *J*_{F-H} = 16 Hz, *J*_{H-H} = 8 Hz) 7.91 (t, 4H, *J* = 8 Hz), 7.76-7.65 (m, 20H), 7.4-7.2 (m, 9H). ³¹P{¹H} NMR (162 MHz, 25 °C, CD₃CN) δ = 40.3 (s, *J*_{P-Se} = 700 Hz, 1P, SePPh₂(2-BF₃Ph)), 22.9 (s, 1P, PPh₄). ¹⁹F{¹H} NMR (376 MHz, 25 °C, CD₃CN) δ = -132.6 (m, 3F, BF₃). ¹³C{¹H} NMR (126 MHz, 25 °C, CD₃CN) δ = 136.9 (d, *J*_{C-P} = 97 Hz, *C*_{ipso}), 136.4 (s, PPh₄ *C*_{para}), 135.9 (s), 135.8 (d, *J*_{C-P} = 16 Hz, *C*³-Ar), 135.7 (d, *J*_{C-P} = 13 Hz, PPh₄ *C*_{meta}), 133.4 (d, *J*_{C-P} = 13 Hz, *C*_{ortho}), 132.0 (s), 131.3 (d, *J*_{C-P} = 13 Hz, PPh₄ *C*_{ortho}), 130.9 (s, *C*_{para}), 128.3 (d, *J*_{C-P} = 13 Hz, *C*_{meta}), 126.4 (d, *J*_{C-P} = 25 Hz, *C*⁶-Ar), 119.0 (d, *J*_{C-P} = 113 Hz, PPh₄ *C*_{ipso}). ¹¹B{¹H} NMR (160 MHz, 25 °C, CDCl₃) δ = 2.4 (broad q, *J*_{B-F} = 51 Hz). IR (KBr pellet): 3048 (m) 1586 (m) 1482 (m) 1434 (s) 1315 (w) 1260 (w) 1181 (m) 1162 (m) 1109 (s) 1052 (w) 978 (m) 955 (m) 935 (s) 759 (m) 725 (s) 691 (s) 610 (m). Elem. Anal: Calc'd ([PPh₄][SePPh₂(2-BF₃Ph)]) C 67.5 H 4.6 N 0. Found: C 67.7 H 4.9 N 0.

Procedure for oxidative addition of C₆F₆

UV-vis

To a stirring THF solution (1 mL) of Ni(COD)₂ (14 mg, 0.051 mmol) was added a THF solution (1 mL) of **K1** (30 mg, 0.099 mmol, 1.9 eq) and an excess of C₆F₆ (200 mg, 1.07 mmol, 21 eq), resulting in a deep red solution. After stirring for one hour, the solution had become brown-yellow, and NMR indicated oxidative addition of the C-F bond via the appearance of characteristic ¹⁹F NMR peaks at -383 (Ni-F) and -117 (*o*-C-F) ppm and the disappearance of ³¹P peaks associated with **K1** (Figures S29-31). Further characterization of the oxidative addition product could not be obtained due to the instability of the resulting species. Samples for UV-vis were prepared by dissolving Ni(COD)₂ (10 mg, 0.035 mmol), **K1** (22 mg, 0.072 mmol, 2 equiv.), and C₆F₆ (89 μL, 0.76 mmol, 21 equiv.) in 2.9 mL THF, resulting in a 12 mM solution. Diluting 75 μL of this solution in 2.5 mL resulted in a 0.36 mM solution which was used to monitor the decay of the Ni complex by UV-vis. The decay of the absorbance at 464 nm was monitored to determine the rate of decay of the in situ formed Ni complex (Figure S46). Monitoring the decay under identical conditions in the absence of C₆D₆ indicates minimal decay (Figure 47).

NMR Kinetics

K1

A THF stock solution was prepared by adding 66 μL of CF₃Ph (0.54 mmol) and 125 μL of C₆F₆ (1.08 mmol) to 9 mL of THF. In a 20 mL scintillation vial Ni(COD)₂ (10 mg, 0.036 mmol), **K1** (22 mg, 0.072 mmol, 2 equiv.) and PPh₃O (10 mg, 0.036, 1 equiv.) were dissolved in 3 mL of the

stock solution (delivering 0.18 mmol of CF₃Ph, 5 equiv., and 0.36 mmol C₆F₆, 10 equiv.). Approximately 500 μL of this solution was pipetted into an NMR tube, which was then covered with a small piece of tubing connected to a plastic adapter, removed from the glovebox, frozen in LN₂, placed under vacuum on the schlenk line and sealed under vacuum. The sample was kept frozen until the time of the first scan. NMR spectra of the reaction were collected every 2 hours for 16 hours, then again at 20 hours.

PCy₃

A THF stock solution was prepared by adding 66 μL of CF₃Ph (0.54 mmol) and 125 μL of C₆F₆ (1.08 mmol) to 9 mL of THF. In a 20 mL scintillation vial Ni(COD)₂ (10 mg, 0.036 mmol), PCy₃ (20 mg, 0.072 mmol, 2 equiv.) and PPh₃O (10 mg, 0.036, 1 equiv.) were dissolved in 3 mL of the stock solution (delivering 0.18 mmol of CF₃Ph (5 equiv.) and 0.36 mmol C₆F₆ (10 equiv.)). Approximately 500 μL of this solution was pipetted into an NMR tube, which was then covered with a small piece of tubing connected to a plastic adapter, removed from the glovebox, frozen in LN₂, placed under vacuum on the schlenk line and sealed under vacuum. The sample was kept frozen until the time of the first scan. NMR spectra were collected every 3 hours for 18 hours, then every 5 hours for 35 more hours, for 53 hours of monitoring total.

PEt₃

A THF stock solution was prepared by adding 32 μL of PEt₃ (0.216 mmol), 66 μL of CF₃Ph (0.54 mmol) and 125 μL of C₆F₆ (1.08 mmol) to 9 mL of THF. In a 20 mL scintillation vial Ni(COD)₂ (10 mg, 0.036 mmol) and PPh₃O (10 mg, 0.036, 1 equiv.) were dissolved in 3 mL of the stock solution (delivering 0.072 mmol of PEt₃ (2 equiv.), 0.18 mmol of CF₃Ph (5 equiv.), and 0.36 mmol C₆F₆ (10 equiv.)). Approximately 500 μL of this solution was pipetted into an NMR tube, which was then covered with a small piece of tubing connected to a plastic adapter, removed from the glovebox, frozen in LN₂, placed under vacuum on the schlenk line and sealed under vacuum. The sample was kept frozen until the time of the first scan. Spectra of the reaction were collected every 3 hours for 18 hours, then every 5 hours for 36 more hours, then every 12 hours for 60 more hours, for a total of 114 hours. Previous reports suggest the reaction reaches completion after 4 weeks, and the partial conversion observed here is consistent with that time frame.¹⁵

NMR methods

T₁ measurements of the reaction mixtures were used to decide collection parameters for monitoring the course of the reaction. Fluorine NMR was collected without decoupling with the following parameters: NS = 16, O1P = -113 ppm, SW = 140 ppm, D1 = 25 s and AQ = 2s. ³¹P{1H} was collected using the following parameters: NS = 31, O1P = 35 ppm, SW = 429 ppm, D1=35 s, and AQ = 2s. The spectra were collected using an automated Bruker Avance III HD nanobay 400 MHz. The rate of formation was determined using Mnova by generating a concentration graph, and fitting the concentration data to a three parameter exponential fit to the equation $y = B + F * \exp(-x * G)$, with G the observed rate.

Procedures for catalytic C-F borylation

Trial reactions – A 4 mL screw thread cap vial was charged with solid Ni(COD)₂ (10 mg, 0.036 mmol), K1 (22 mg, 0.072 mmol, 2 equiv.) and B₂pin₂ (amount specified in reaction tables). The solid mixture was then dissolved in 1 mL THF to give dark red solutions. Next, 1,3-difluorobenzene (40 μL, 0.4 mmol, 11 equiv.), CF₃Ph (20 μL, 0.16 mmol, 4.5 equiv.) and any additives were added to the reactions. Solutions were heated at 50 °C for the specified amounts of time. To work up the reactions, the 1 mL reaction was diluted to 5 mL in a scintillation vial. From that solution, 50 μL were diluted to 400 μL within an NMR tube, giving a 4 mM solution of CF₃Ph and what would be a 10 mM solution of product if there were 100% conversion of the fluoroarene. All yields are reported relative to added 1,3-difluorobenzene, consistent with the yields reported in the main text. See Tables S17-S24 for the yields from trial runs. Some of the yields are a slight underestimate because an excess of 1,3-difluorobenzene was added relative to B₂pin₂ (11 equiv. arene vs 10 equiv. B₂pin₂ relative to Ni(COD)₂). Yield was determined by comparing the integration of the CF₃Ph peak to the product peak using the following equation-¹⁶

$$\text{Moles of product} = \frac{\text{Integration of product}}{\# \text{ of fluorines in product}} \times \frac{\# \text{ of fluorines in CF}_3\text{Ph}}{\text{Integration of CF}_3\text{Ph}} \times \text{moles of CF}_3\text{Ph}$$

Yield = moles of product/theoretical yield * 100

Theoretical yield for borylated products is 0.4 mmol, theoretical yield for coupled products is 0.2 mmol.

Catalytic reactions – Stock solutions were prepared for three reactions at a time by dissolving Ni(COD)₂ (30 mg, 0.108 mmol, 3 equiv.), K1 (66 mg, 0.216 mmol, 6 equiv.), and B₂pin₂ (552 mg, 2.16 mmol, 60 equiv.) in 3 mL THF. Next the substrate (1.2 mmol, 33 equiv.), CF₃Ph (60 μL, 0.48 mmol, 13.5 equiv.), and MeOH (90 μL, 2.16 mmol, 60 equiv.) was added. The solution was divided into three vials which each already contained CsOH (54 mg, 0.36 mmol, 1 equiv.). The reactions were then heated at 50 °C for 4 hours. See Figure 5 in main text for the yields from these reactions. To characterize the yield of the C₆FH₅ reaction, the 1 mL reaction was diluted to 5 mL in a scintillation vial. From this solution, 45 μL was subsequently diluted to 3 mL, giving what would be a 1.2 mM solution if there were 100% conversion. This solution was filtered through a short silica plug in a pipette. The integration of the C₆H₅-Bpin was compared to an integral calibration curve prepared with stock solutions of C₆H₅-Bpin. The methods for workup and yield determination by NMR for the remaining catalytic reactions are identical to those for the trial reactions. Literature sources were used to assign the NMR shifts and MS of substrates and products:

Compound	Reference
1,2-difluorobenzene	17
1-Bpin-2-C ₆ FH ₄	
1,3-difluorobenzene	

1-Bpin-3-C ₆ FH ₄	
1,2,4-trifluorobenzene	
1,3,5-trifluorobenzene	
1-Bpin-3,5-C ₆ F ₂ H ₄	
1,3-Bpin-5-C ₆ FH ₃	
MS of C ₆ F ₅ -Bpin	
2,2'-F ₂ -1,1'-Ph ₂	18
1,4-difluorobenzene	19
1-Bpin-4-C ₆ FH ₄	20
2,2',5,5'-F ₄ -1,1'-Ph ₂	21

NMR Characterization Spectra

Ph₂PCH₂BF₃K (K1)

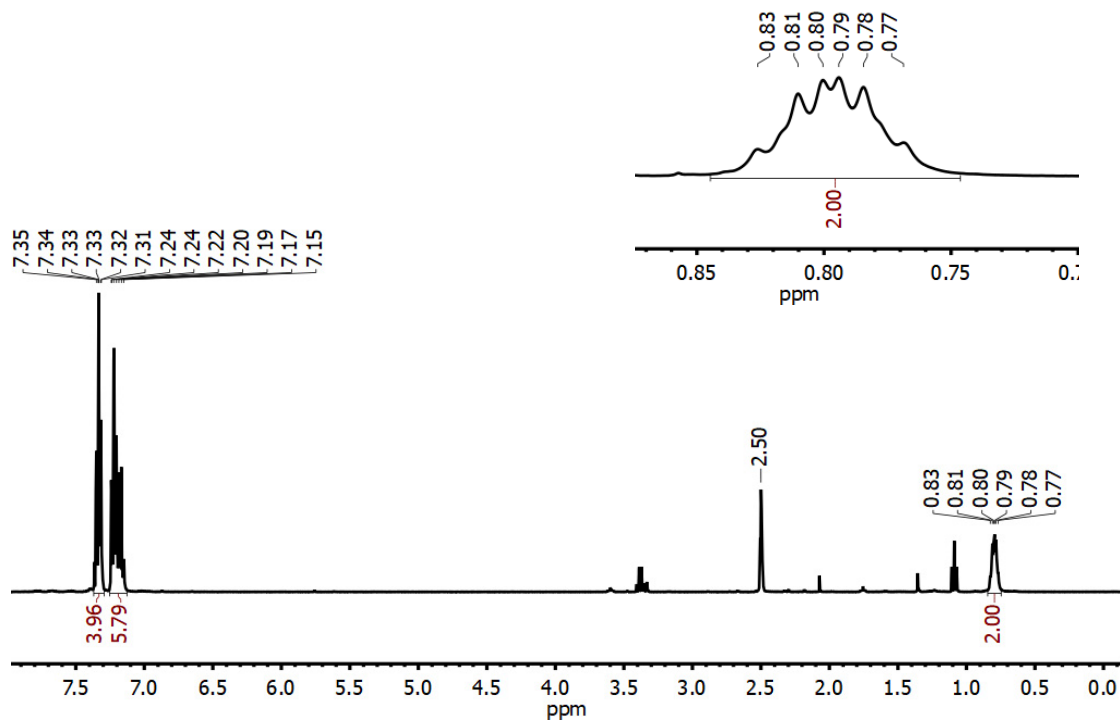


Figure S1. ¹H NMR spectrum of K1 in DMSO-*d*₆ with inset showing CH₂ peak.

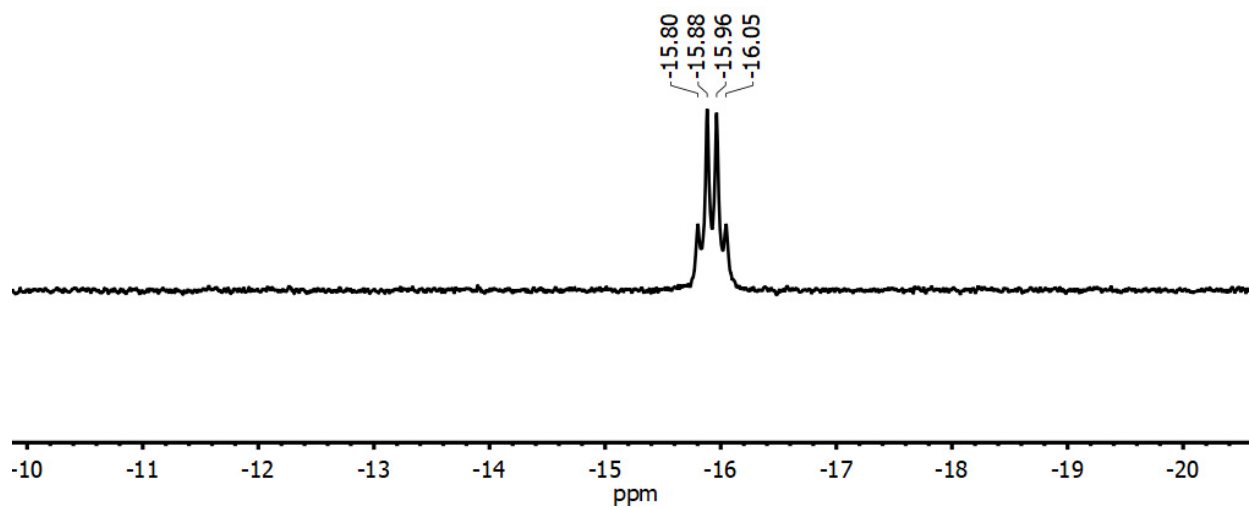


Figure S2. ³¹P{¹H} NMR spectrum of K1 in DMSO-*d*₆.

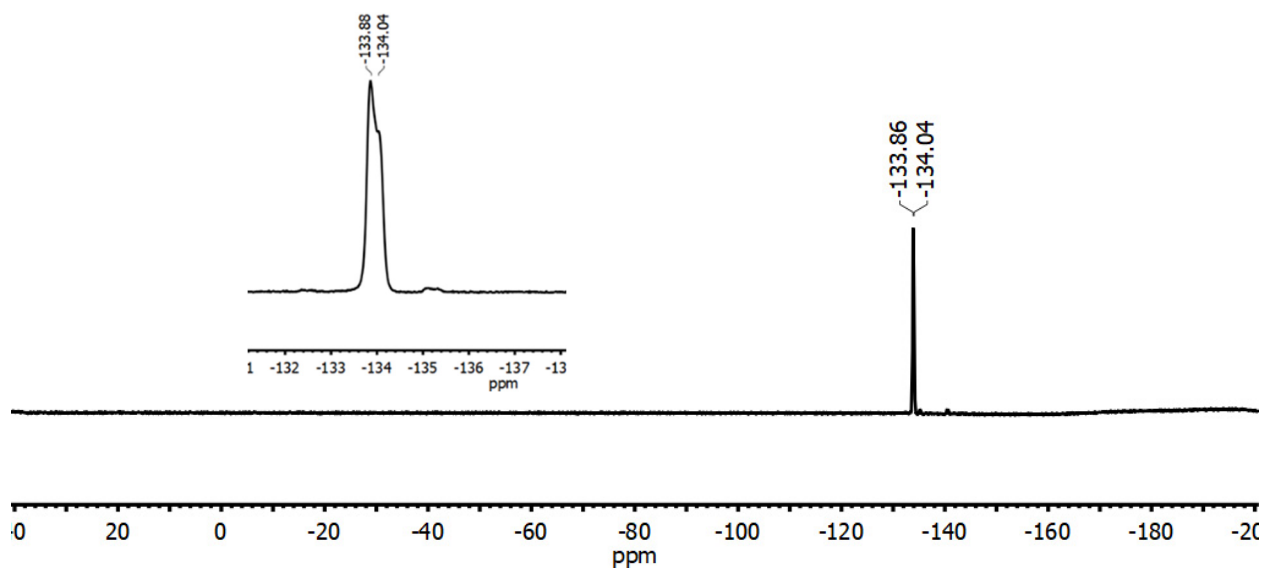


Figure S3. $^{19}\text{F}\{^1\text{H}\}$ NMR spectrum of K1 in $\text{DMSO-}d_6$. Broad feature around -190 ppm is a result of Teflon within the probe.

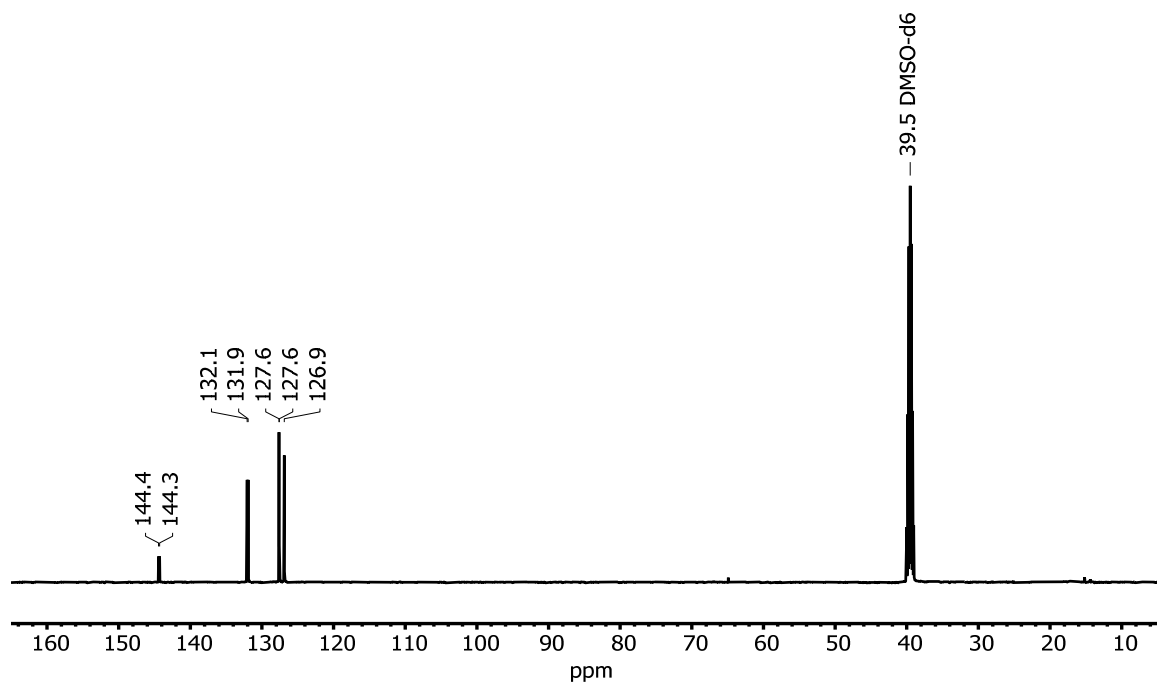


Figure S4. $^{13}\text{C}\{^1\text{H}\}$ NMR spectrum of K1 collected in $\text{DMSO-}d_6$.

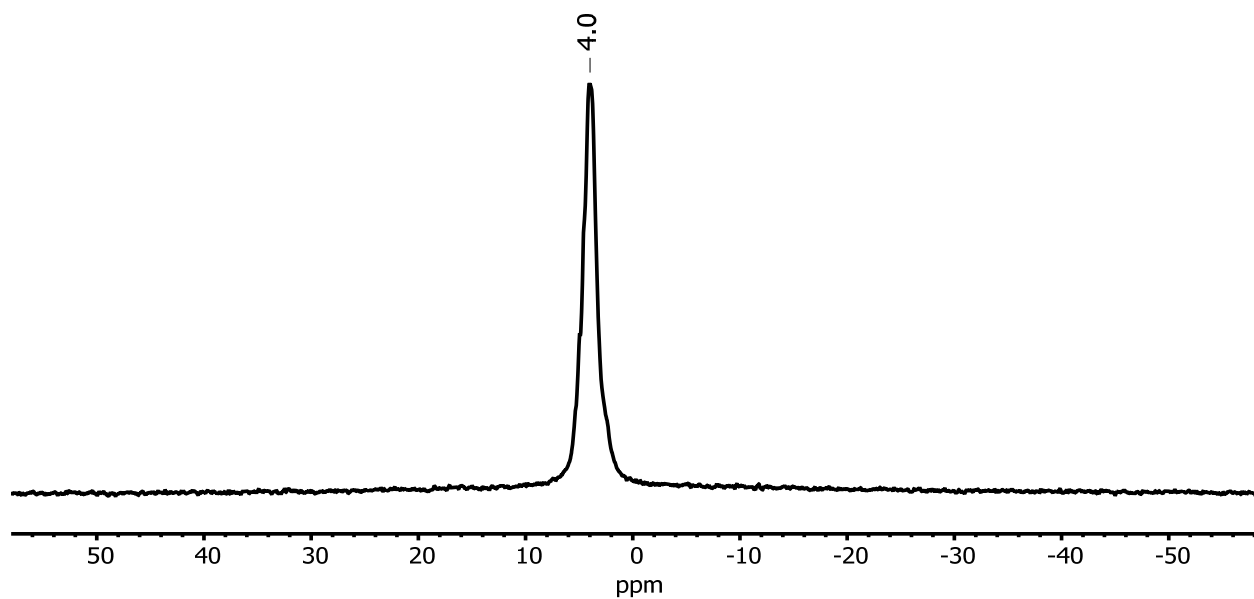


Figure S5. $^{11}\text{B}\{^1\text{H}\}$ NMR spectrum of K1 in $\text{DMSO-}d_6$ collected in a quartz NMR tube.

[PPh₄][Rh(acac)(CO)(PPh₂(CH₂BF₃))] (2)

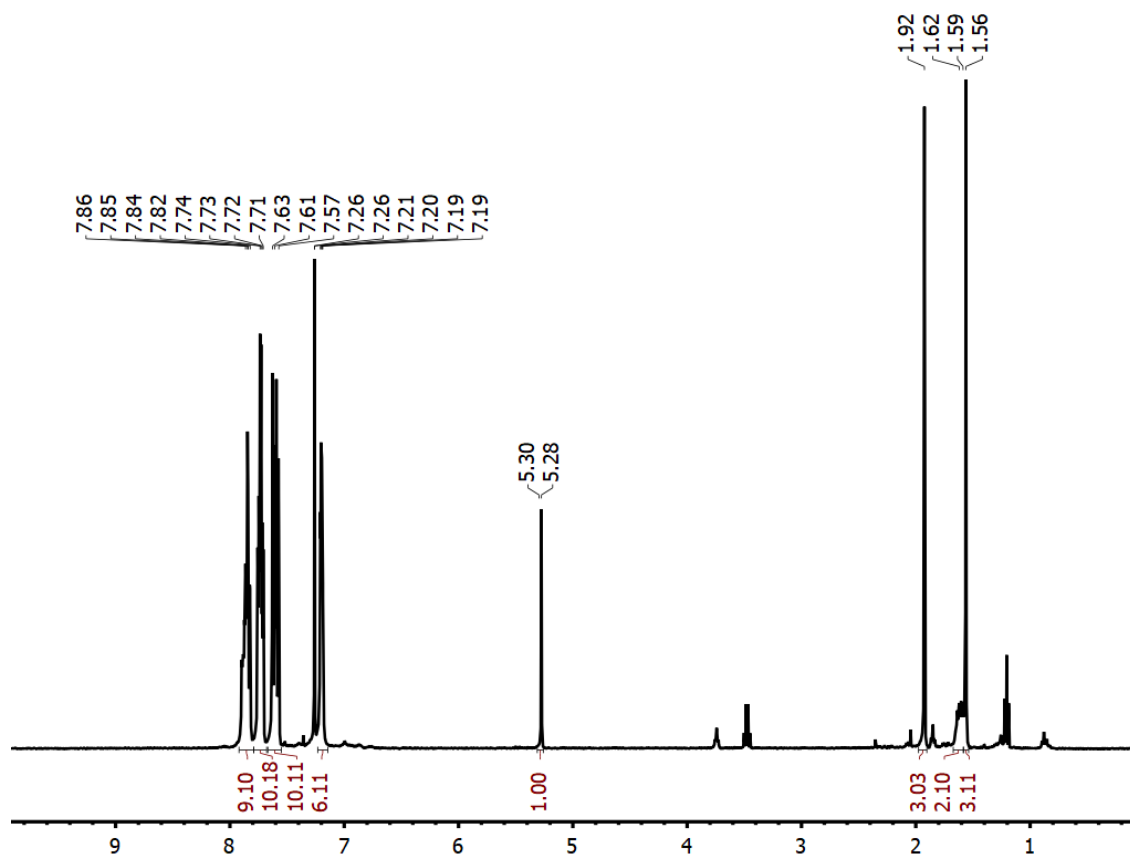


Figure S6. ^1H NMR spectrum of **2** collected in CDCl_3 .

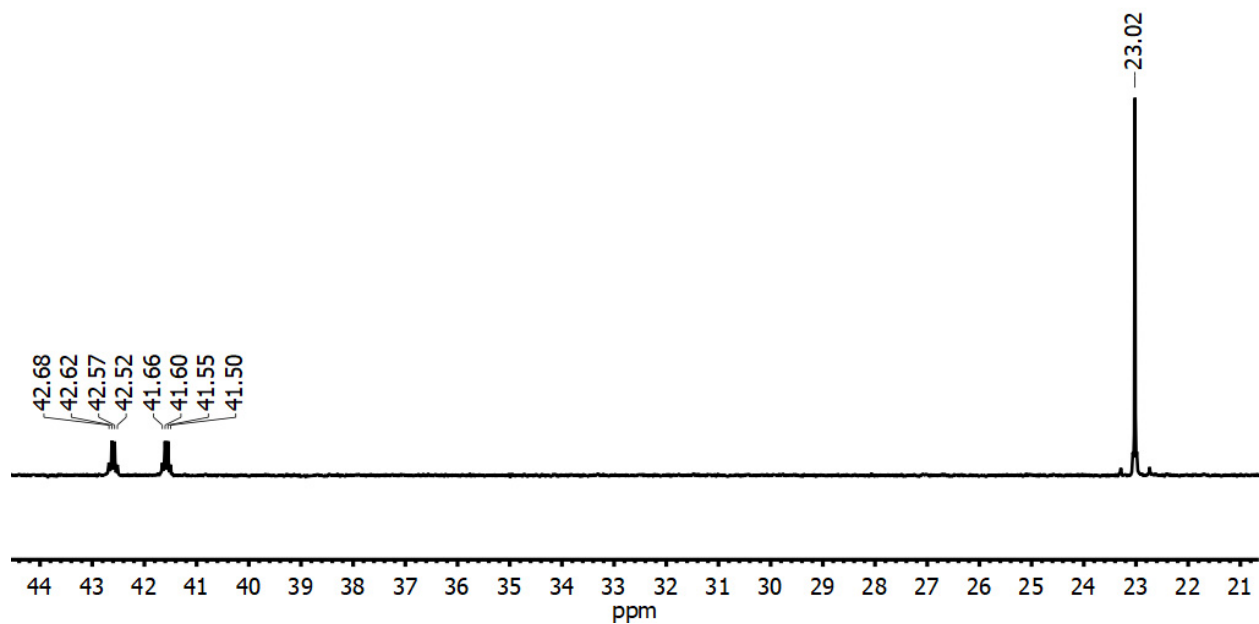


Figure S7. $^{31}\text{P}\{^1\text{H}\}$ NMR spectrum of **2** collected in CDCl_3 .

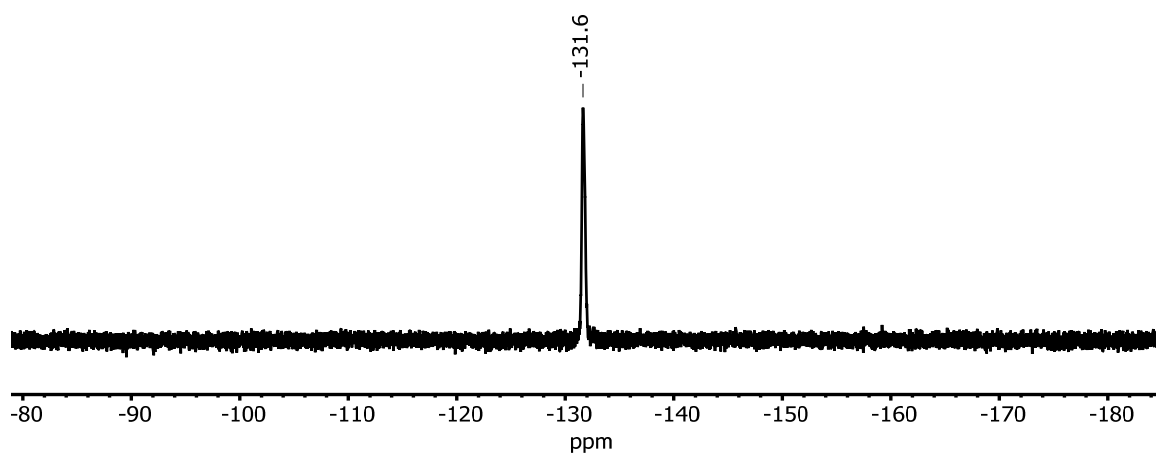


Figure S8. $^{19}\text{F}\{^1\text{H}\}$ NMR spectrum of **2** collected in CDCl_3 .

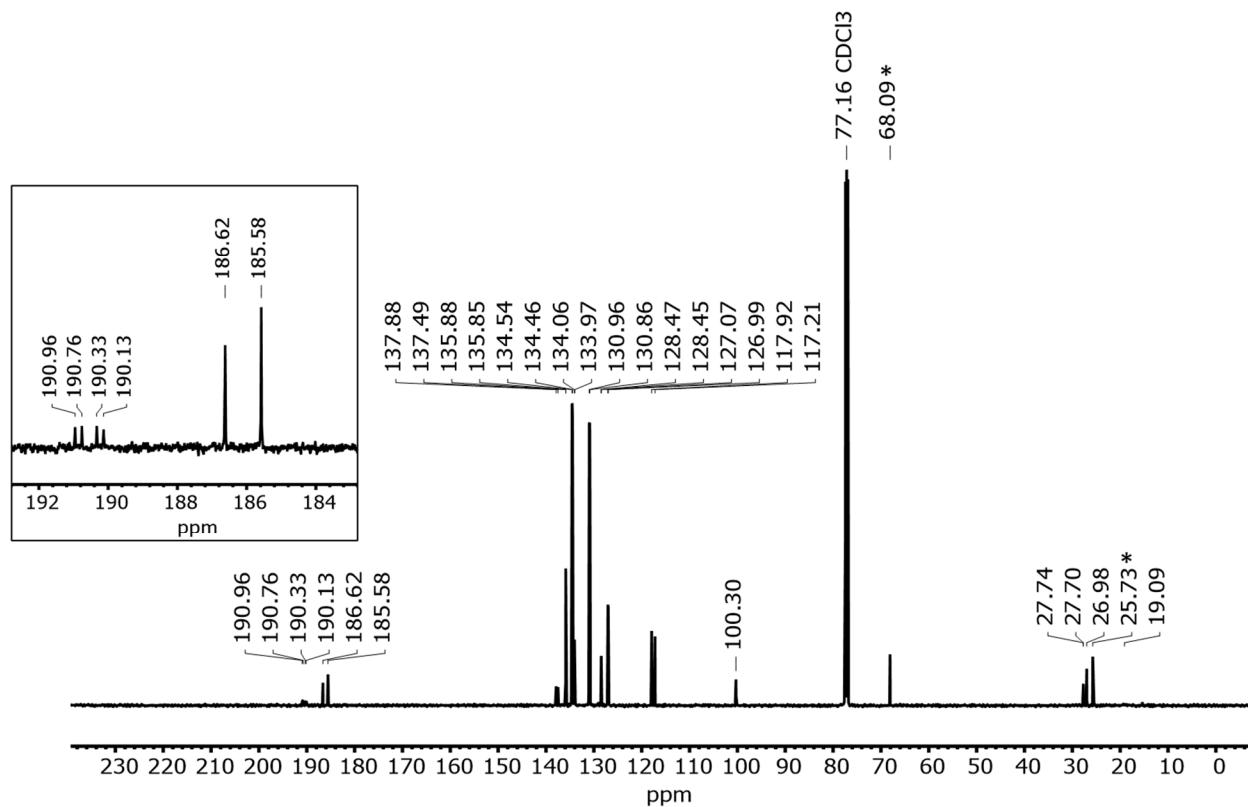


Figure S9. $^{13}\text{C}\{^1\text{H}\}$ NMR spectrum of **2** collected in CDCl_3 . Inset depicts doublet of doublets corresponding to the Rh-CO carbon. Asterisks indicate THF impurity.

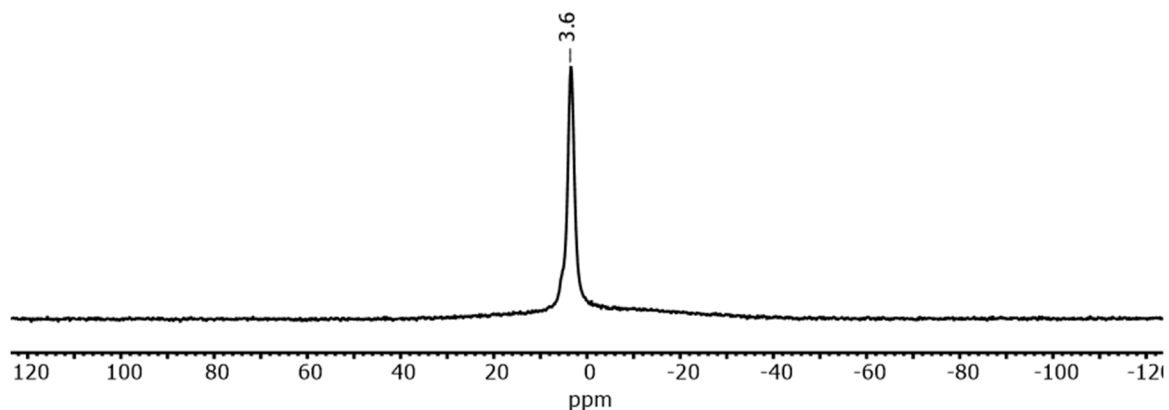


Figure S10. $^{11}\text{B}\{^1\text{H}\}$ NMR spectrum of **2** in CDCl_3 collected in a quartz NMR tube, the broad peak centered at 0 in the baseline is a result of borosilicate in the NMR probe.

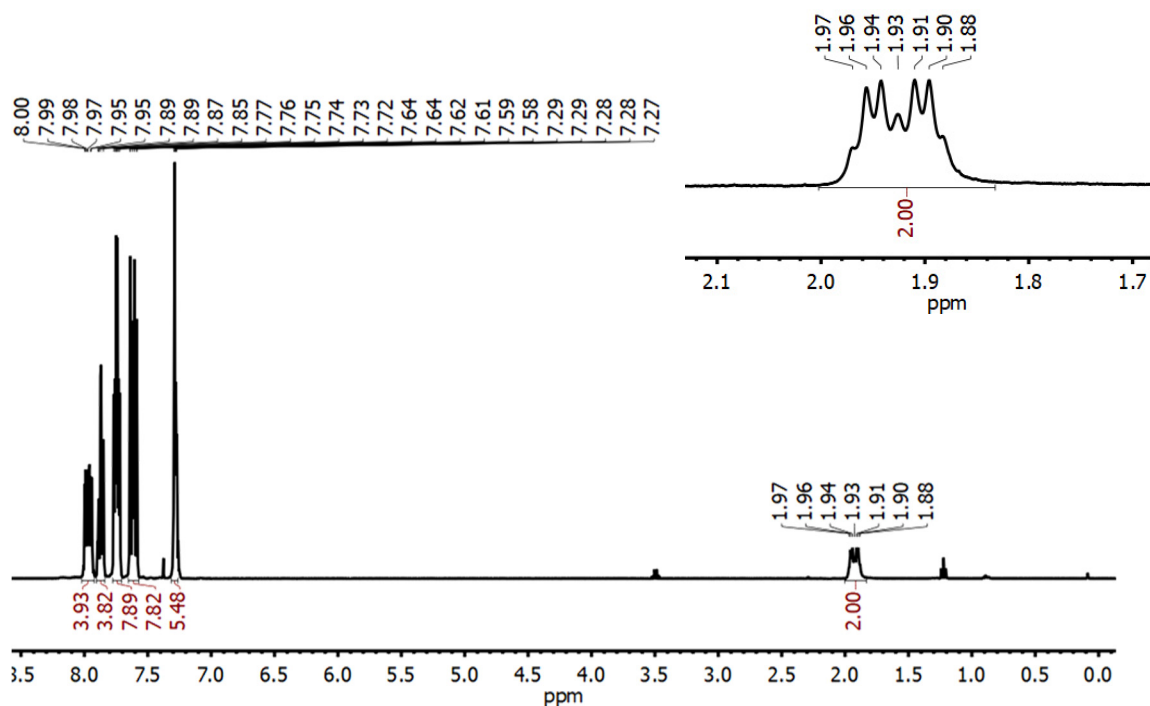


Figure S11. ¹H NMR spectrum of [PPh₄][1^{Se}] in CDCl₃, with inset showing splitting on the CH₂ group.

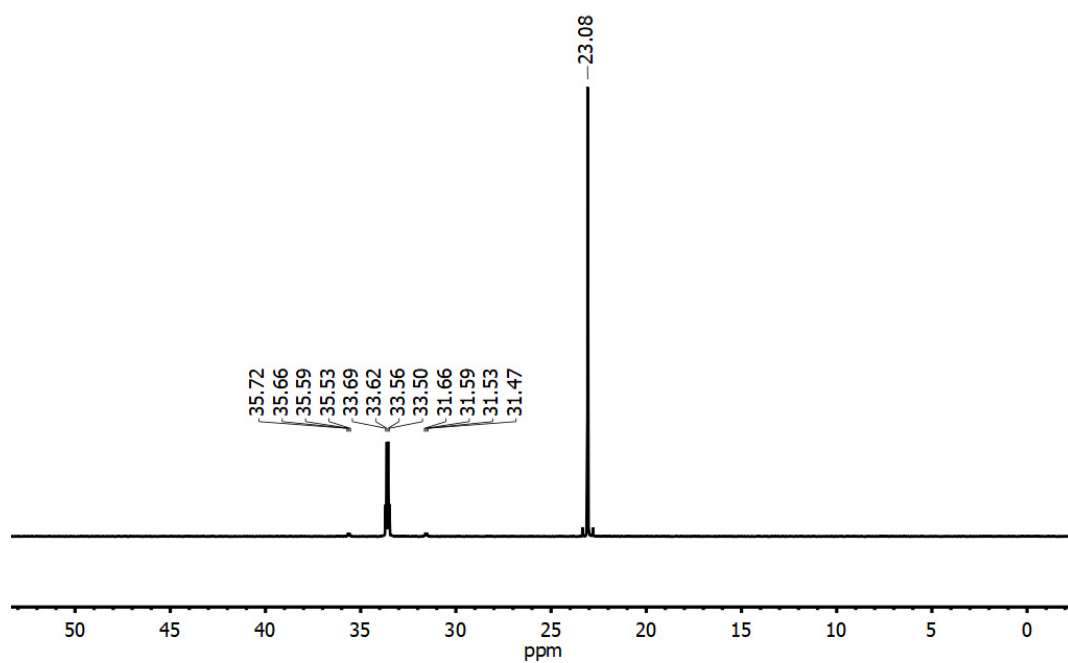


Figure S12. ³¹P{¹H} NMR spectrum of [PPh₄][1^{Se}] in CDCl₃.

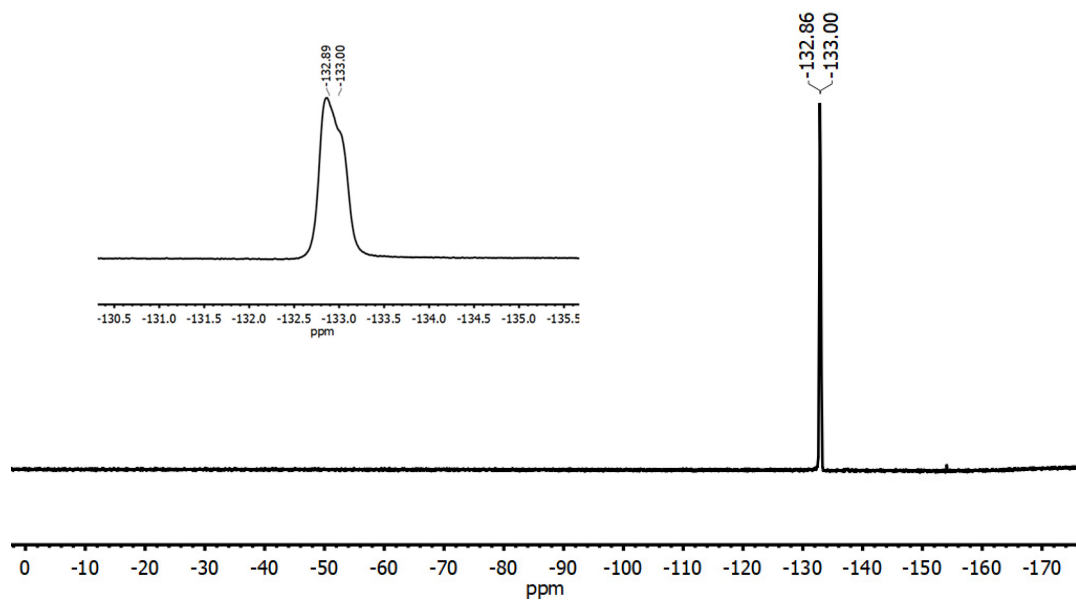


Figure S13. $^{19}\text{F}\{^1\text{H}\}$ NMR spectrum of $[\text{PPh}_4][\text{1}^{\text{Se}}]$ in CDCl_3 .

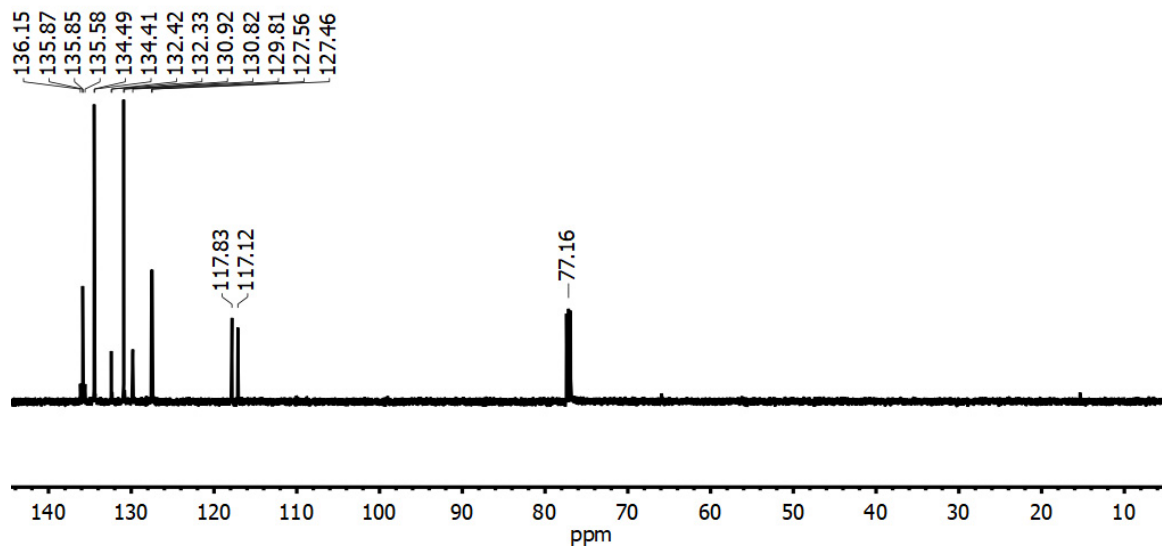


Figure S14. $^{13}\text{C}\{^1\text{H}\}$ NMR spectrum of $[\text{PPh}_4][\text{1}^{\text{Se}}]$ in CDCl_3 .

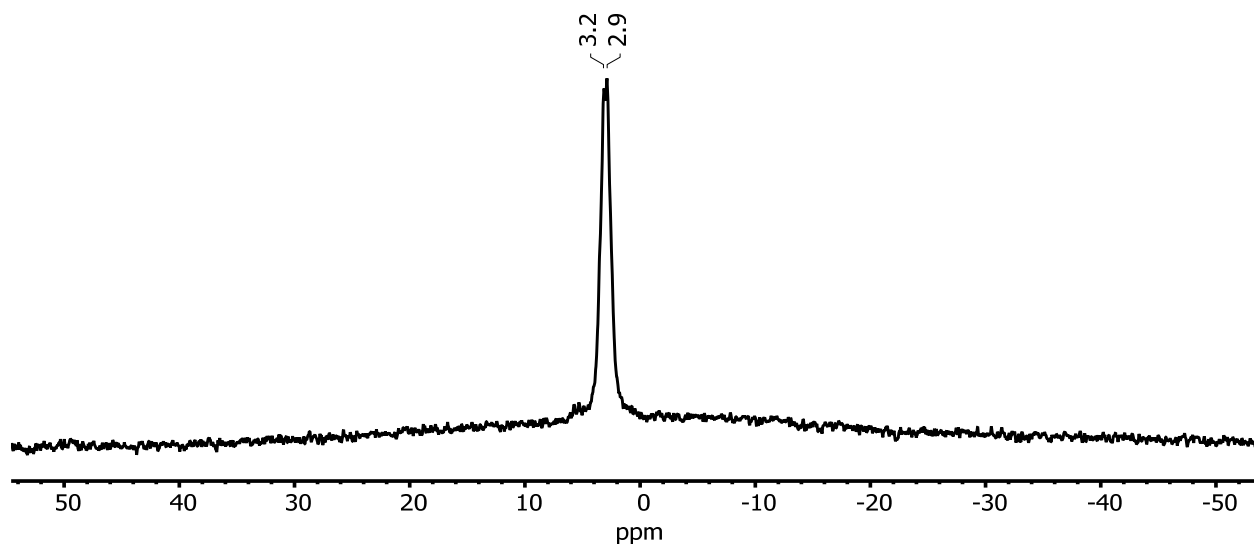


Figure S15. $^{11}\text{B}\{^1\text{H}\}$ NMR spectrum of $[\text{PPh}_4][^1\text{Se}]$ in CDCl_3 collected in a quartz NMR tube.

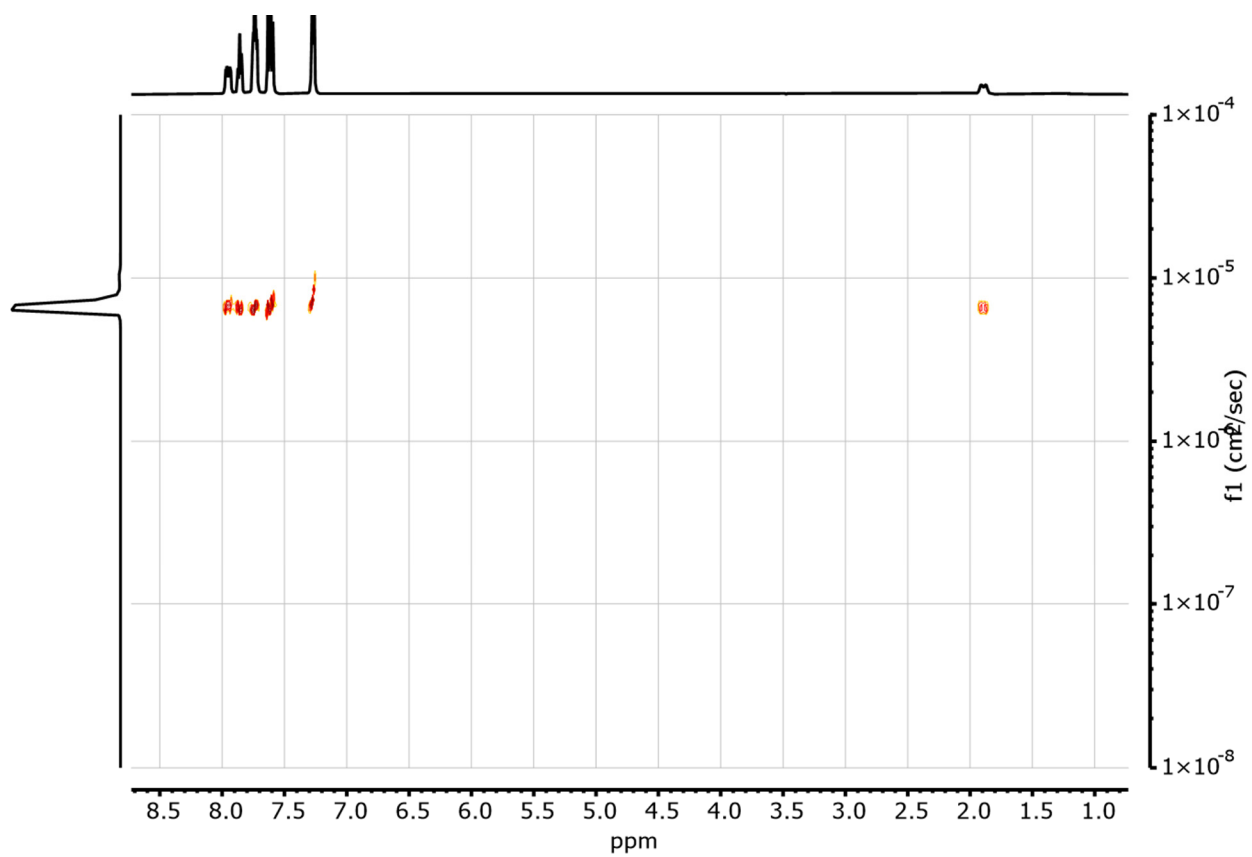


Figure S16. DOSY NMR spectrum of $[\text{PPh}_4][^1\text{Se}]$ in CDCl_3 . The diffusion value is $6.64 \text{ cm}^2/\text{sec}$. Smearing is observed at 7.26 ppm due to the solvent peak.

[TEA][SePPh₂(CH₂BF₃)] ([TEA][1^{Se}])

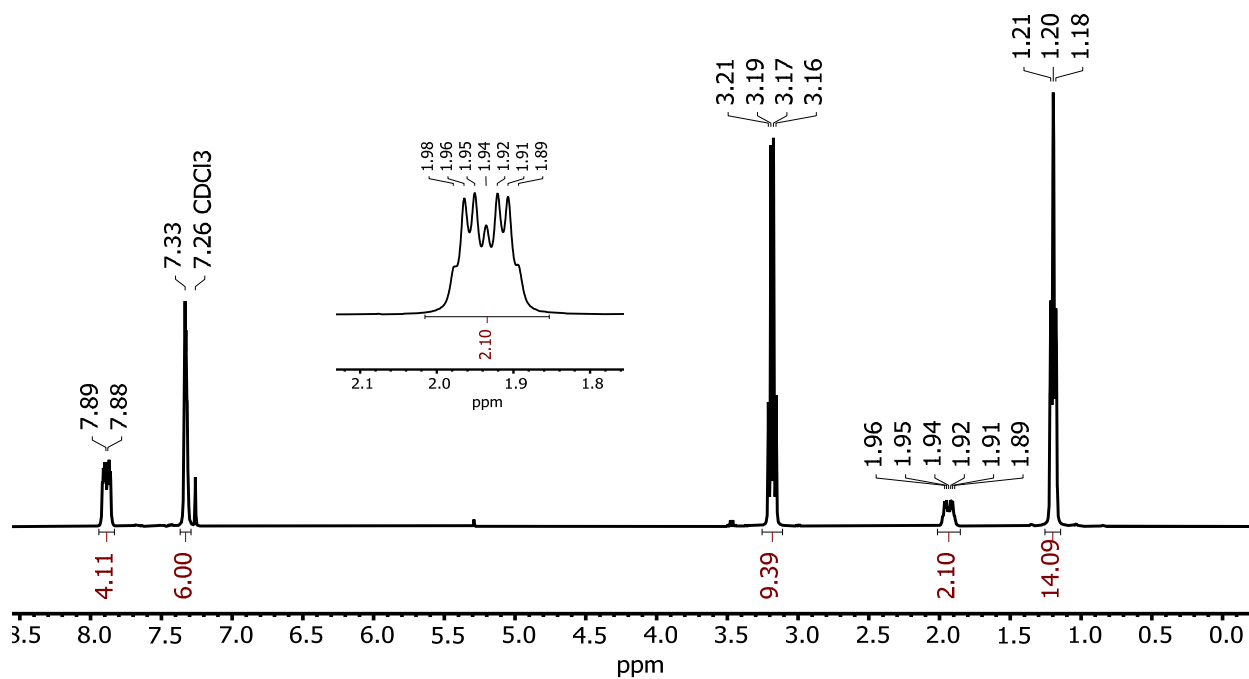


Figure S17. ¹H NMR spectrum of [TEA][1^{Se}] in CDCl₃, with inset showing splitting on the CH₂ group.

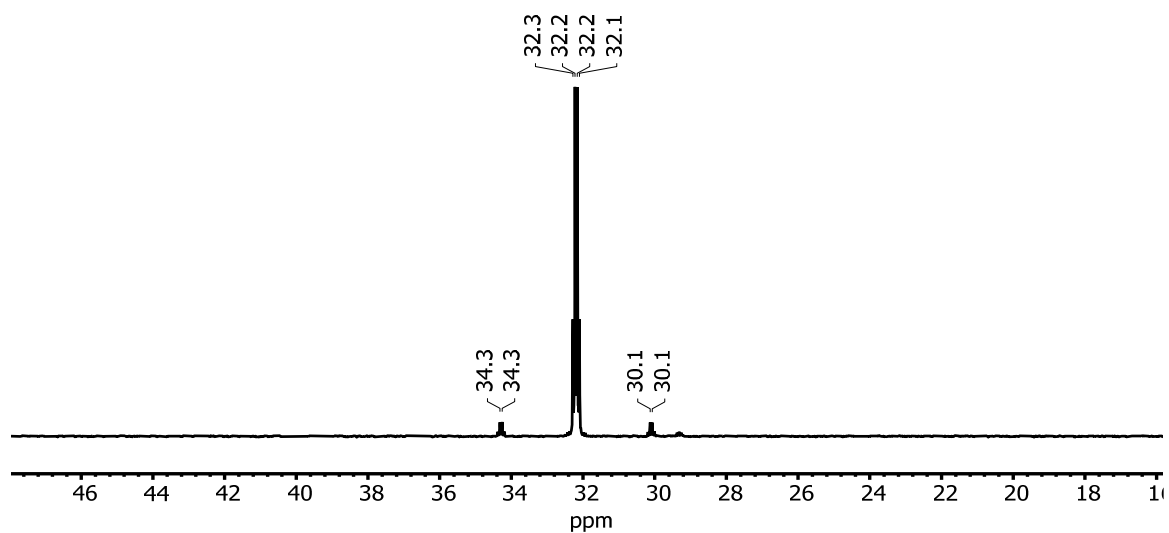


Figure S18. ³¹P{¹H} NMR spectrum of [TEA][1^{Se}] in CDCl₃.

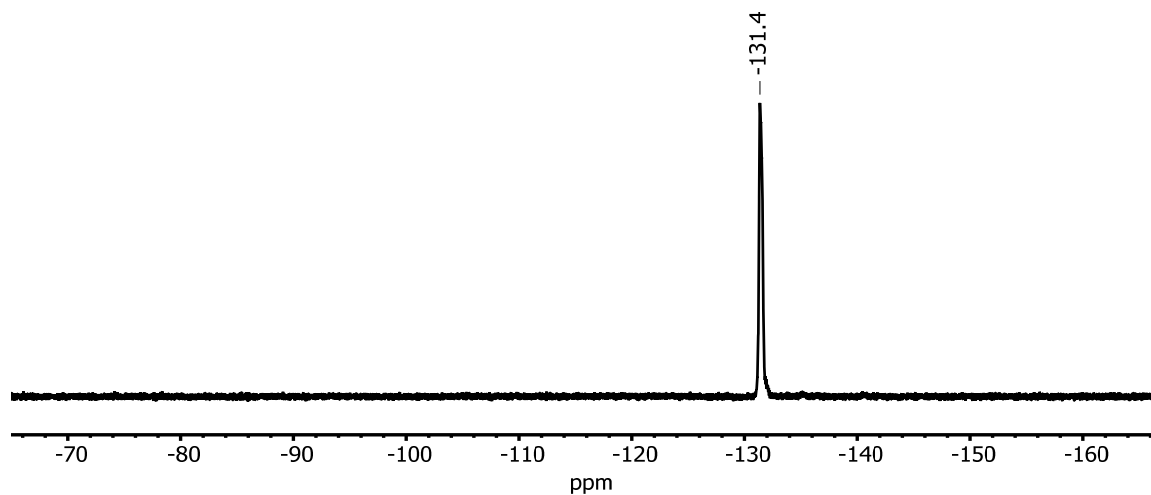


Figure S19. $^{19}\text{F}\{^1\text{H}\}$ NMR spectrum of $[\text{TEA}][\mathbf{1}^{\text{Se}}]$ in CDCl_3 .

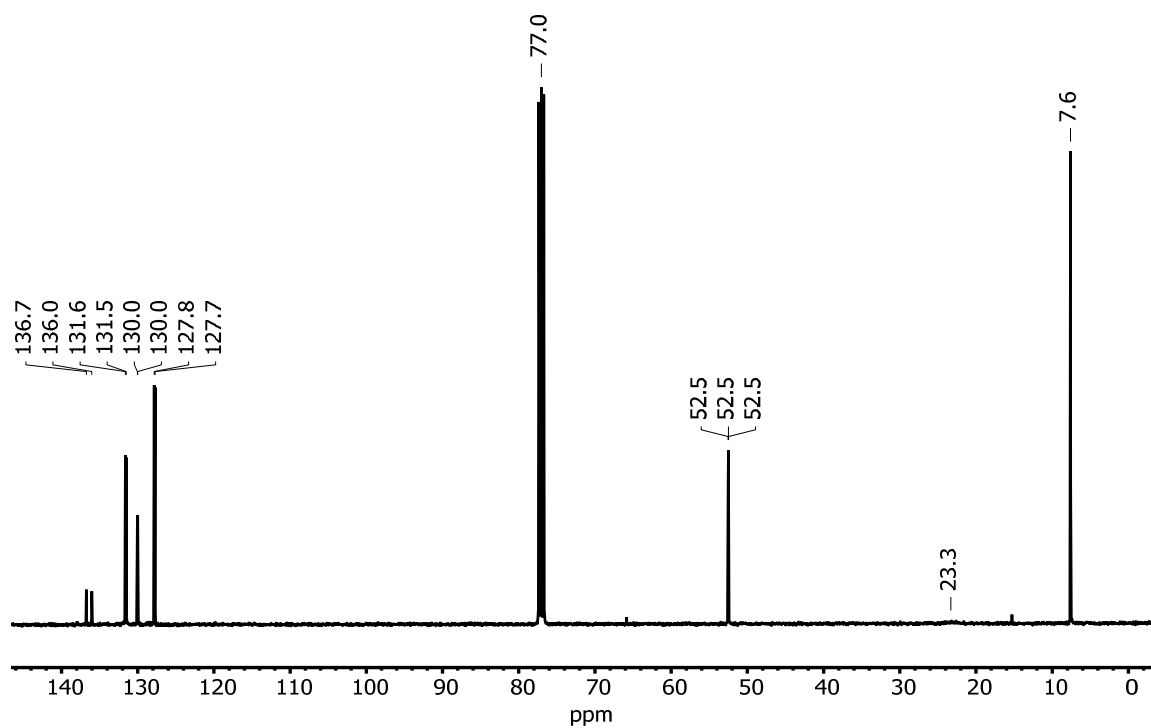


Figure S20. $^{13}\text{C}\{^1\text{H}\}$ NMR spectrum of $[\text{TEA}][\mathbf{1}^{\text{Se}}]$ in CDCl_3 .

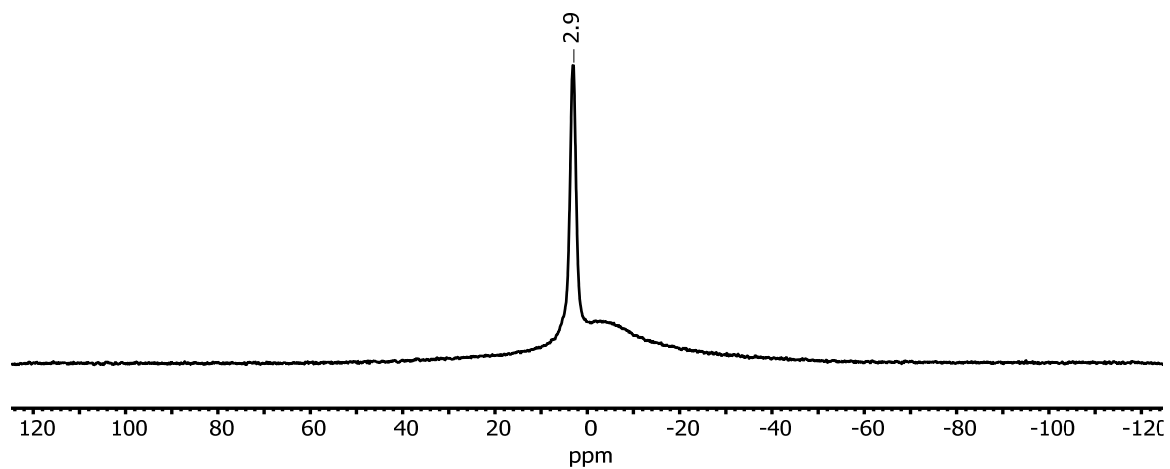


Figure S21. $^{11}\text{B}\{^1\text{H}\}$ NMR spectrum of $[\text{TEA}][\mathbf{1}^{\text{Se}}]$ collected in CDCl_3 ; the broad peak centered around 0 ppm is a result of borosilicate in the NMR tube and the NMR probe.

[PPh₄][SePPh₂(2-BF₃Ph)] ([PPh₄][3^{Se}])

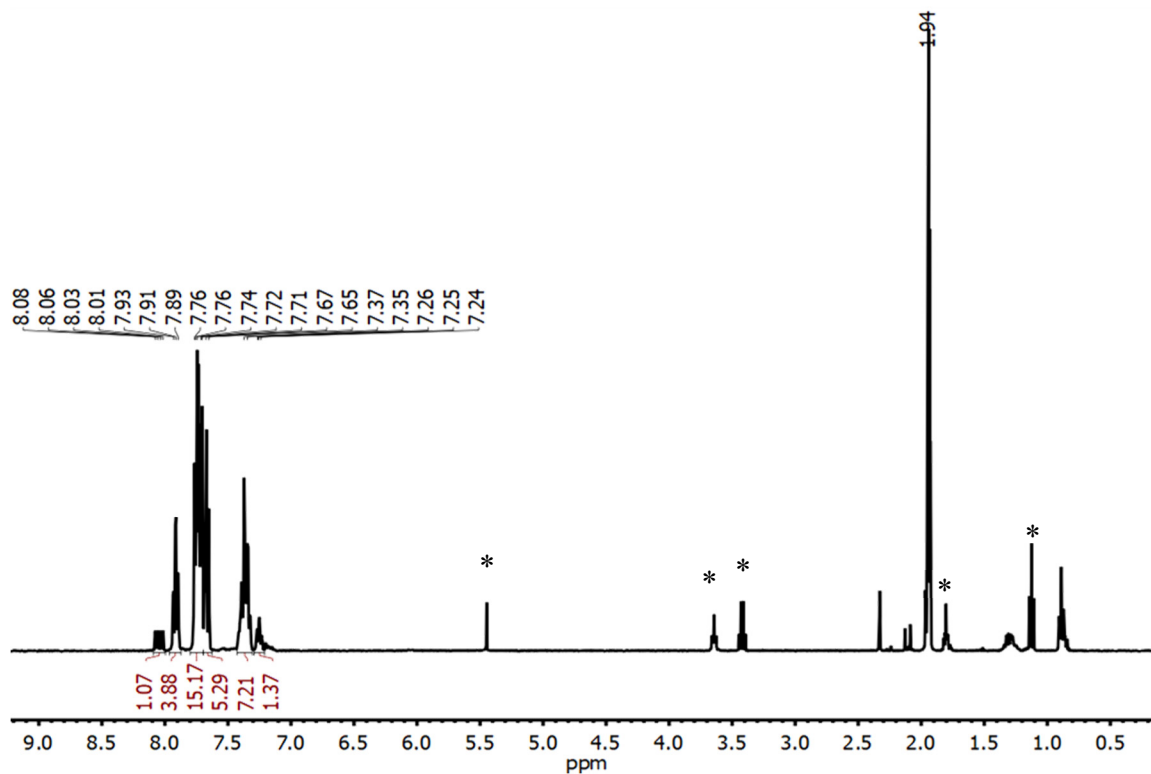


Figure S22. ¹H NMR spectrum of [PPh₄][3^{Se}] in CD₃CN; observed solvent impurities include DCM, THF and Et₂O.

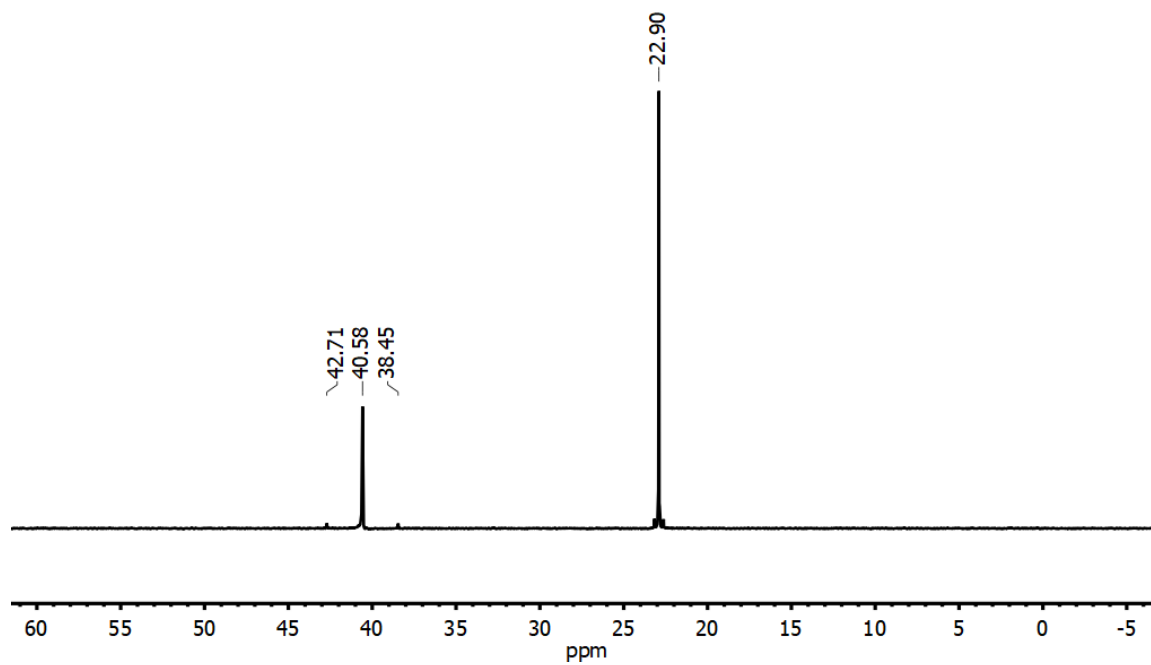


Figure S23. ³¹P{¹H} NMR spectrum of [PPh₄][3^{Se}] in CD₂Cl₂.

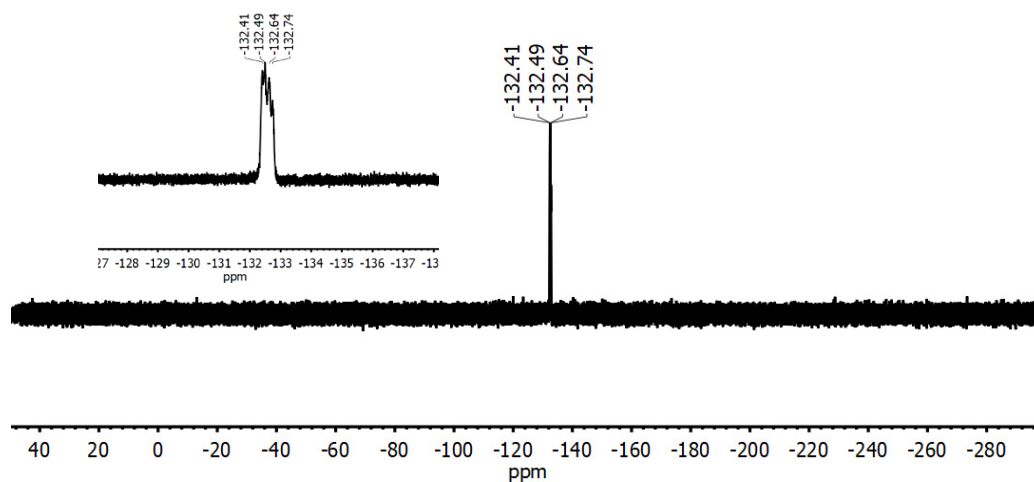


Figure S24. $^{19}\text{F}\{^1\text{H}\}$ NMR spectrum of $[\text{PPh}_4][\text{3}^{\text{Se}}]$ in CD_3CN .

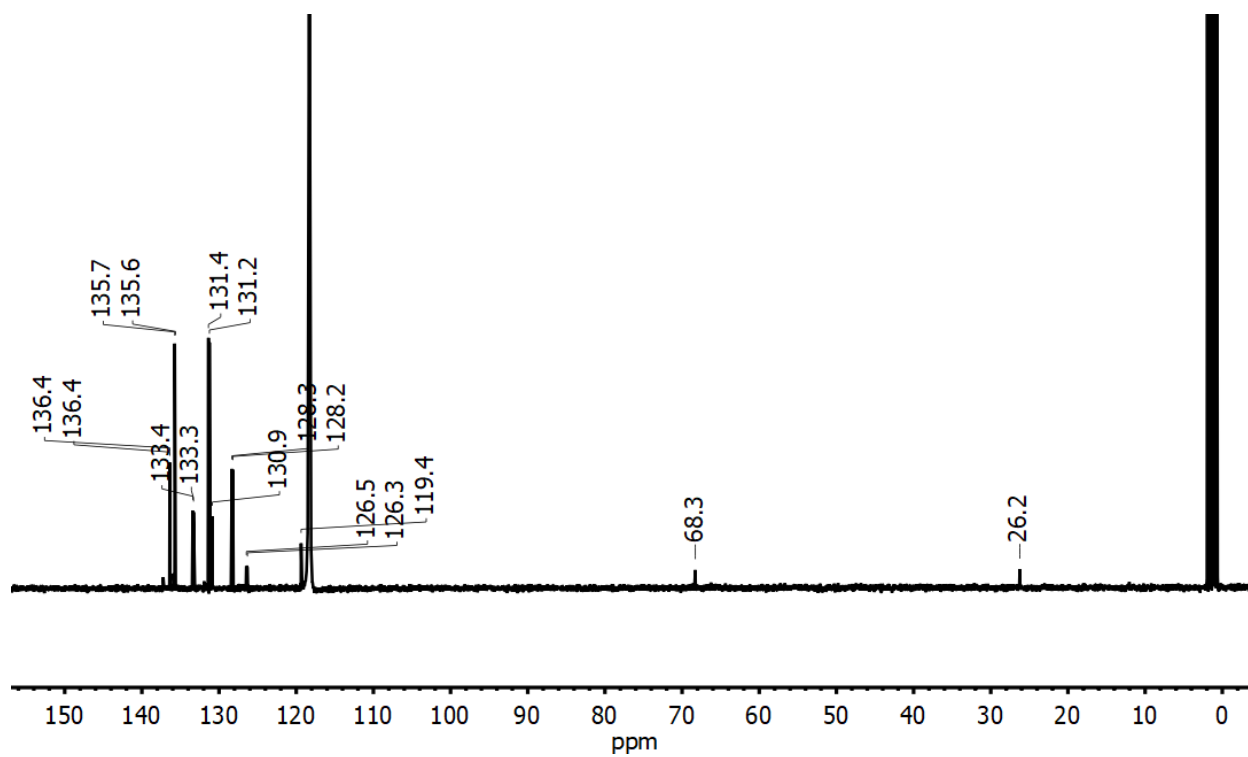


Figure S25. $^{13}\text{C}\{^1\text{H}\}$ NMR spectrum of $[\text{PPh}_4][\text{3}^{\text{Se}}]$ in CD_3CN .

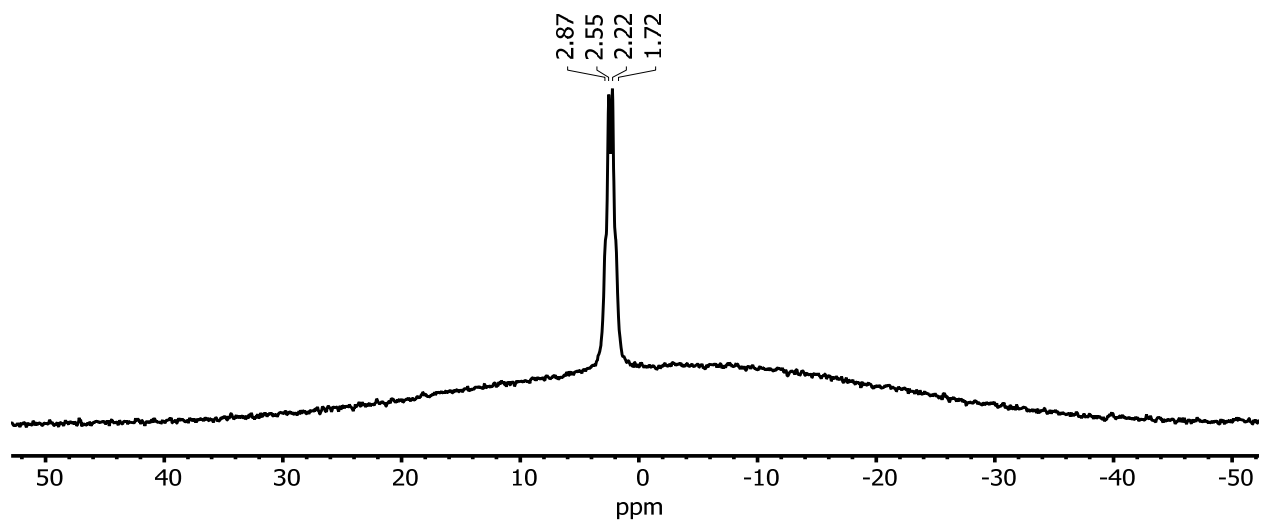


Figure S26. $^{11}\text{B}\{^1\text{H}\}$ NMR spectrum of $[\text{PPh}_4][\text{3}^{\text{Se}}]$ in CD_3CN collected in a quartz NMR tube; the broad peak in the baseline around 0 is a result of borosilicate in the NMR probe.

Variable solvent ^{31}P NMR spectra of $[\text{PPh}_4][\text{1}^{\text{Se}}]$, $[\text{TEA}][\text{1}^{\text{Se}}]$ and $[\text{PPh}_4][\text{3}^{\text{Se}}]$

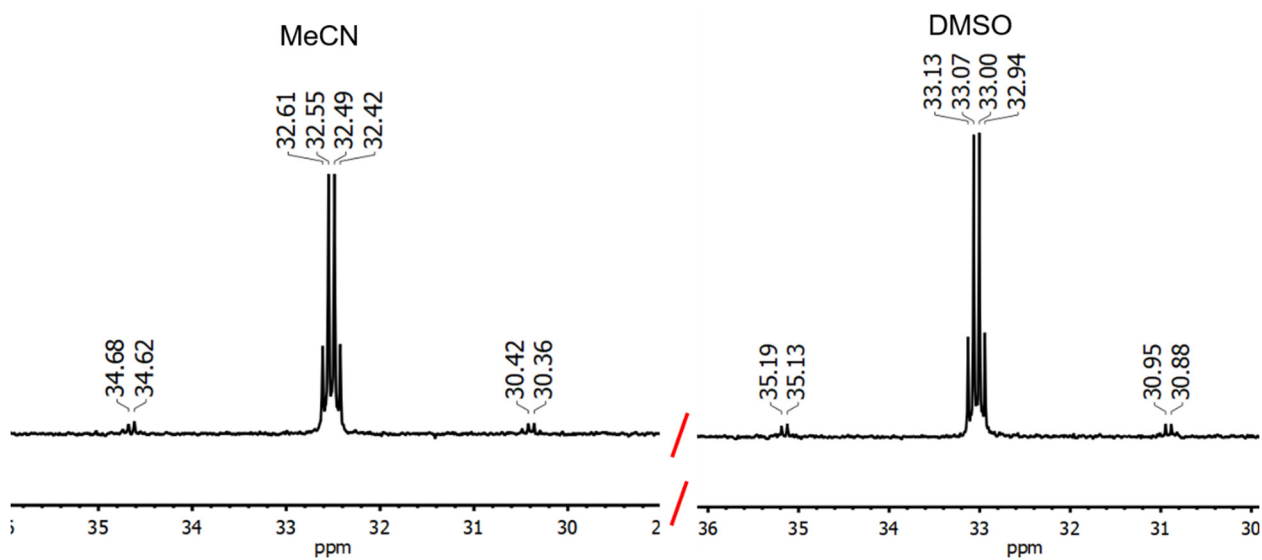


Figure S27. $^{31}\text{P}\{^1\text{H}\}$ NMR spectra of $[\text{PPh}_4][\text{1}^{\text{Se}}]$ in CD_3CN (left) and $\text{DMSO-}d_6$ (right) showing the P-Se phosphorus resonance.

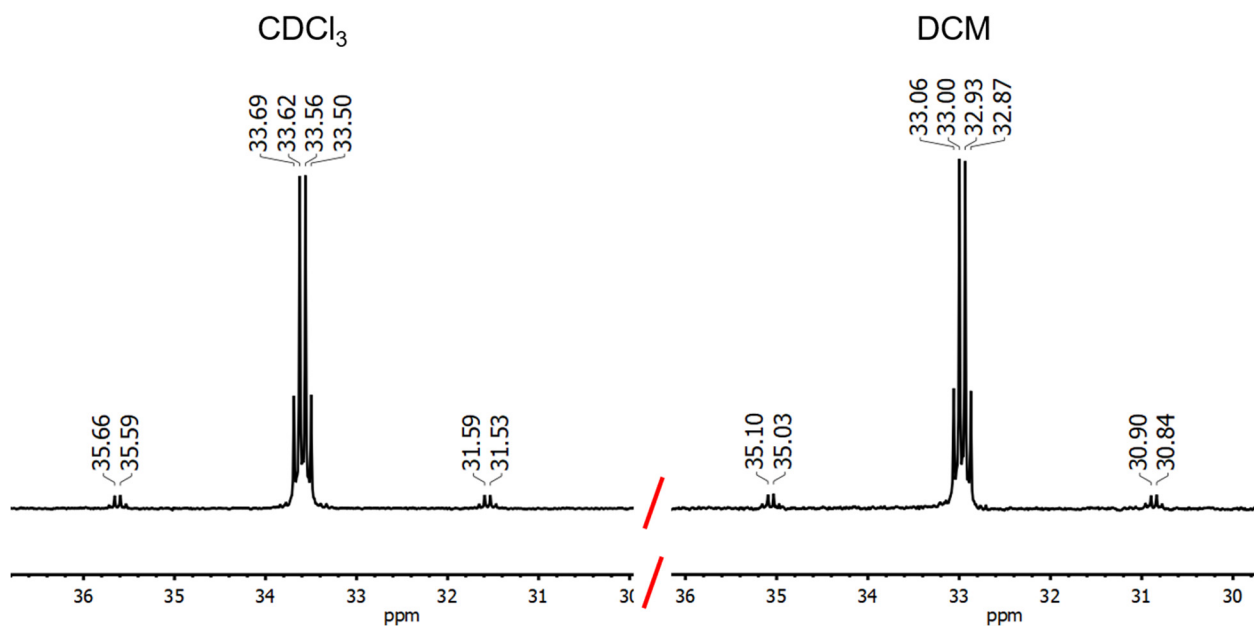


Figure S28. $^{31}\text{P}\{^1\text{H}\}$ NMR spectra of $[\text{PPh}_4][\text{1}^{\text{Se}}]$ in CDCl_3 (left) and CD_2Cl_2 (right) showing the P-Se phosphorus resonance.

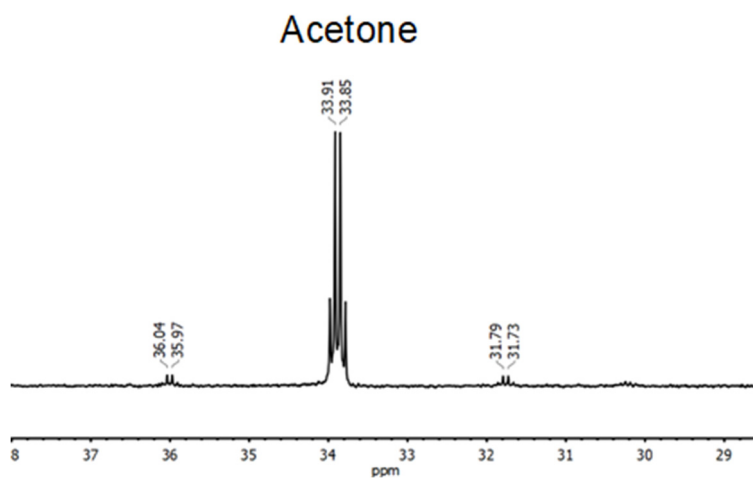


Figure S29. $^{31}\text{P}\{^1\text{H}\}$ NMR spectrum of $[\text{PPh}_4][\text{1}^{\text{Se}}]$ in $(\text{CD}_3)_2\text{CO}$ showing the P–Se phosphorus resonance.

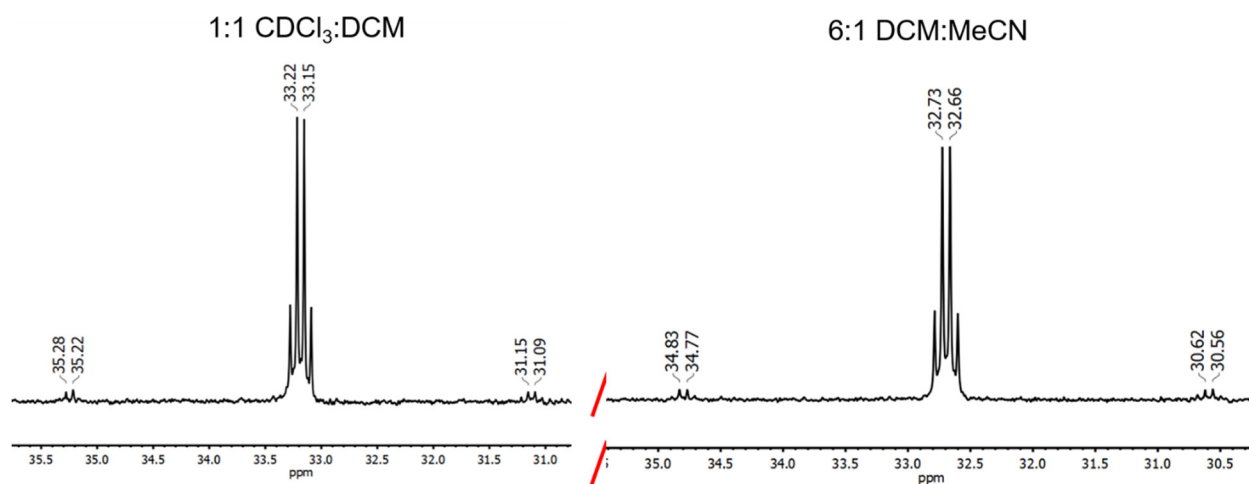


Figure S30. $^{31}\text{P}\{^1\text{H}\}$ NMR spectra of $[\text{PPh}_4][\text{1}^{\text{Se}}]$ in the indicated solvent mixtures showing the P–Se phosphorus resonance.

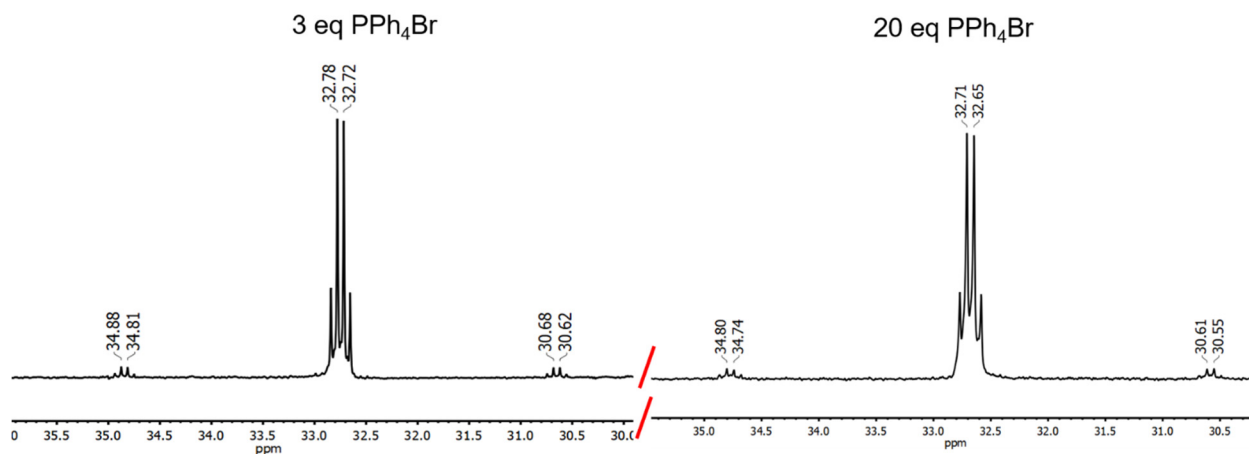


Figure S31. $^{31}\text{P}\{^1\text{H}\}$ NMR spectra of $[\text{PPh}_4][^1\text{Se}]$ in CH_2Cl_2 with addition of different equivalents of PPh_4Br . While the changing electrolyte concentration could influence the solvent dielectric, and hence the coupling constant, literature examples with tetra-alkyl ammonium salts suggest that very little change is expected for changing electrolyte concentration over this concentration range (~ 1 M).²²

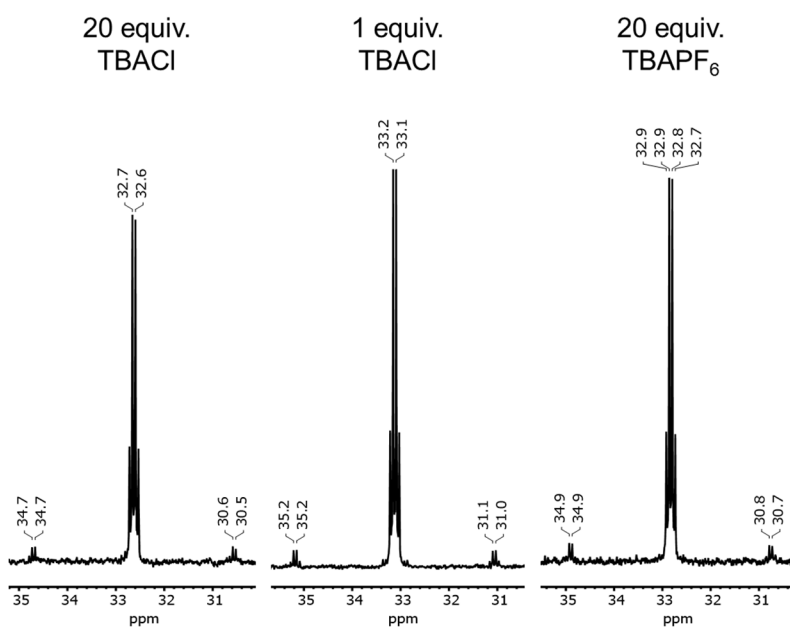


Figure S32. $^{31}\text{P}\{^1\text{H}\}$ NMR spectra of $[\text{PPh}_4][^1\text{Se}]$ in CDCl_3 with addition of tetrabutylammonium (TBA) salts.

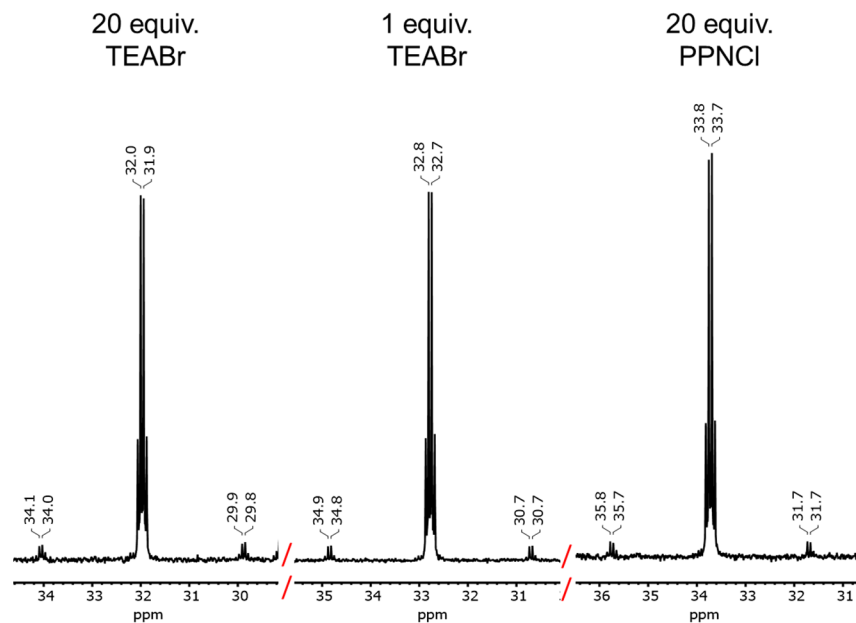


Figure S33. $^{31}\text{P}\{^1\text{H}\}$ NMR spectra of $[\text{PPh}_4][^1\text{Se}]$ in CDCl_3 with addition of tetraethylammonium (TEA) and bis(triphenylphosphine)iminium (PPN) salts.

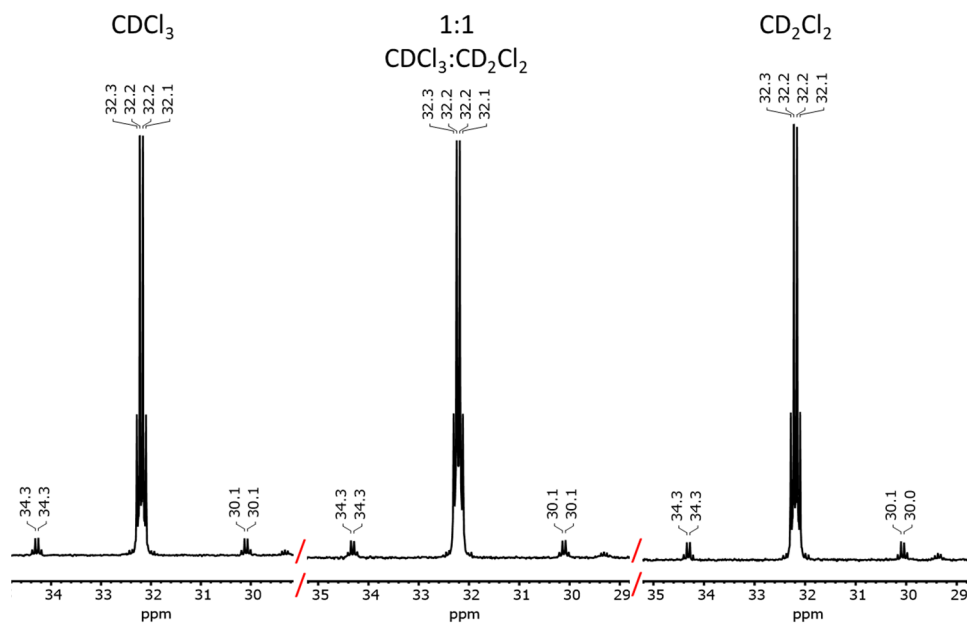


Figure S34. $^{31}\text{P}\{^1\text{H}\}$ NMR spectrum of $[\text{TEA}][^1\text{Se}]$ in the indicated solvents showing the P-Se phosphorus resonance.

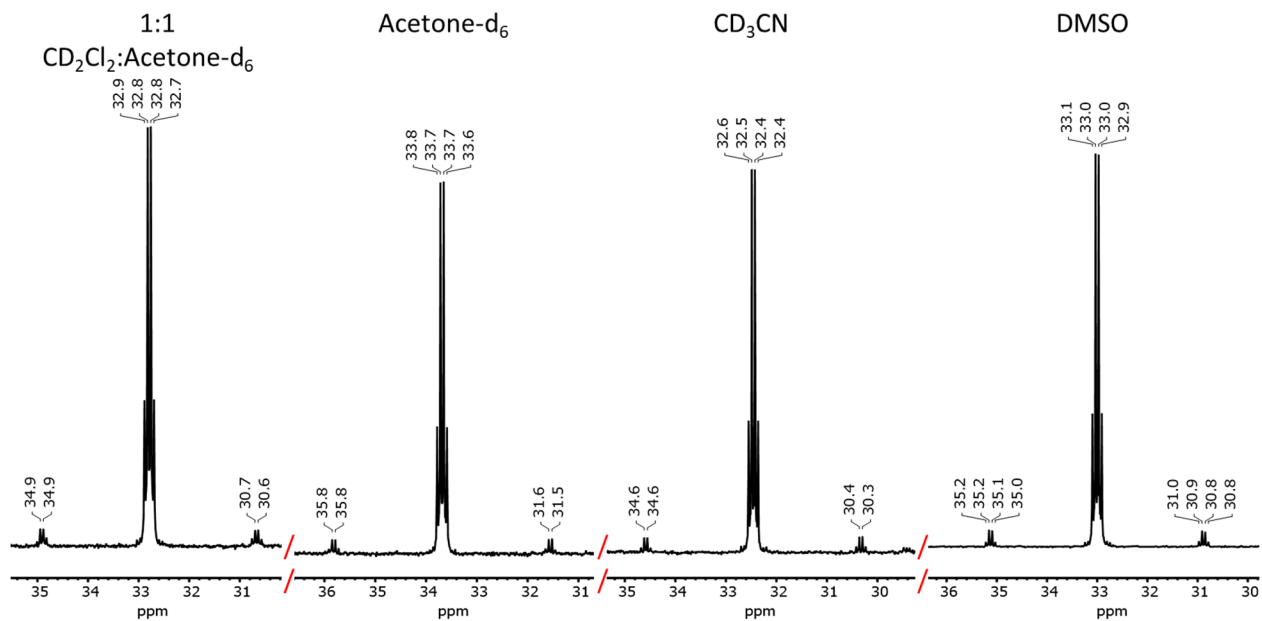


Figure S35. $^{31}\text{P}\{^1\text{H}\}$ NMR spectrum of $[\text{TEA}][\text{1}^{\text{Se}}]$ in the indicated solvents.

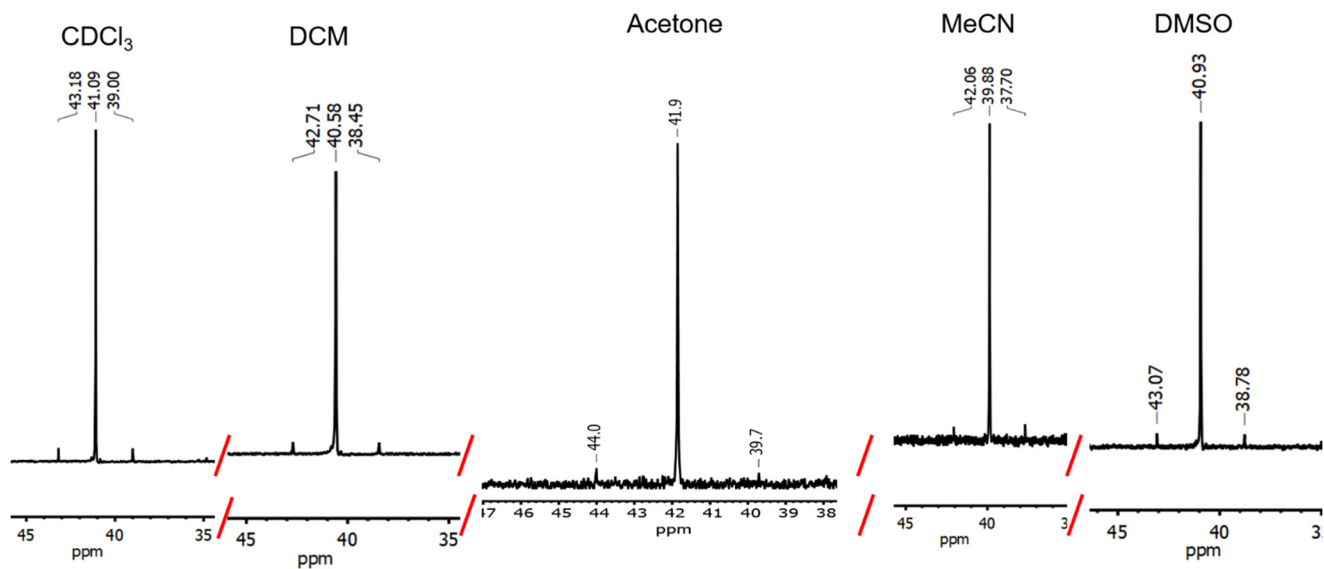


Figure S36. $^{31}\text{P}\{^1\text{H}\}$ NMR spectra of $[\text{PPh}_4][\text{3}^{\text{Se}}]$ in different solvents.

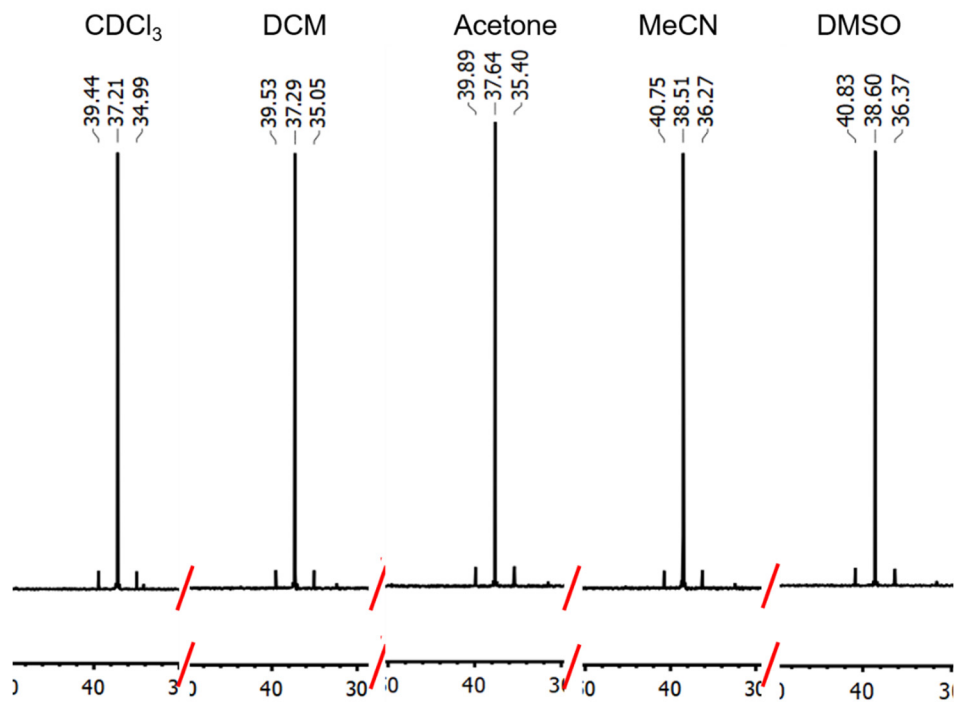


Figure S37. $^{31}\text{P}\{^1\text{H}\}$ NMR spectra of SePPh₂Et in the indicated solvents.

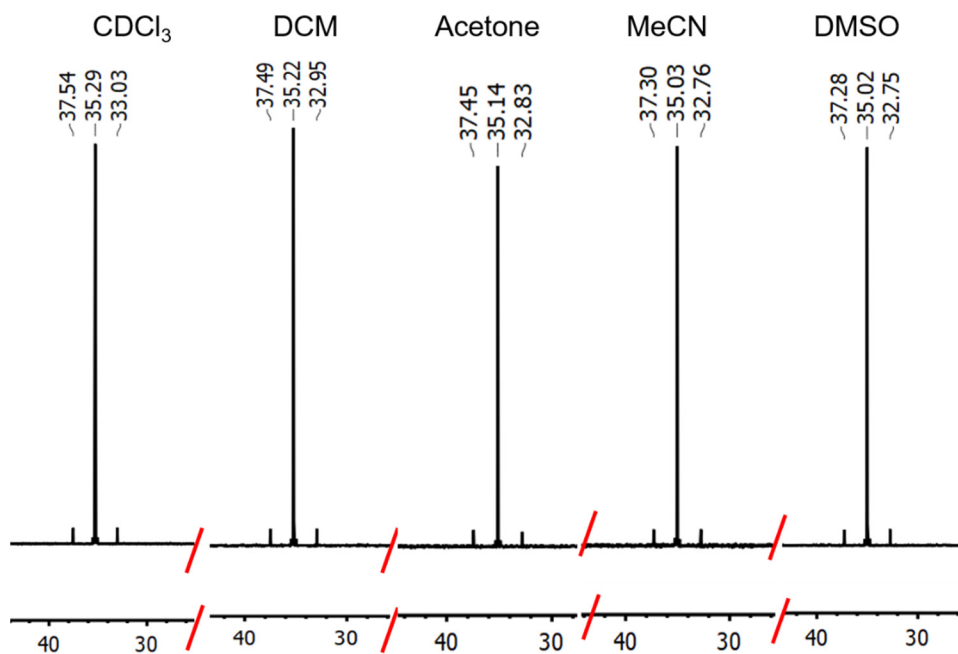


Figure S38. $^{31}\text{P}\{^1\text{H}\}$ NMR spectra of SePPh₃ in the indicated solvents.

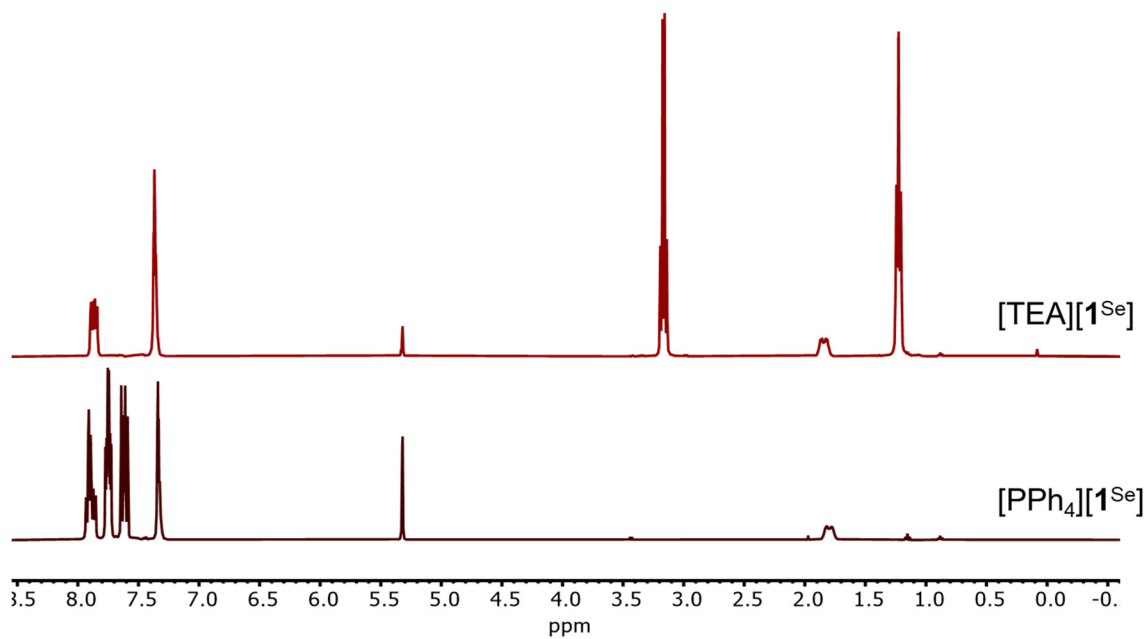


Figure S39. ^1H NMR spectra of $[\text{TEA}][\mathbf{1}^{\text{Se}}]$ and $[\text{PPh}_4][\mathbf{1}^{\text{Se}}]$ in CD_2Cl_2 .

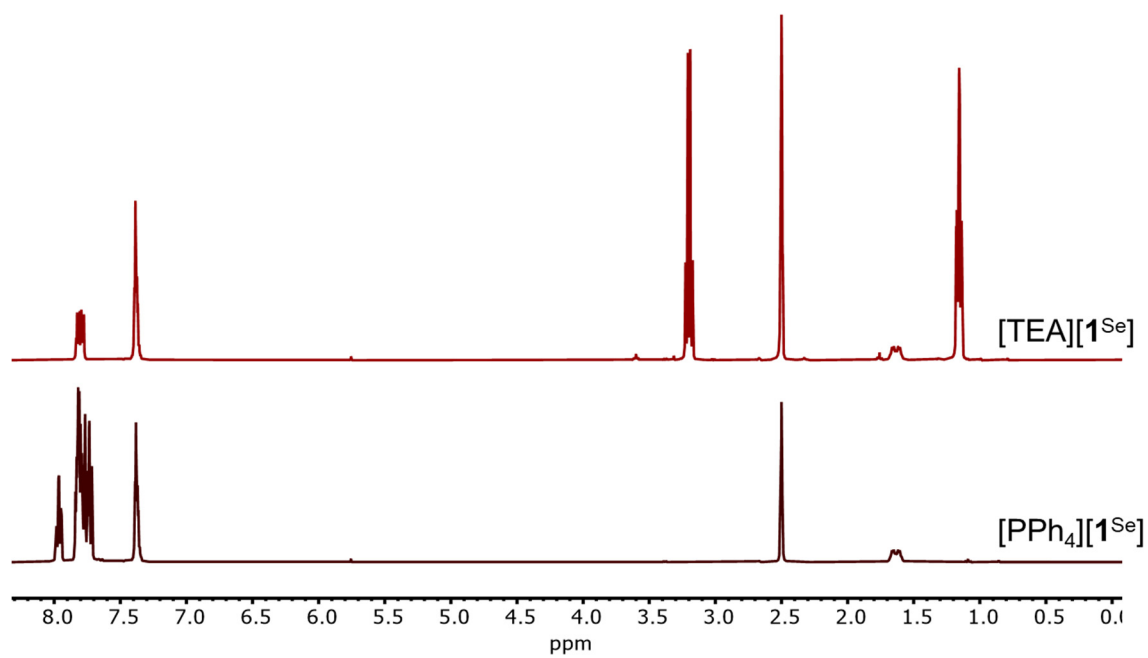


Figure S40. ^1H NMR spectra of $[\text{TEA}][\mathbf{1}^{\text{Se}}]$ and $[\text{PPh}_4][\mathbf{1}^{\text{Se}}]$ in $\text{DMSO-}d_6$.

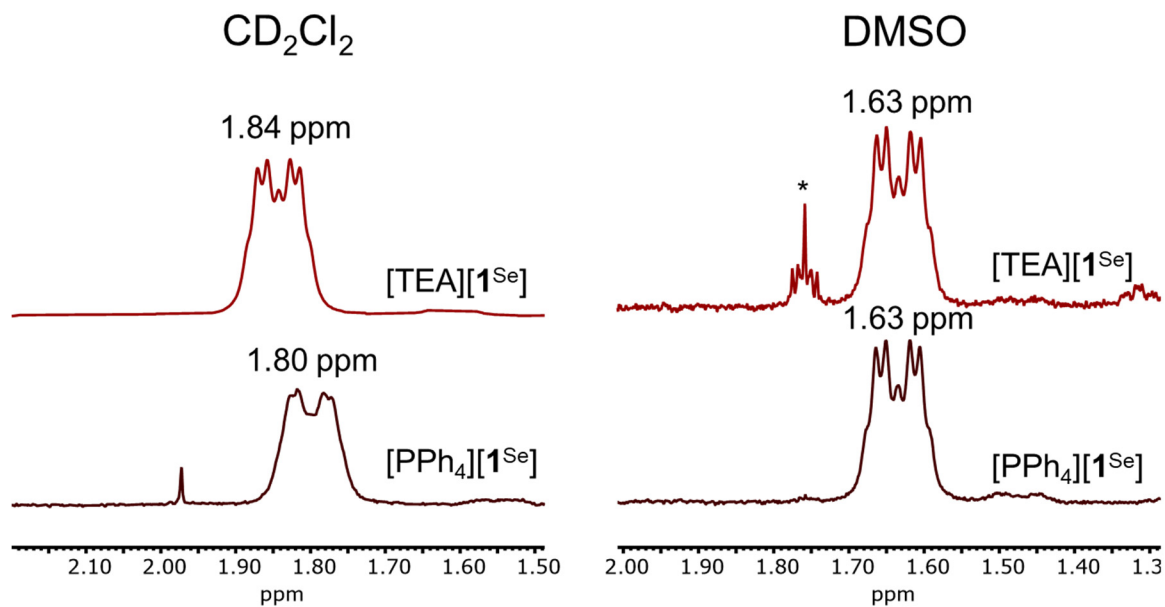


Figure S41. ^1H NMR spectra showing methylene resonance of $[\text{TEA}][\mathbf{1}^{\text{Se}}]$ and $[\text{PPh}_4][\mathbf{1}^{\text{Se}}]$ in CD_2Cl_2 and $\text{DMSO-}d_6$. The * indicates a small THF impurity.

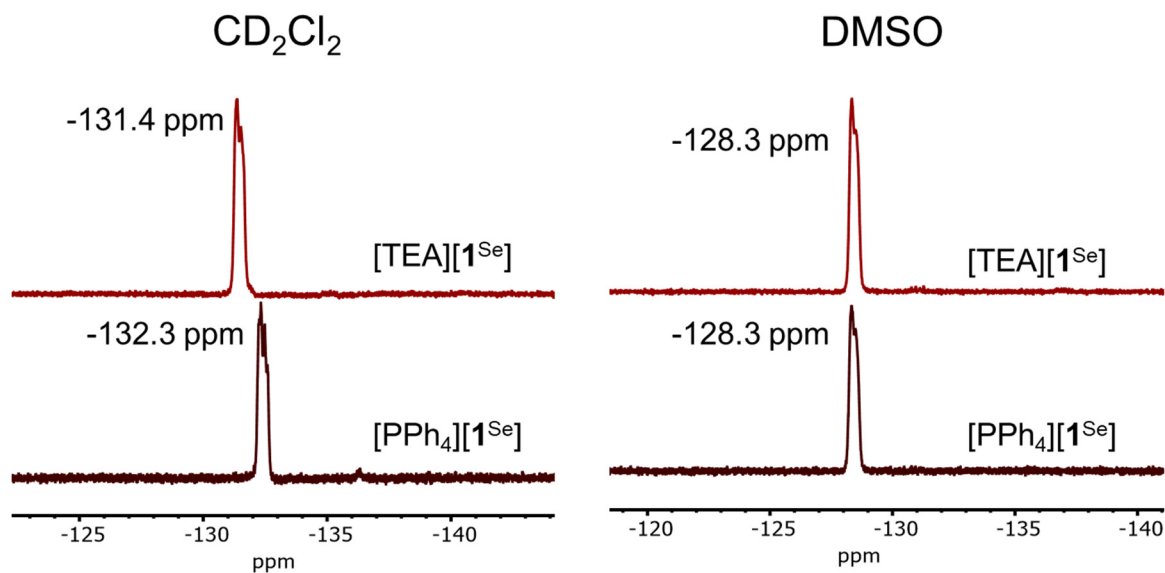


Figure S42. ^{19}F NMR spectra showing the BF_3 resonance of $[\text{TEA}][\mathbf{1}^{\text{Se}}]$ and $[\text{PPh}_4][\mathbf{1}^{\text{Se}}]$ in CD_2Cl_2 and $\text{DMSO-}d_6$.

NMR spectra of the reaction kinetics of C₆F₆ oxidative addition

K1 with Ni(COD)₂

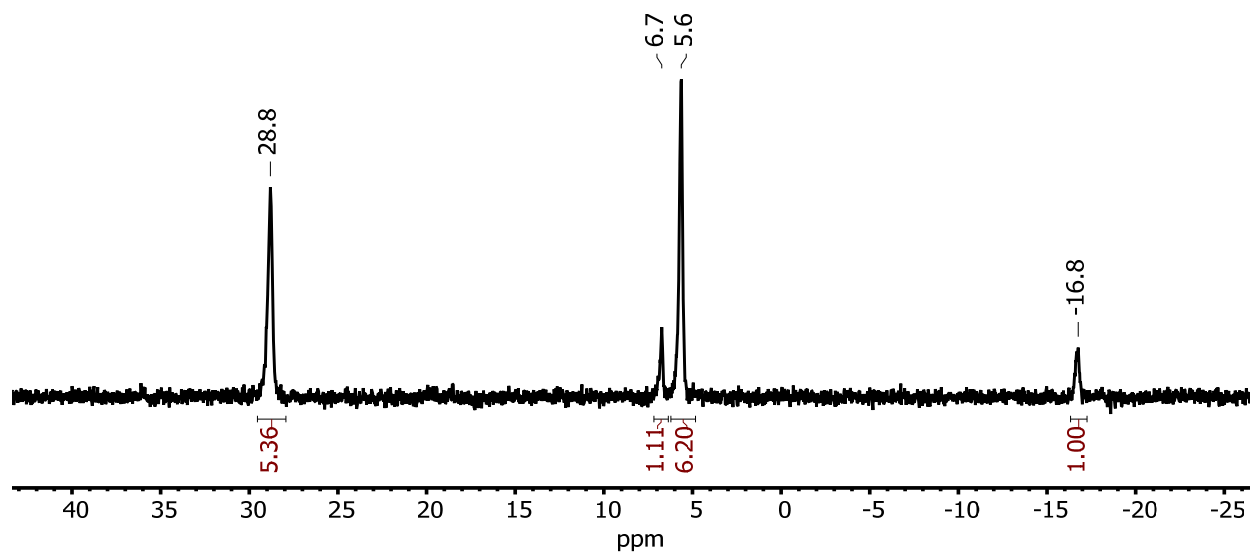


Figure S43. ³¹P{¹H} NMR spectrum of the reaction of K1 and Ni(COD)₂ in THF.

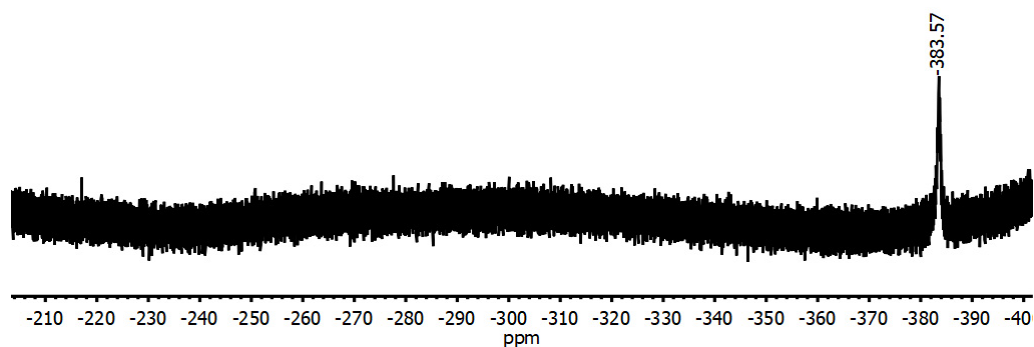


Figure S44. ¹⁹F{¹H} NMR spectrum of the reaction of K1, Ni(COD)₂, and C₆F₆ after 1 hr at RT. This upfield region shows the characteristic Ni–F peak.

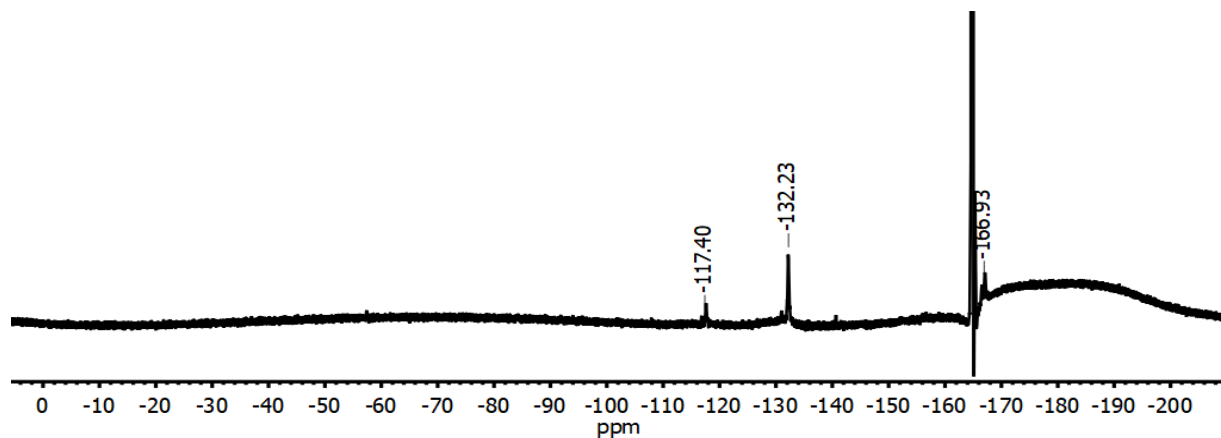


Figure S45. $^{19}\text{F}\{^1\text{H}\}$ NMR spectrum of the reaction of K1, $\text{Ni}(\text{COD})_2$, and C_6F_6 after 1 hr at RT. The broad peak centered around -180 ppm is Teflon within the NMR probe. The peak at -164.6 ppm that is cut off is excess C_6F_6 .

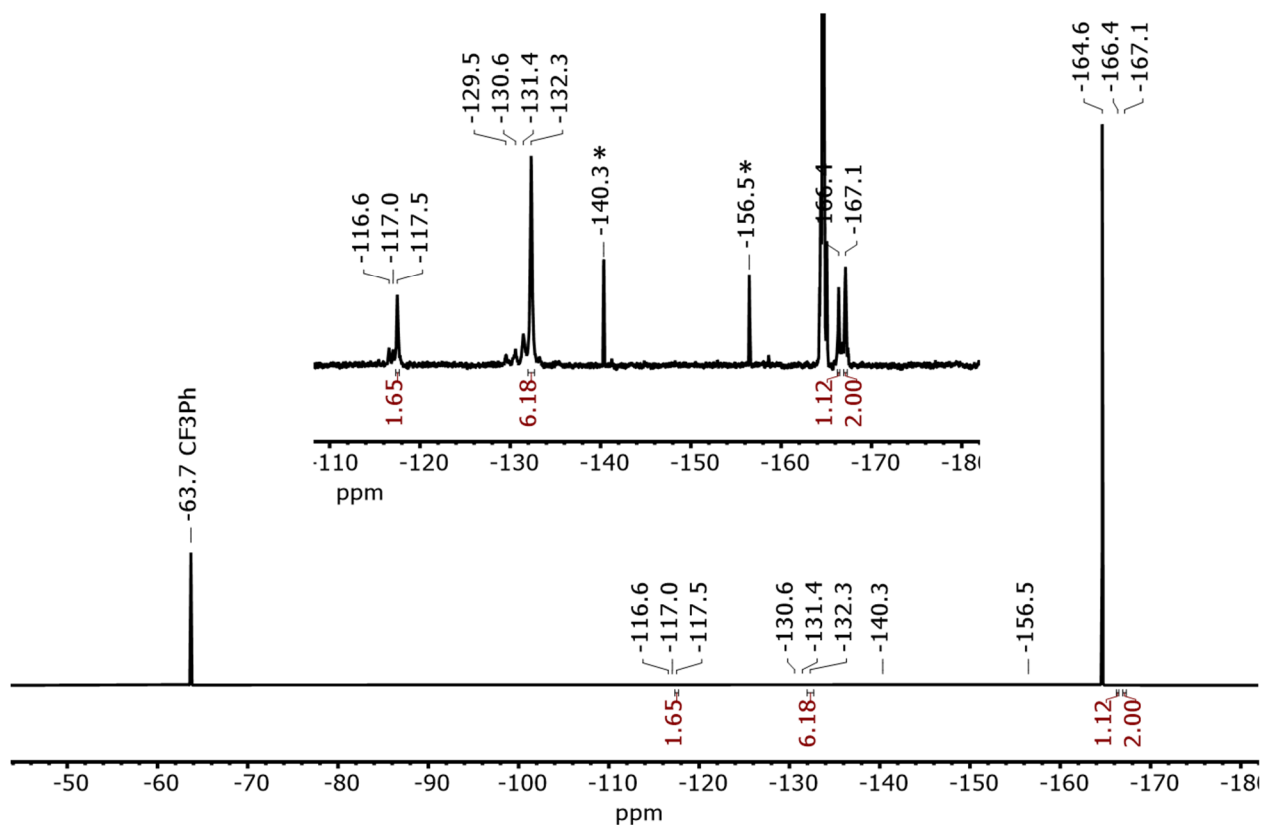


Figure S46. ^{19}F NMR spectrum of the reaction between K1 (24 mM), $\text{Ni}(\text{COD})_2$ (12 mM) and C_6F_6 (120 mM) in THF with CF_3Ph (60 mM) and PPh_3O (12 mM) as internal integral standards after 20 h at RT. Oxidative addition product peaks assigned: -117.5 (2F, F_{ortho}), -132.3 (6F, BF_3), -166.4 (1F, F_{para}) -167.1 (2F, F_{meta}) based on comparison to reference 15. Peaks at -140.3 and -156.5 ppm are not always observed and are assigned as unknown impurities. The peak at -164.6 ppm is unreacted C_6F_6 .

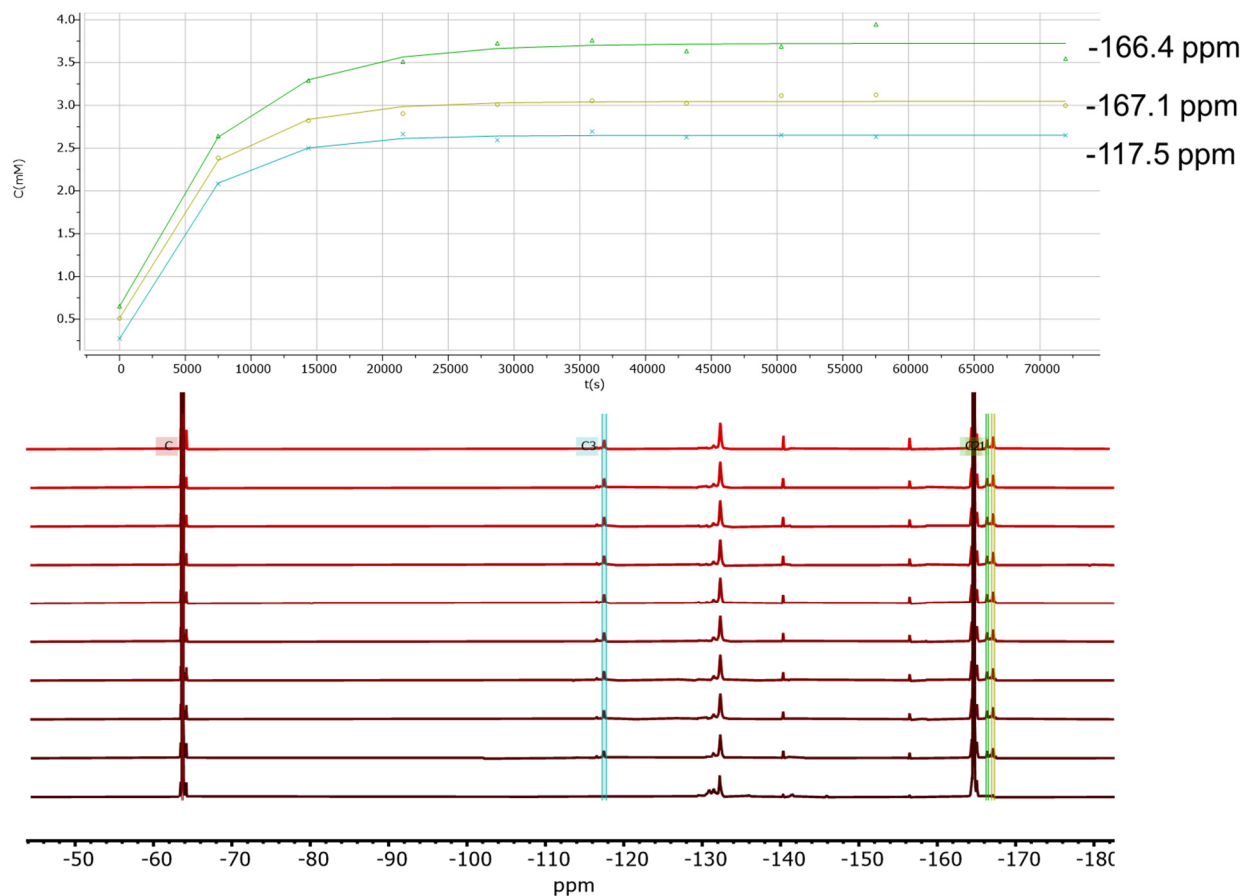


Figure S47. Time course monitoring of the ¹⁹F NMR spectrum of the reaction between K1 (24 mM), Ni(COD)₂ (12 mM) and C₆F₆ (120 mM) in THF with CF₃Ph (60 mM) and OPPh₃ (12 mM) as internal integral standards over the course of 20 h at RT. The observed rate of formation and % completion for the oxidative addition product for the following peaks are: -166.4 ppm (1.4E-4 s⁻¹, 3.5 mM, 30%), -167.1 ppm (1.7E-4 s⁻¹, 3.0 mM, 25%), -117.5 ppm (1.9E-4 s⁻¹, 2.6 mM, 22%). The average observed rate of formation and % yield are 1.7(3)E-4 s⁻¹ and 25(4)%.

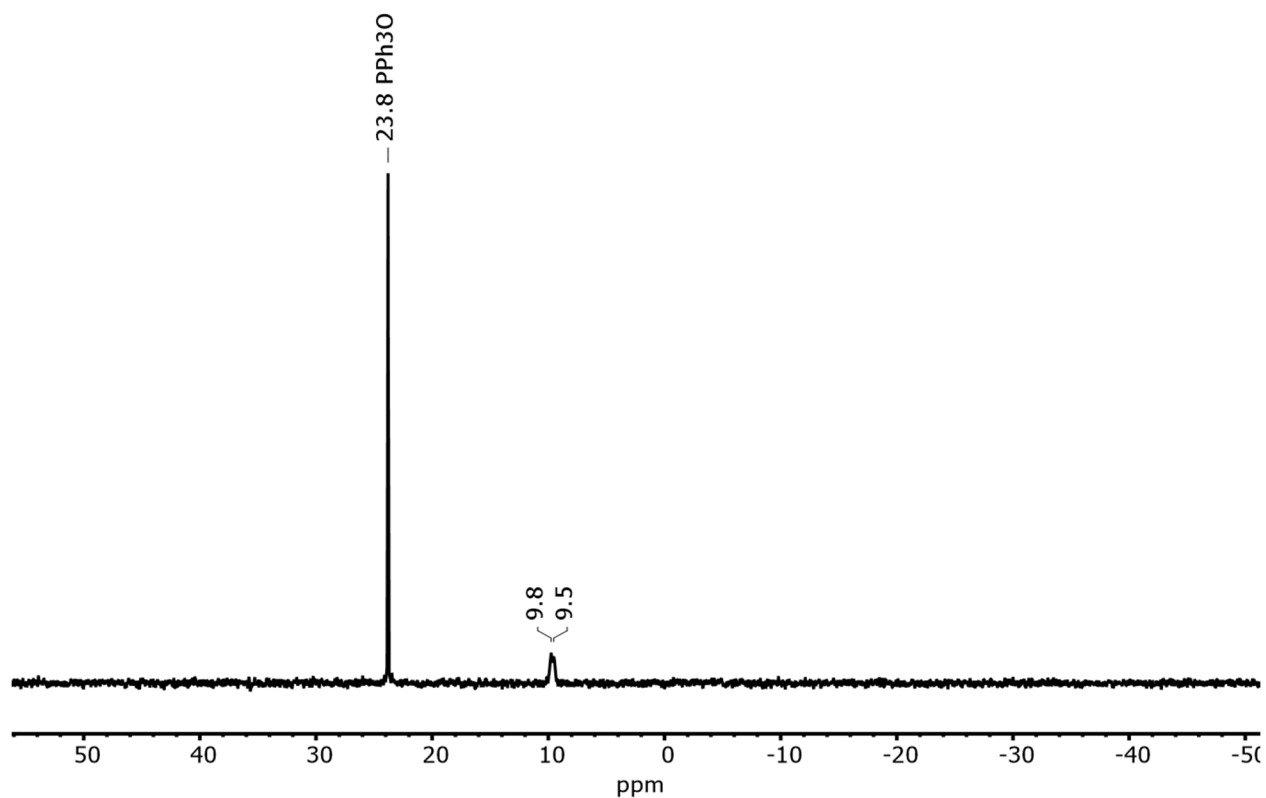


Figure S48. $^{31}\text{P}\{^1\text{H}\}$ NMR spectrum of the reaction between **K1** (24 mM), $\text{Ni}(\text{COD})_2$ (12 mM) and C_6F_6 (120 mM) in THF with CF_3Ph (60 mM) and OPPh_3 (12 mM) as internal integral standards after 16 h at RT. The phosphorus resonance for the oxidative addition product is assigned as the doublet at 9.6 ppm on the basis of coupling to ^{19}F on the Ni-F.

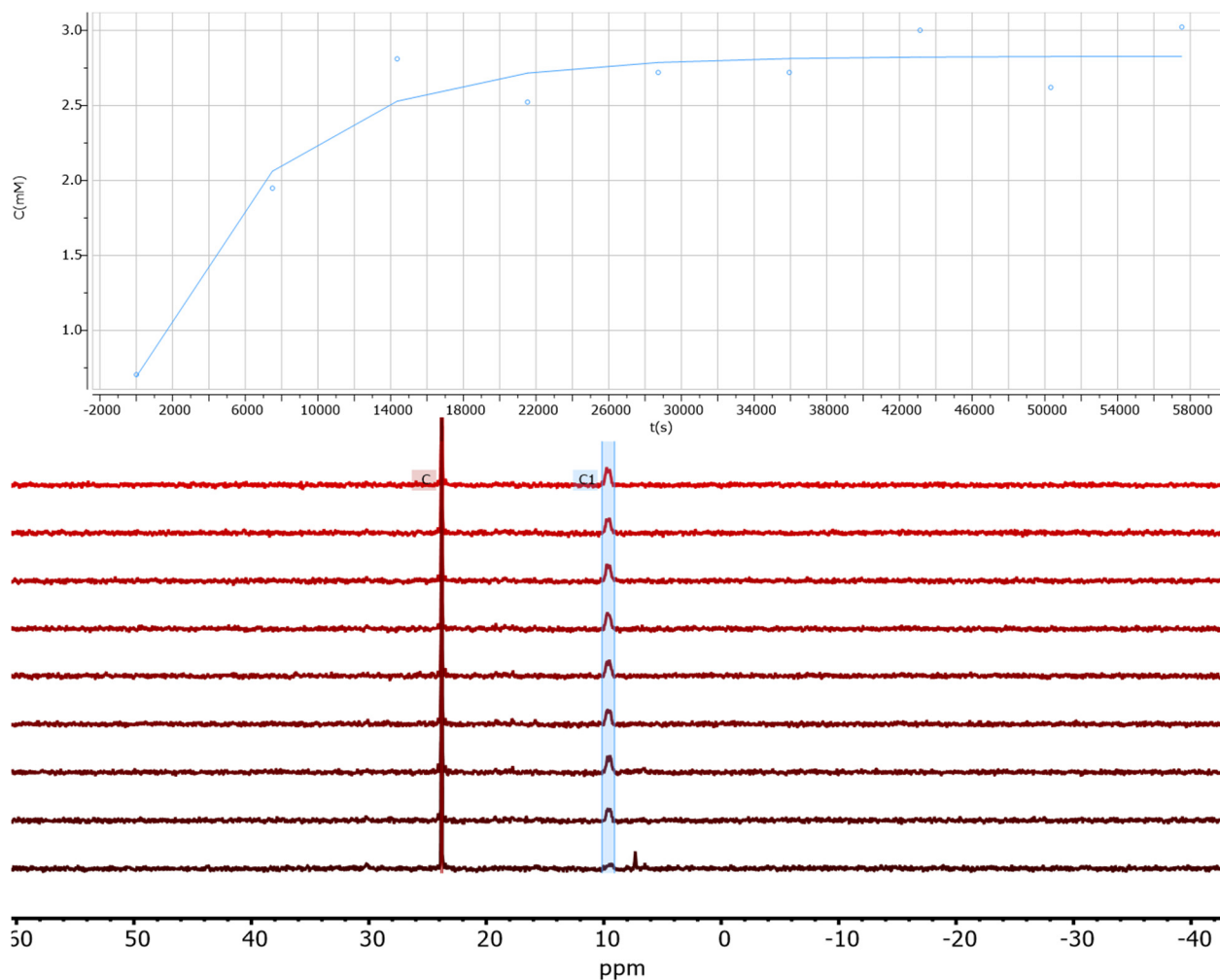


Figure S49. Time course monitoring of the $^{31}\text{P}\{^1\text{H}\}$ NMR spectrum of the reaction between K1 (24 mM), $\text{Ni}(\text{COD})_2$ (12 mM) and C_6F_6 (120 mM) in THF with CF_3Ph (60 mM) and OPPh_3 (12 mM) as internal integral standards over the course of 16 h at RT. The observed rate of formation and % completion for the oxidative addition peak at 9.6 ppm is $1.4\text{E}-4 \text{ s}^{-1}$ and 3.0 mM (25%)

PCy₃ with Ni(COD)₂

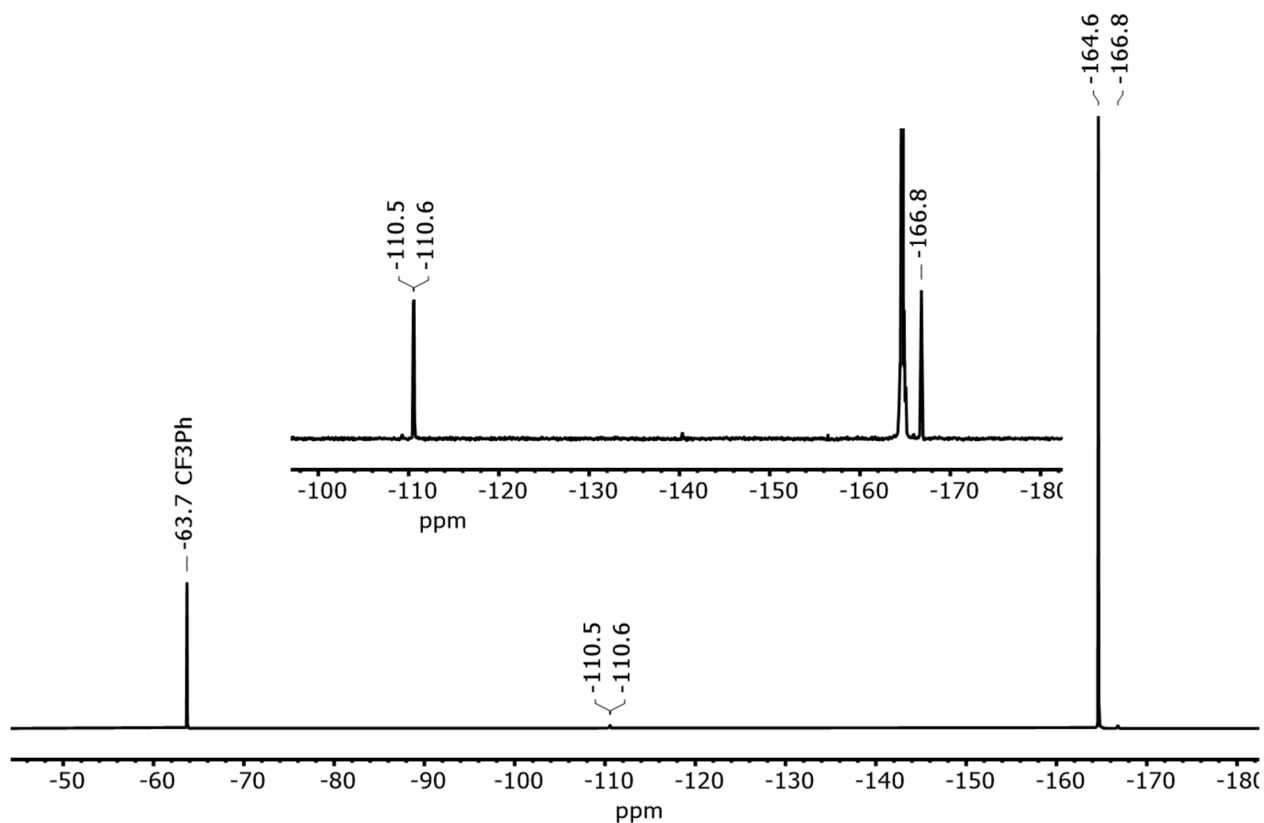


Figure S50. ¹⁹F NMR spectrum of the reaction between PCy₃ (24 mM), Ni(COD)₂ (12 mM) and C₆F₆ (120 mM) in THF with CF₃Ph (60 mM) and OPPh₃ (12 mM) as internal integral standards after 53 h at RT. Oxidative addition product peaks assigned: -110.6 (2F, F_{ortho}), -166.8 (2F, F_{meta}) based on comparison to reference 15. The F_{para} peak is hidden under the C₆F₆ peak, but can be observed in the ¹⁹F {¹H} NMR spectrum. The peak at -164.6 ppm is the unreacted C₆F₆.

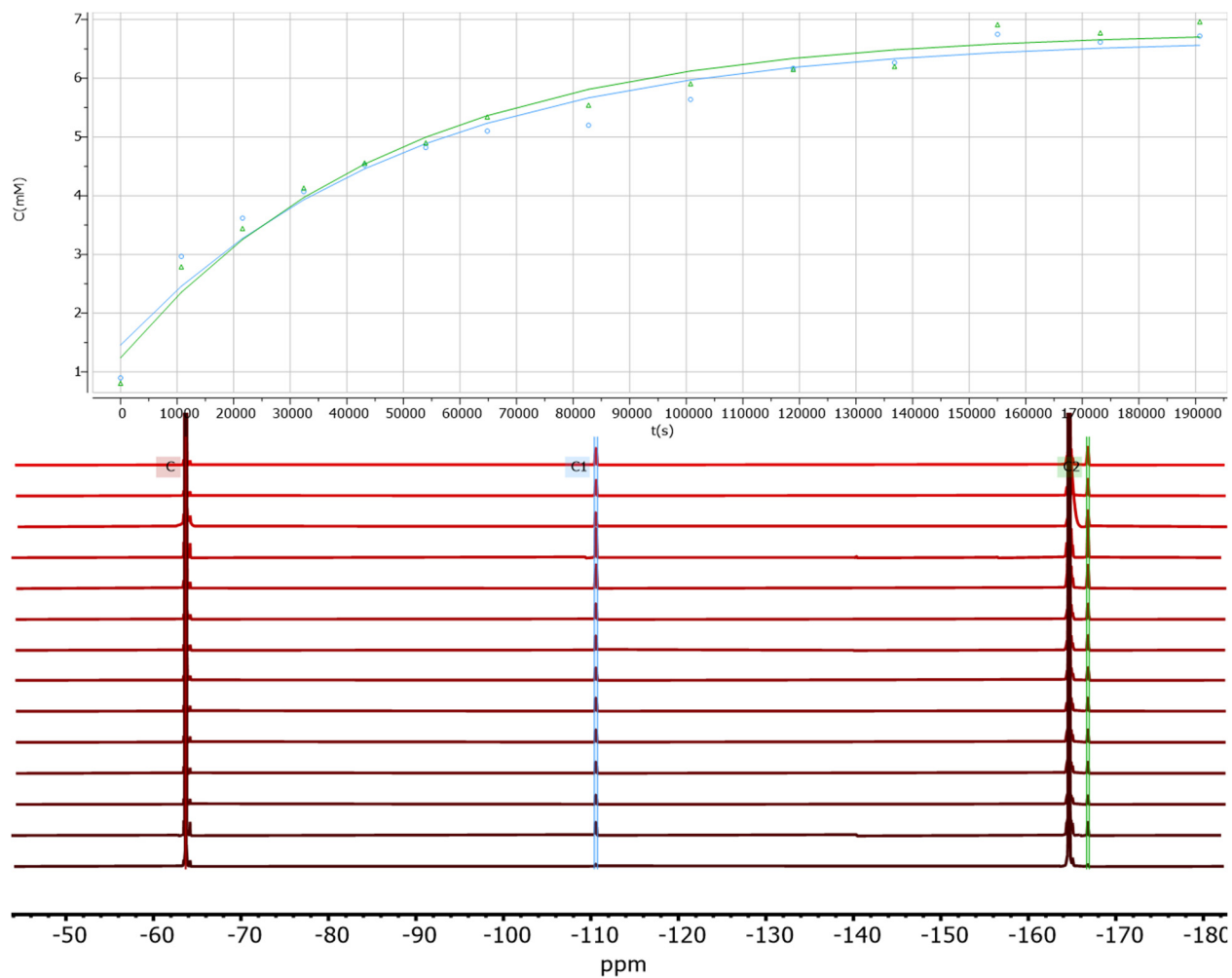


Figure S51. Time course monitoring of the ^{19}F NMR spectrum of the reaction between PCy_3 (24 mM), $\text{Ni}(\text{COD})_2$ (12 mM) and C_6F_6 (120 mM) in THF with CF_3Ph (60 mM) and OPPh_3 (12 mM) as internal integral standards over the course of 52 h at RT. The observed rate of formation and % completion for the oxidative addition product for the following peaks are: -110.6 ppm ($2.0\text{E}-5$ s^{-1} , 6.7 mM, 56%), -166.8 ppm ($2.1\text{E}-5$ s^{-1} , 7.0 mM, 58%). The average observed rate of formation and % yield are $2.10(7)\text{E}-5$ s^{-1} and 57(2)%.

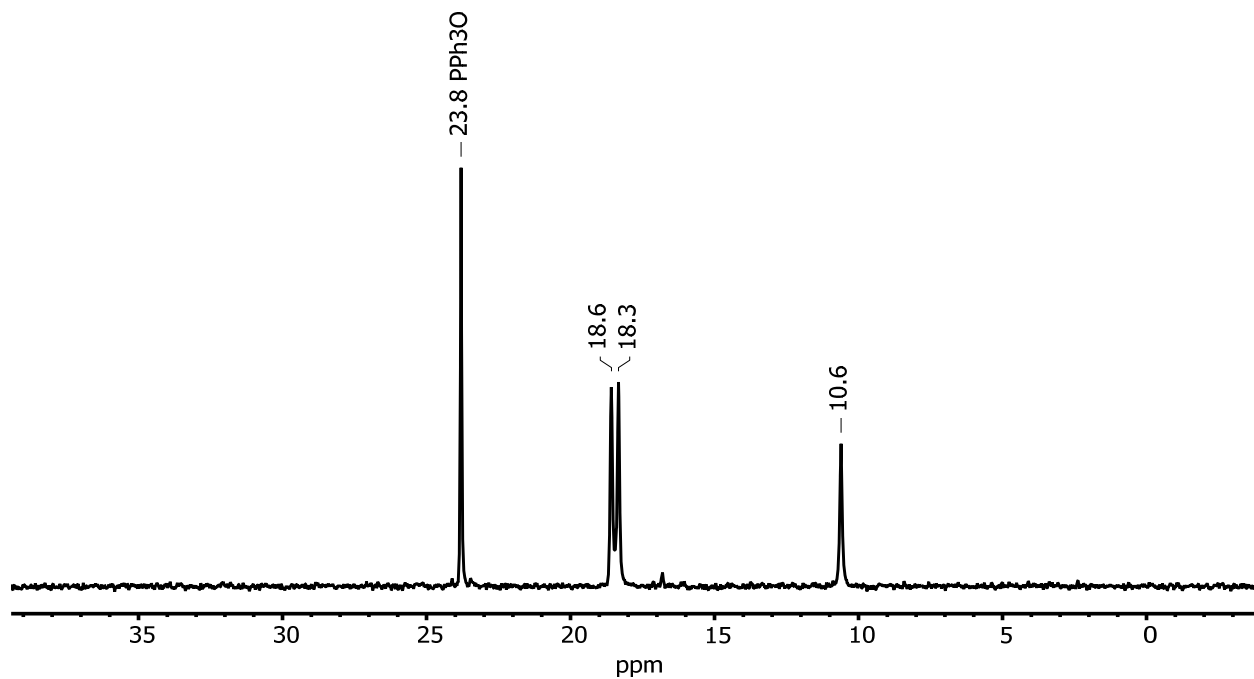


Figure S52. $^{31}\text{P}\{^1\text{H}\}$ NMR spectrum of the reaction between PCy_3 (24 mM), $\text{Ni}(\text{COD})_2$ (12 mM) and C_6F_6 (120 mM) in THF with CF_3Ph (60 mM) and OPPh_3 (12 mM) as internal integral standards after 53 h at RT. The phosphorus resonance for the oxidative addition product is assigned as the doublet at 18.5 ppm on the basis of coupling to ^{19}F in the Ni-F. The starting phosphine is assigned as the peak at 10.6 ppm.

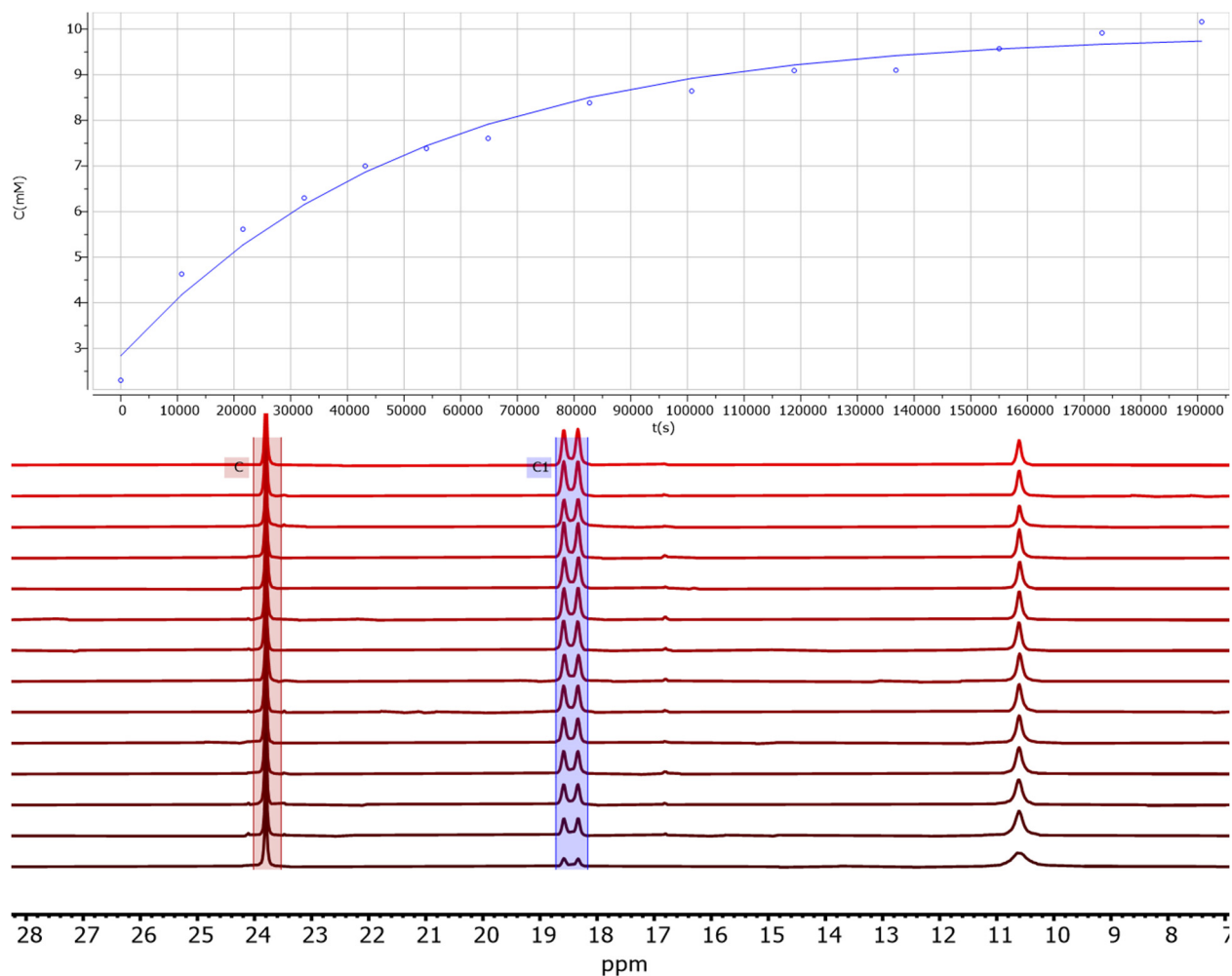


Figure S53. Time course monitoring of the $^{31}\text{P}\{^1\text{H}\}$ NMR spectrum of the reaction between PCy_3 (24 mM), $\text{Ni}(\text{COD})_2$ (12 mM) and C_6F_6 (120 mM) in THF with CF_3Ph (60 mM) and OPPh_3 (12 mM) as internal integral standards over the course of 53 h at RT. The observed rate of formation and % completion for the oxidative addition peak at 18.5 ppm is $2.0\text{E}-5 \text{ s}^{-1}$ and 10.0 mM (83%)

PEt₃ with Ni(COD)₂

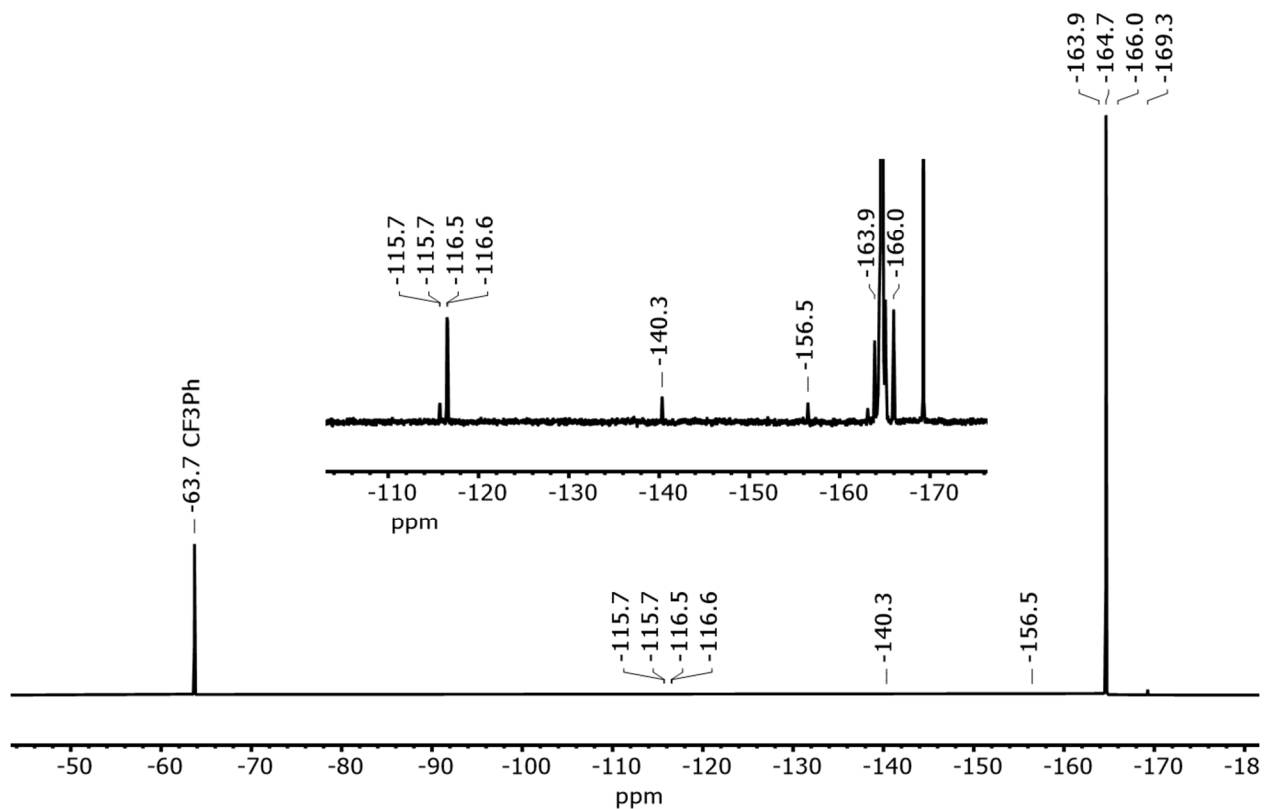


Figure S54. ¹⁹F NMR spectrum of the reaction between PEt₃ (24 mM), Ni(COD)₂ (12 mM) and C₆F₆ (120 mM) in THF with CF₃Ph (60 mM) and OPPh₃ (12 mM) as internal integral standards after 114 h at RT. Oxidative addition product peaks assigned: -116.6 (2F, F_{ortho}), -163.9 (1F, F_{para}), and -166.0 (2F, F_{meta}) based on comparison to reference 15. Peaks at -140.3 and -156.5, and -169.3 ppm are not always observed and are assigned as unknown impurities. The peak at -164.6 ppm is unreacted C₆F₆.

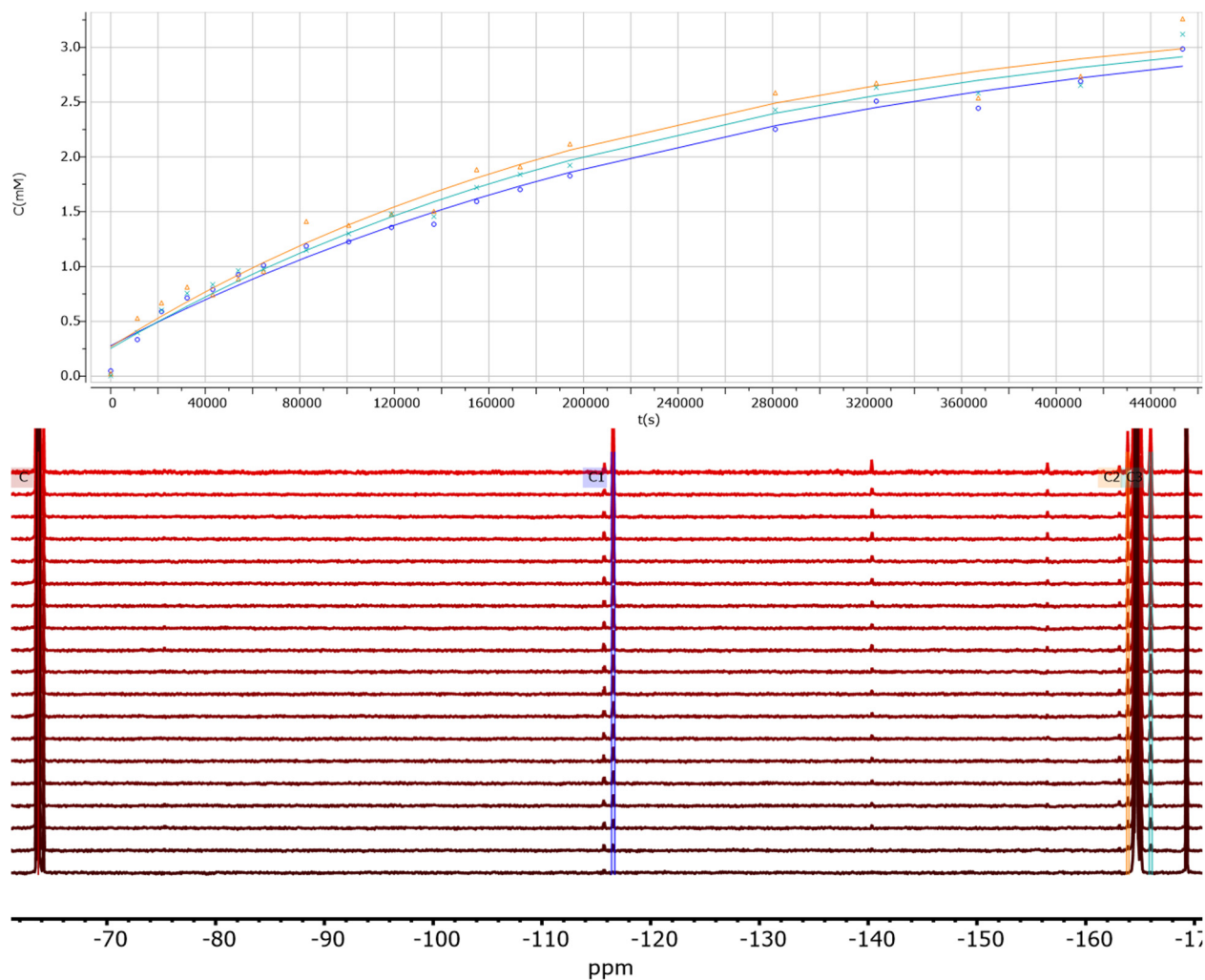


Figure S55. Time course monitoring of the ^{19}F NMR spectrum of the reaction between PEt_3 (24 mM), $\text{Ni}(\text{COD})_2$ (12 mM) and C_6F_6 (120 mM) in THF with CF_3Ph (60 mM) and OPPh_3 (12 mM) as internal integral standards over the course of 114 h at RT. The observed rate of formation and % completion for the oxidative addition product for the following peaks are: -116.6 ppm ($3.5\text{E}-6 \text{ s}^{-1}$, 2.7 mM, 23%), -163.9 ppm ($4.3\text{E}-6 \text{ s}^{-1}$, 2.7 mM, 23%), and 166.0 ($4.0\text{E}-6 \text{ s}^{-1}$, 2.7 mM, 23%). The average observed rate of formation and % yield are $4.0(4)\text{E}-6 \text{ s}^{-1}$ and 23%.

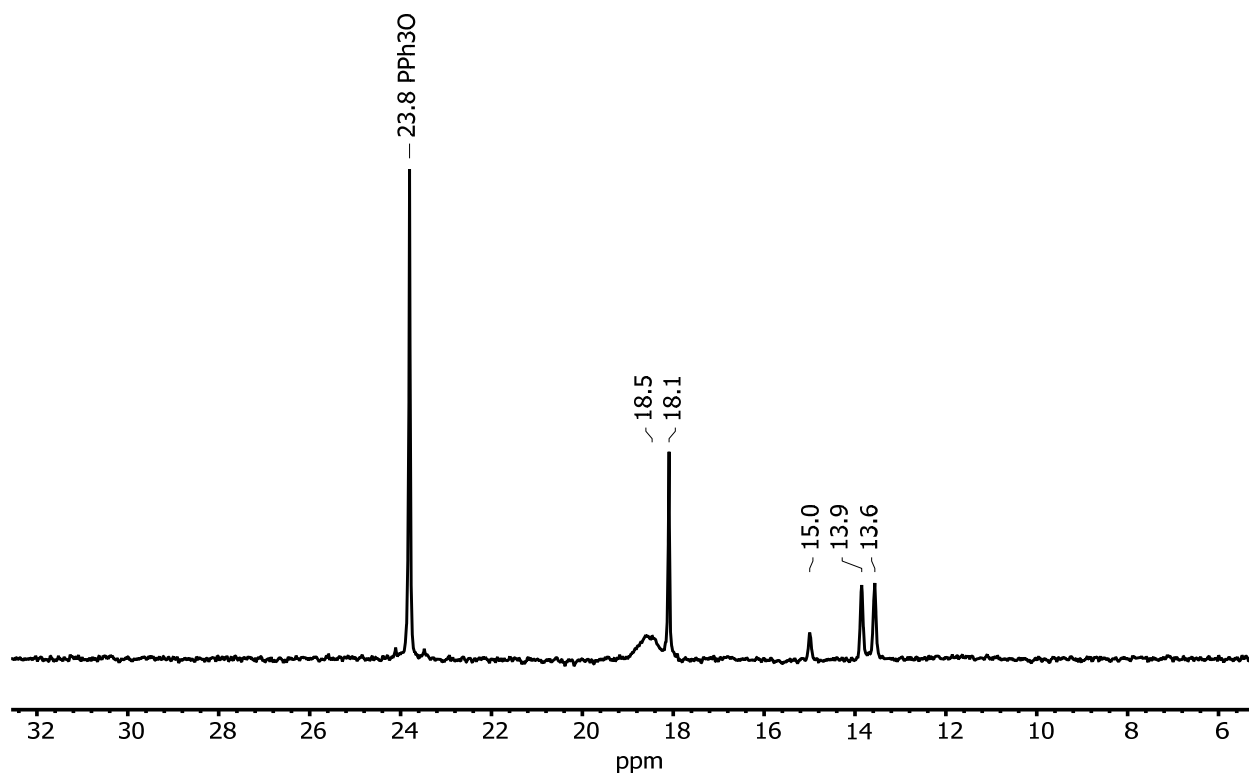


Figure S56. $^{31}\text{P}\{^1\text{H}\}$ NMR spectrum of the reaction between PEt_3 (24 mM), $\text{Ni}(\text{COD})_2$ (12 mM) and C_6F_6 (120 mM) in THF with CF_3Ph (60 mM) and OPPh_3 (12 mM) as internal integral standards after 114 h at RT. The phosphorus resonance for the oxidative addition product is assigned as the doublet at 13.8 ppm on the basis of coupling to ^{19}F in the Ni-F. The starting phosphine is assigned as the resonance at 18.1 ppm.

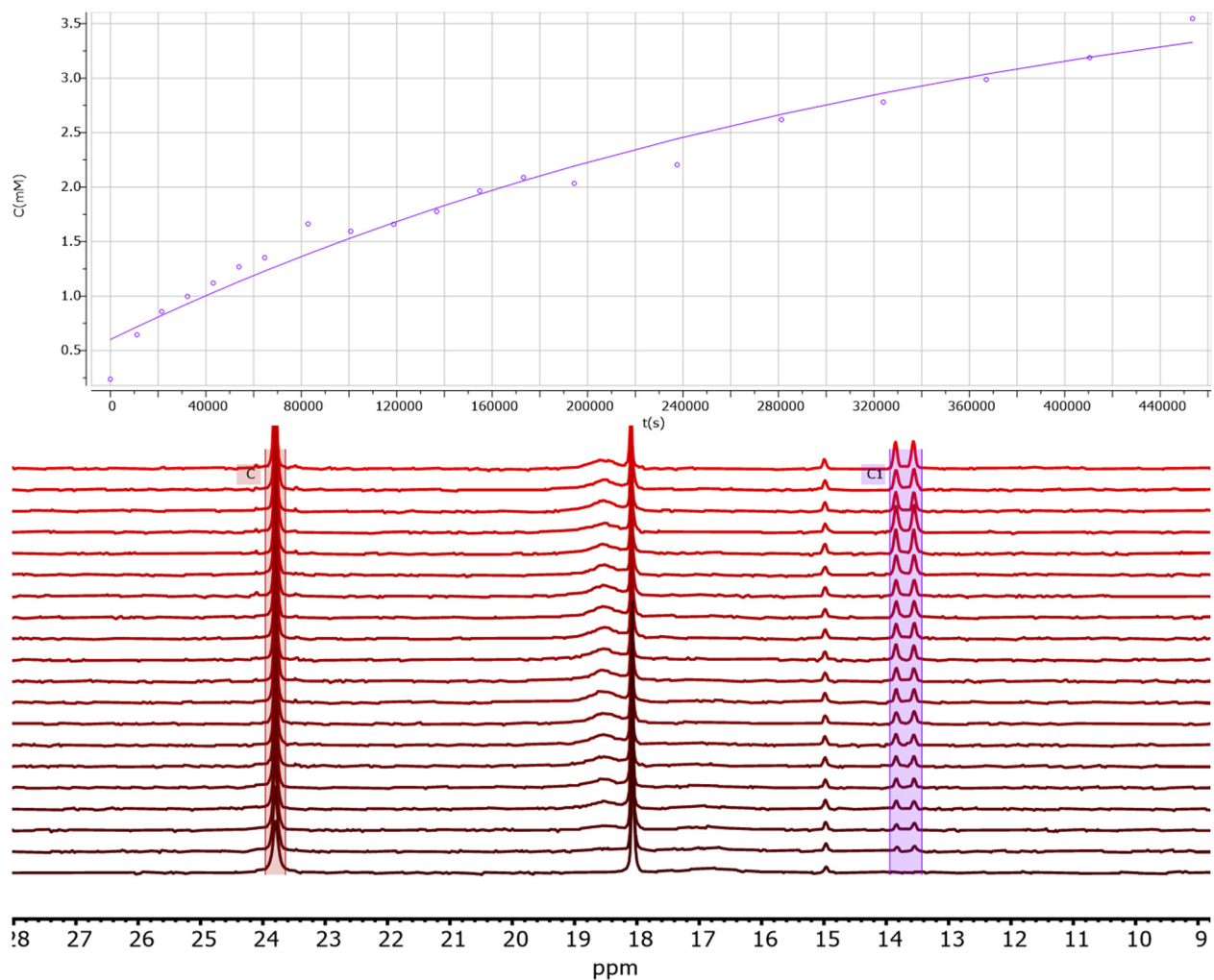
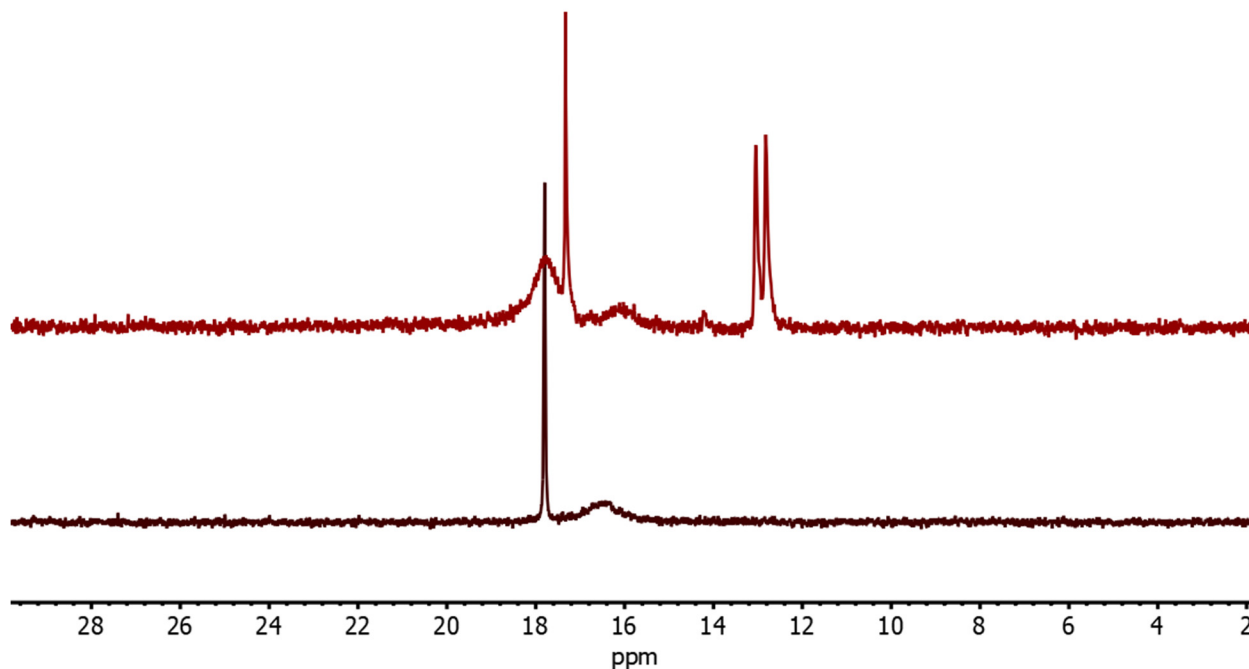


Figure S57. Time course monitoring of the $^{31}\text{P}\{^1\text{H}\}$ NMR spectrum of the reaction between PEt_3 (24 mM), $\text{Ni}(\text{COD})_2$ (12 mM) and C_6F_6 (120 mM) in THF with CF_3Ph (60 mM) and OPPh_3 (12 mM) as internal integral standards over the course of 114 h at RT. The observed rate of formation and % completion for the oxidative addition peak at 13.8 ppm is $2.8\text{E}-6 \text{ s}^{-1}$ and 3.2 mM (27%)

Table S1. Summary of observed rates from NMR monitoring experiments

Phosphine	Average k_{obs}	Average yield	k_{obs} from ^{19}F NMR	yields from ^{19}F NMR	k_{obs} from ^{31}P NMR	yield from ^{31}P NMR
K1	$1.6(2)\text{E-}4 \text{ s}^{-1}$	25(3)% at 20h	$1.4\text{E-}4 \text{ s}^{-1}$ $1.7\text{E-}4 \text{ s}^{-1}$ $1.9\text{E-}4 \text{ s}^{-1}$	30% 25% 22%	$1.4\text{E-}4 \text{ s}^{-1}$	25%
PCy ₃	$2.0(1)\text{E-}5 \text{ s}^{-1}$	66(15)% at 53 h	$2.0\text{E-}5 \text{ s}^{-1}$ $2.1\text{E-}5 \text{ s}^{-1}$	56% 58%	$2.0\text{E-}5 \text{ s}^{-1}$	83%
PEt ₃	$3.7(7)\text{E-}6 \text{ s}^{-1}$	24(2)% at 114h	$3.5\text{E-}6 \text{ s}^{-1}$ $4.3\text{E-}6 \text{ s}^{-1}$ $4.0\text{E-}6 \text{ s}^{-1}$	23% 23% 23%	$2.8\text{E-}6 \text{ s}^{-1}$	27%

**Figure S58.** $^{31}\text{P}\{^1\text{H}\}$ NMR spectrum of the reaction of PEt₃, Ni(COD)₂, and C₆F₆ in THF after 1 hour (bottom, black) and 1 week (top, red) at RT. The features around 17 ppm are unreacted Ni(COD)₂ PEt₃ adducts and the doublet at 13 ppm is the oxidative addition product with $^1J_{\text{P-F}}$ coupling.

NMR spectra of the catalytic C-F borylation reactions

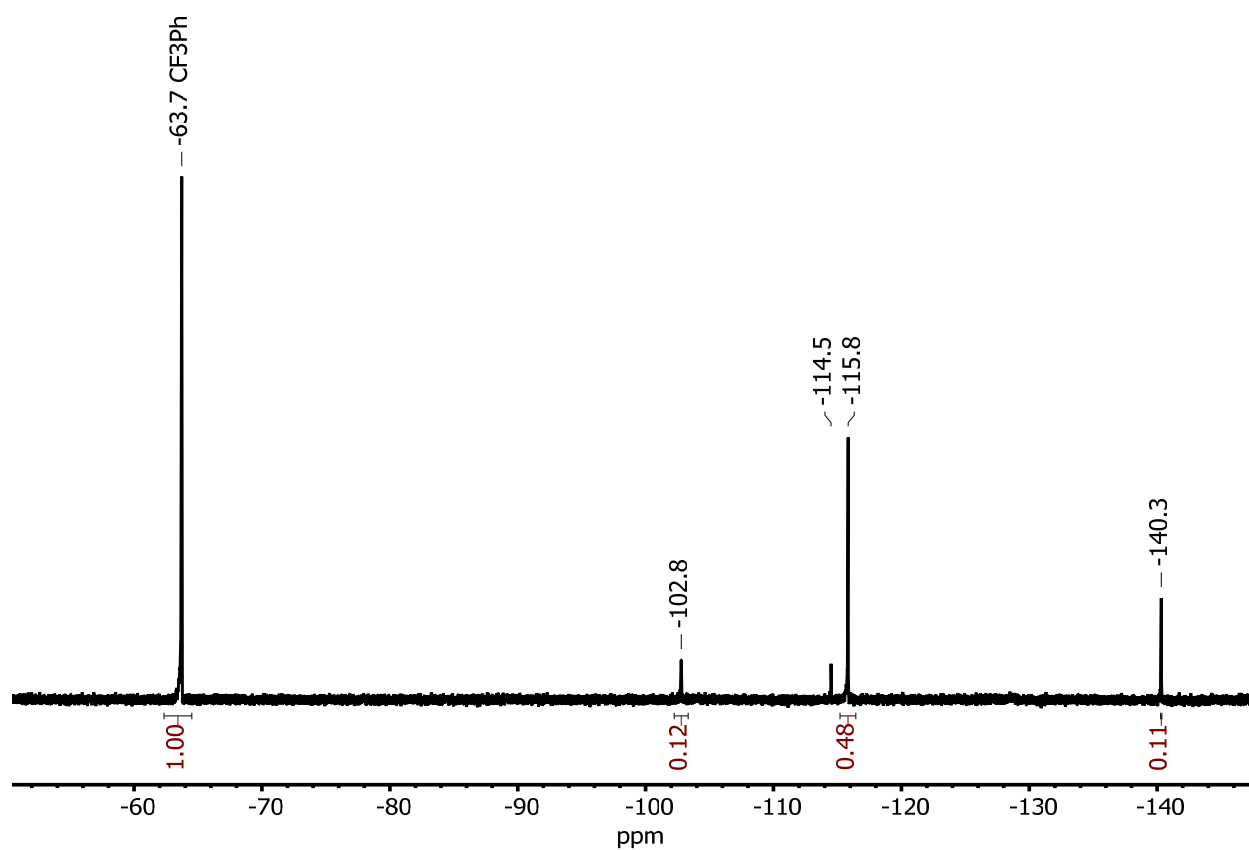


Figure S59. $^{19}\text{F}\{^1\text{H}\}$ NMR spectrum of the reaction mixture from one of the catalytic borylation reactions of 1,2-difluorobenzene following standard catalytic conditions detailed in methods section. The peaks at -102.8, -115.8, and -140.3 ppm are assigned as 1-Bpin-2-C₆FH₄, 2,2'-F₂-1,1'-Ph₂, and 1,2-difluorobenzene, respectively.

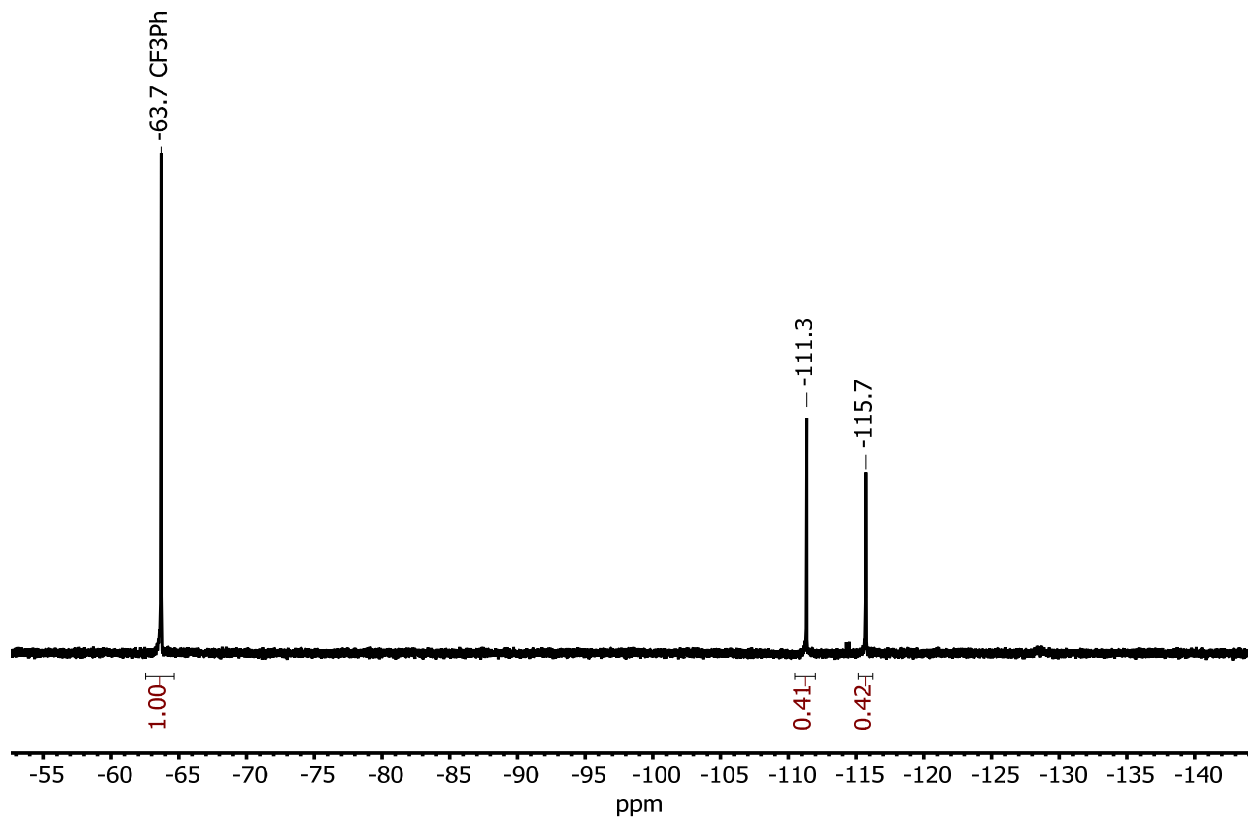


Figure S60. $^{19}\text{F}\{^1\text{H}\}$ NMR spectrum of the reaction mixture from one of the catalytic borylation reactions of 1,3-difluorobenzene following standard catalytic conditions detailed in methods section. The peaks at -111.3 and -115.7 ppm are assigned as 1,3-difluorobenzene and 1-Bpin-3-C₆FH₄, respectively.

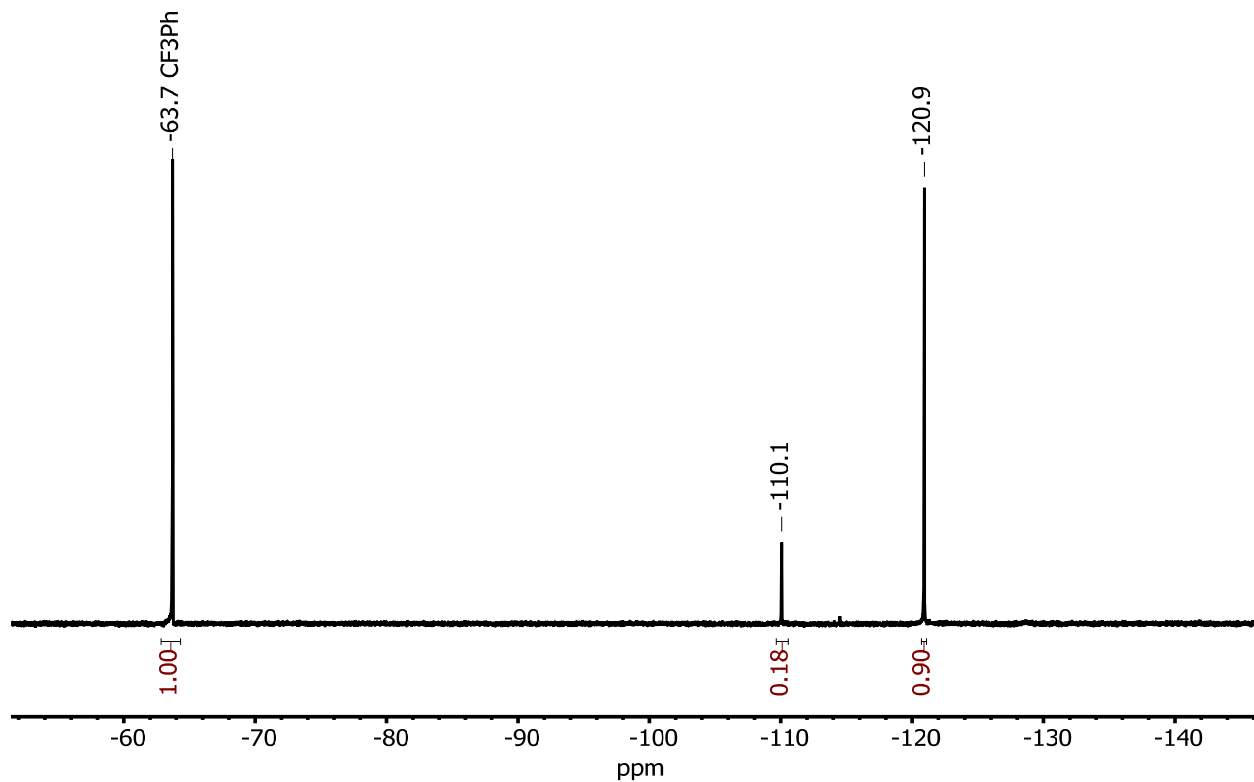


Figure S61. $^{19}\text{F}\{^1\text{H}\}$ NMR spectrum of the reaction mixture from one of the catalytic borylation reactions of 1,4-difluorobenzene following standard catalytic conditions detailed in methods section. The peaks at -110.1 and -120.9 ppm are assigned as 1-Bpin-4-C₆FH₄ and 1,4-difluorobenzene, respectively.

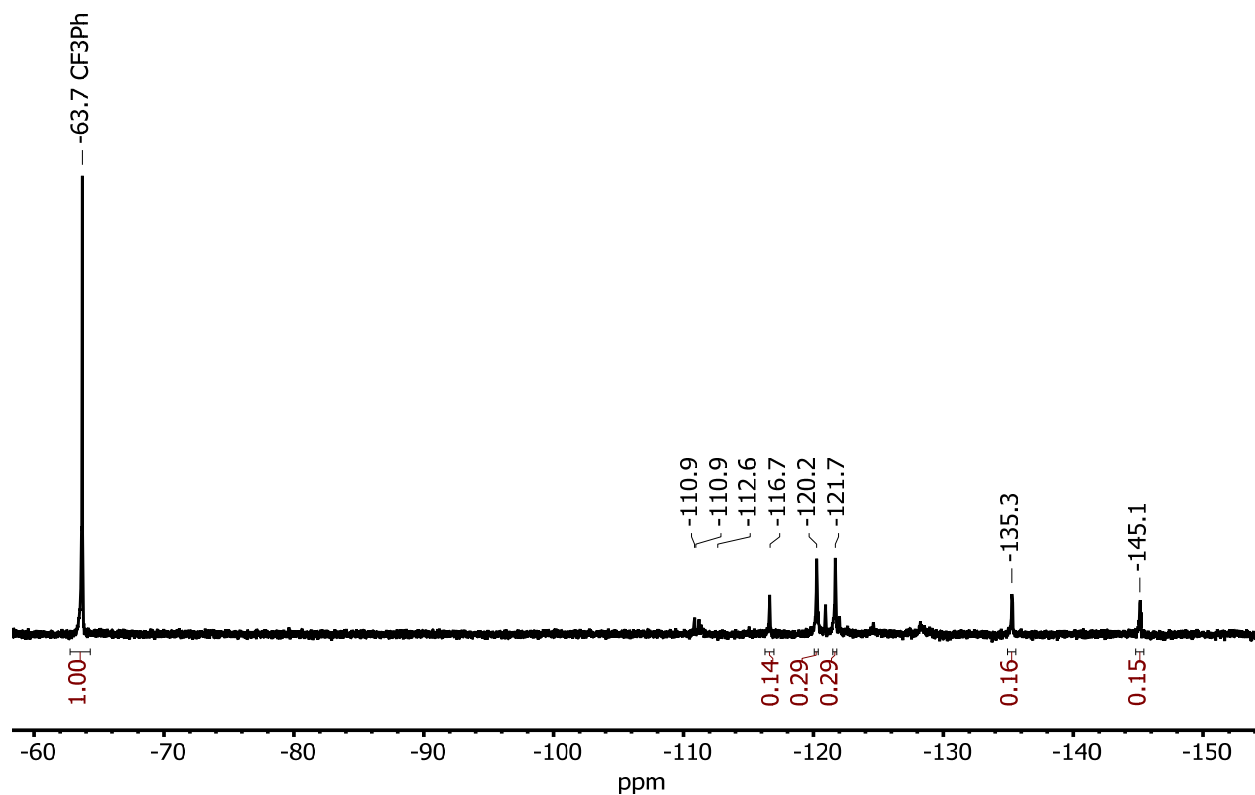


Figure S62. $^{19}\text{F}\{^1\text{H}\}$ NMR spectrum of the reaction mixture from one of the catalytic borylation reactions of 1,2,4-trifluorobenzene following standard catalytic conditions detailed in methods section. The peaks at -116.7, -135.3 and -145.1 ppm are assigned to 1,2,4-trifluorobenzene and the peaks at -120.2 and -121.7 ppm are assigned to 2,2',5,5'-F₄-1,1'-Ph₂.

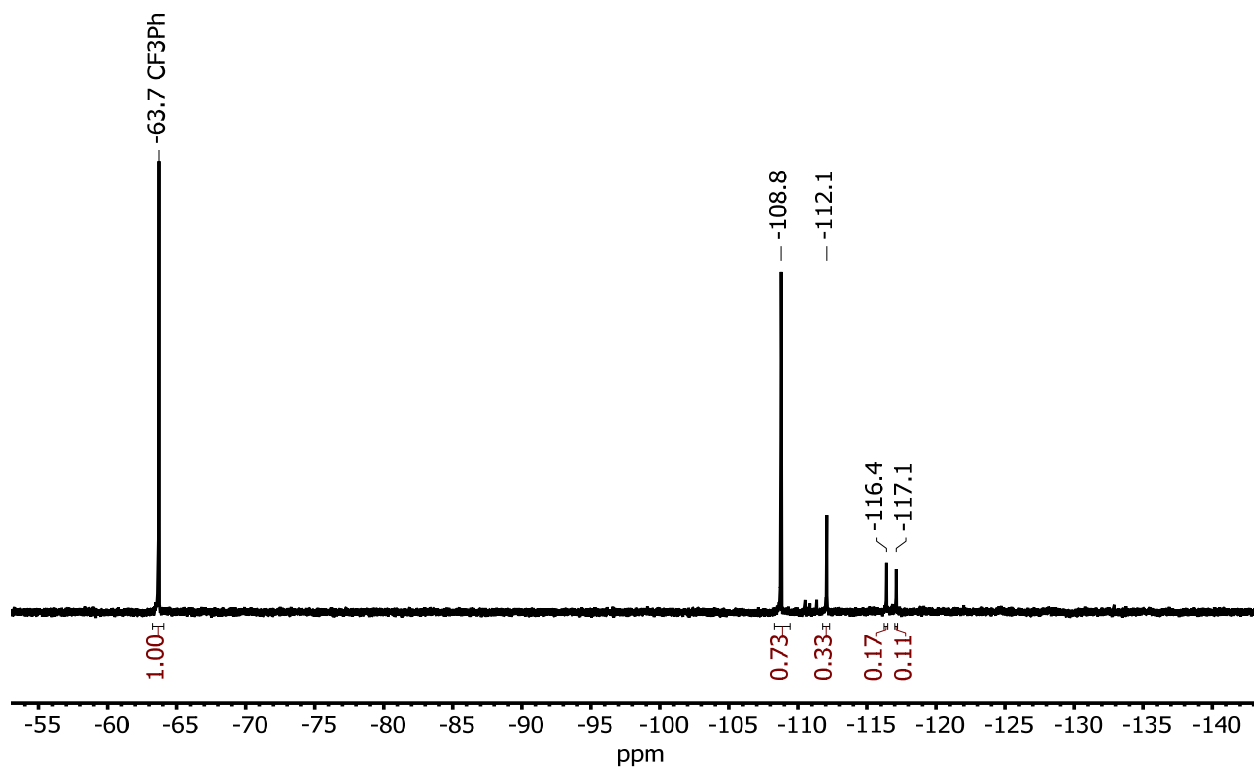


Figure S63. $^{19}\text{F}\{^1\text{H}\}$ NMR spectrum of the reaction mixture from one of the catalytic borylation reactions of 1,3,5-trifluorobenzene following standard catalytic conditions detailed in methods section. The peaks at -108.8, -112.1, and -116.4 ppm are assigned as 1,3,5-trifluorobenzene, 1-Bpin-3,5-C₆F₂H₃, and 1,3-Bpin-5-C₆FH₃, respectively.

GC/MS characterization of C₆H₅Bpin

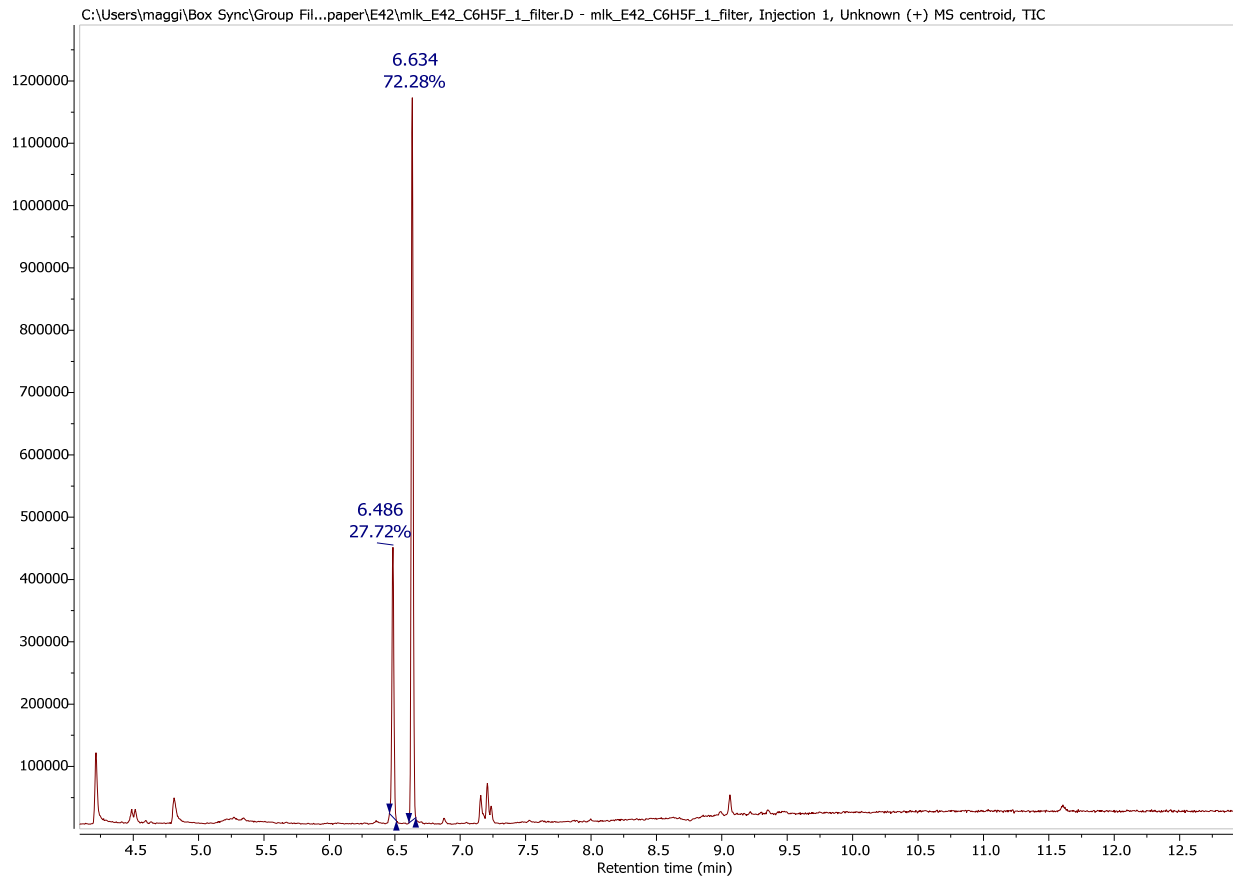


Figure S64. GC trace of the reaction mixture resulting from one of the catalytic borylation reactions of C₆H₅F. The peak at a retention time of 6.486 minutes corresponds to C₆H₅Bpin (see MS below) and the peak at 6.634 minutes corresponds to B₂pin₂.

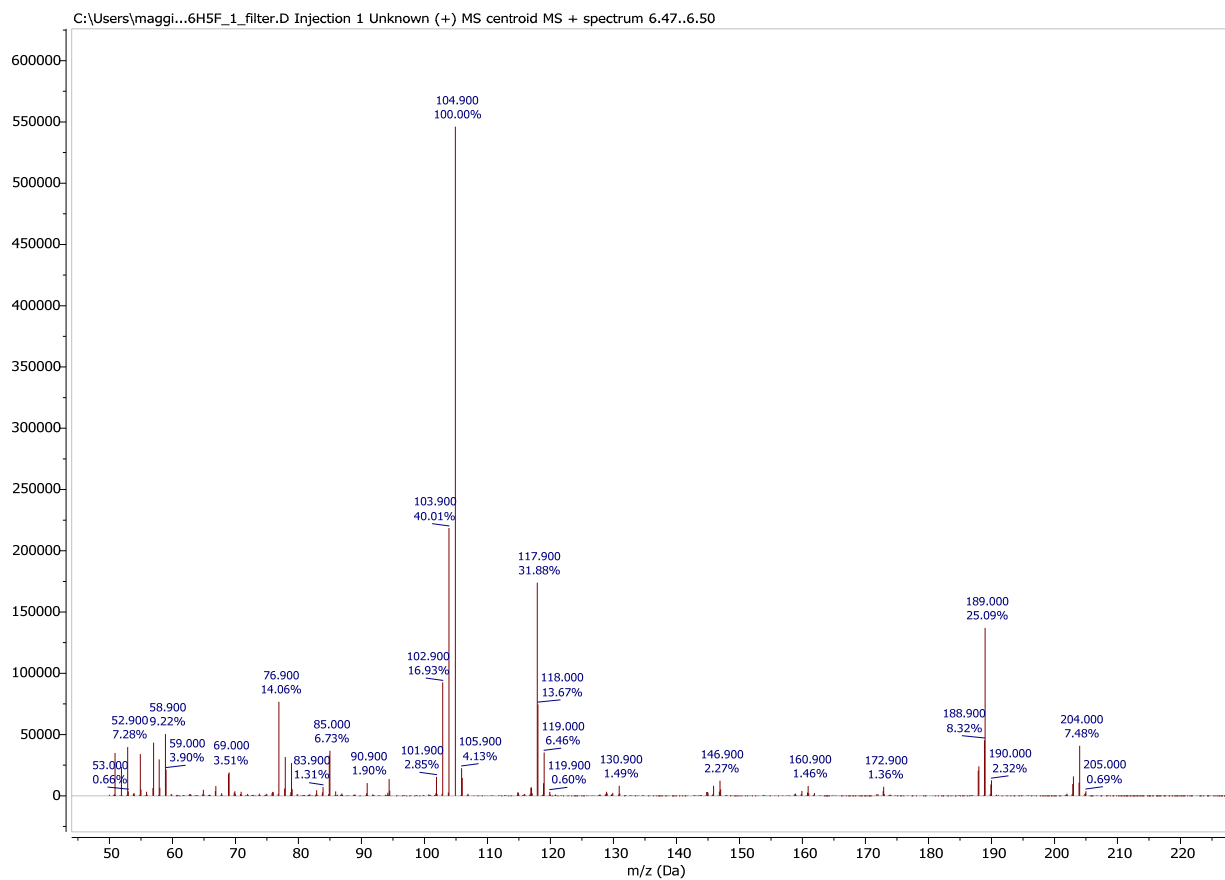


Figure S65. Mass spectrum of the C_6H_5Bpin peak from the reaction mixture GC resulting from one of the catalytic borylation reactions of C_6H_5F .

Infrared Spectra

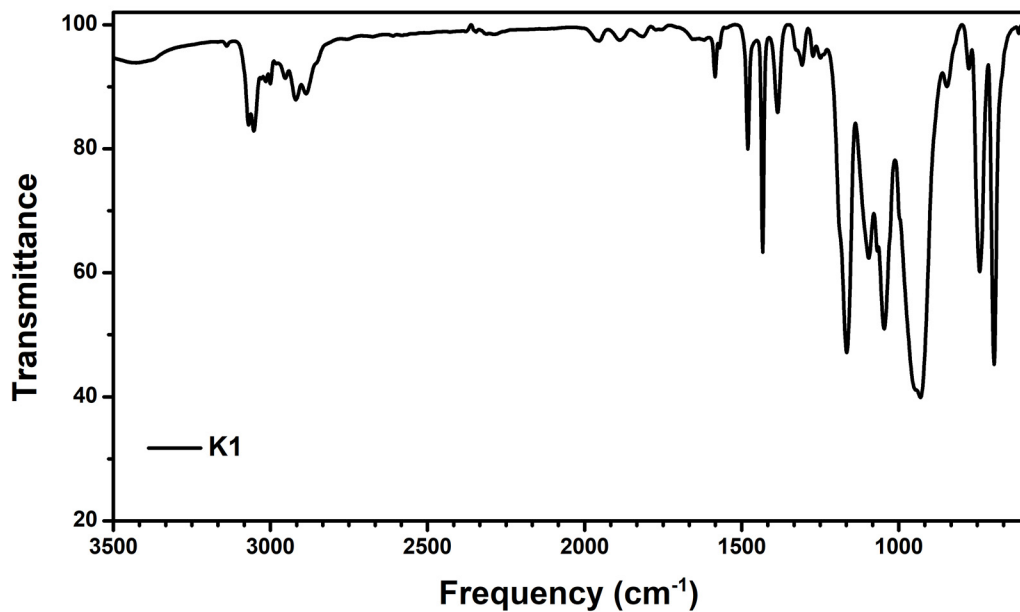


Figure S66. IR spectrum (KBr Pellet) of K1.

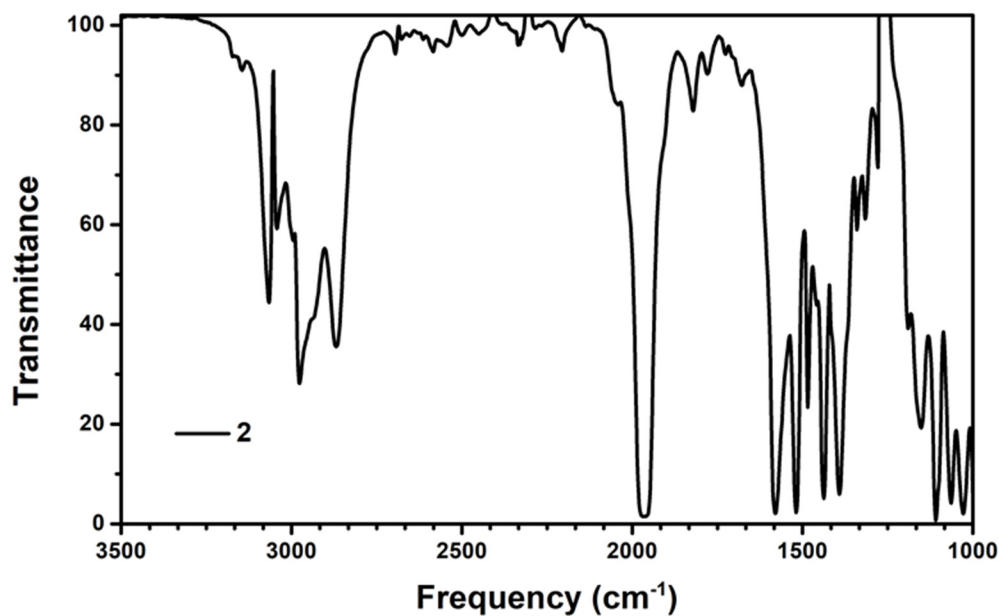


Figure S67. IR spectrum (DCM Solution) of 2. The equation correlating the stretching frequency in Rh(CO)(acac)L compounds and TEP from Ni(CO)₃L is $y = 0.5716x + 938.47$, where y is TEP and x is $\nu(\text{CO})_{\text{Rh}}$.²³

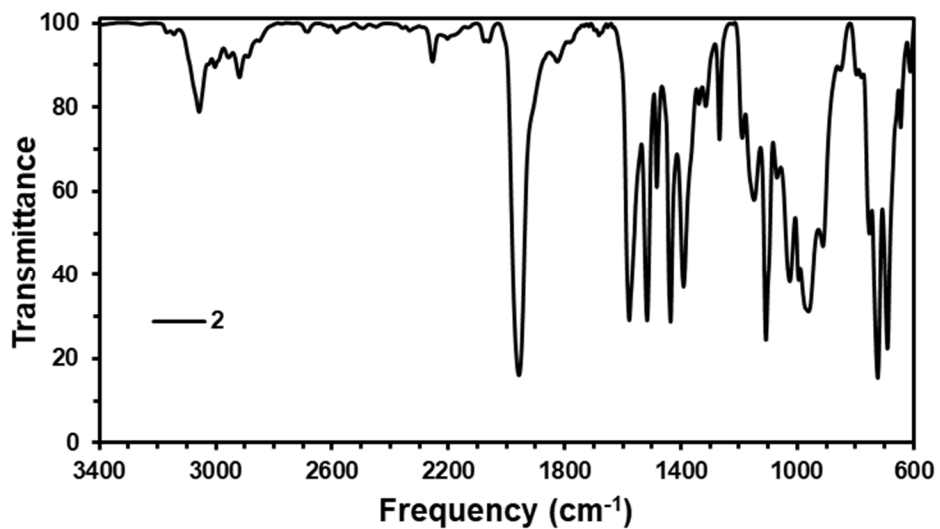


Figure S68. IR spectrum (KBr pellet) of **2**.

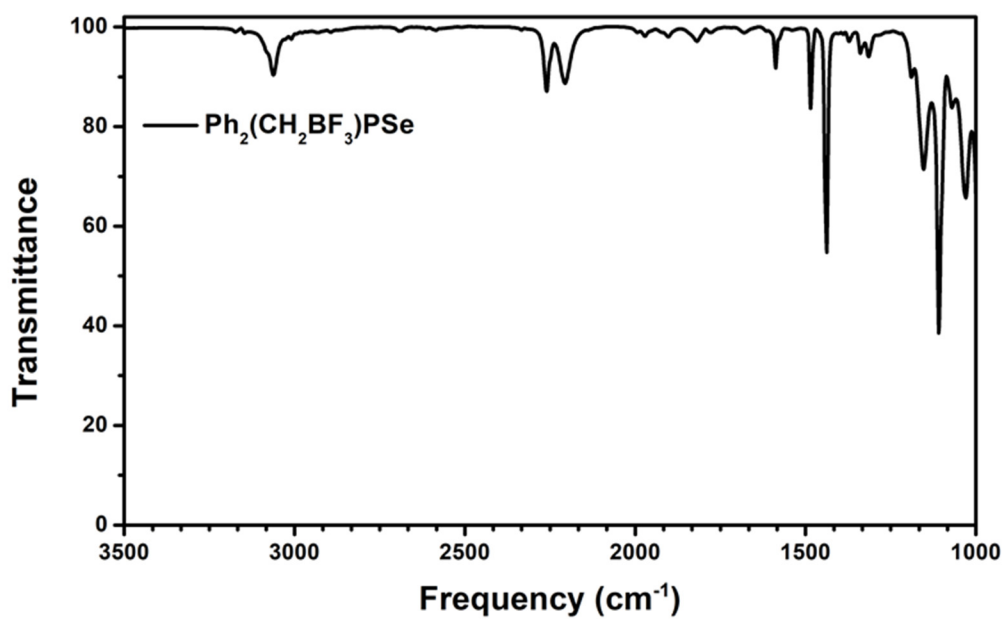


Figure S69. IR spectrum (CDCl₃ solution) of [PPh₄][**1**^{Se}]. Note that the features around 2250 cm⁻¹ are a combination of CO₂ and solvent stretches.

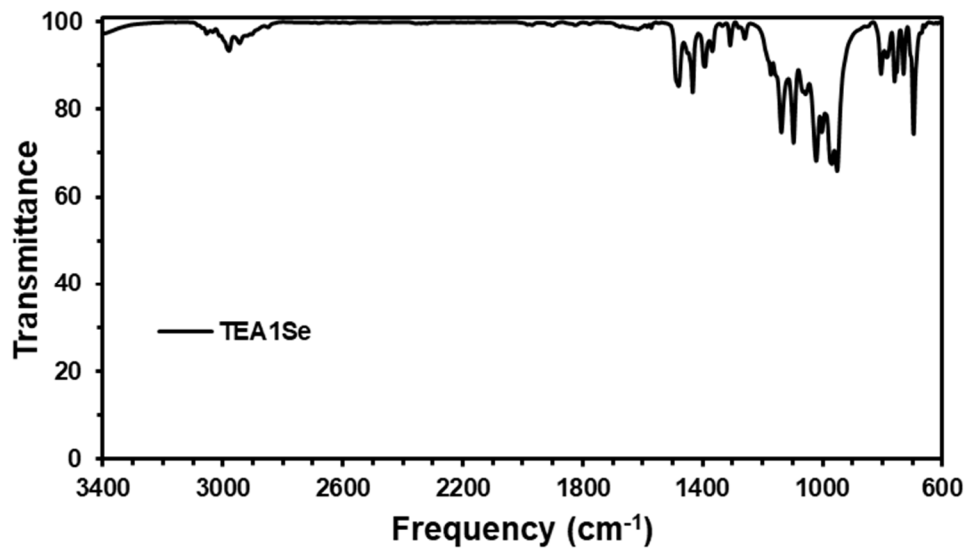


Figure S70. IR spectrum (KBr pellet) of [TEA][1^{Se}].

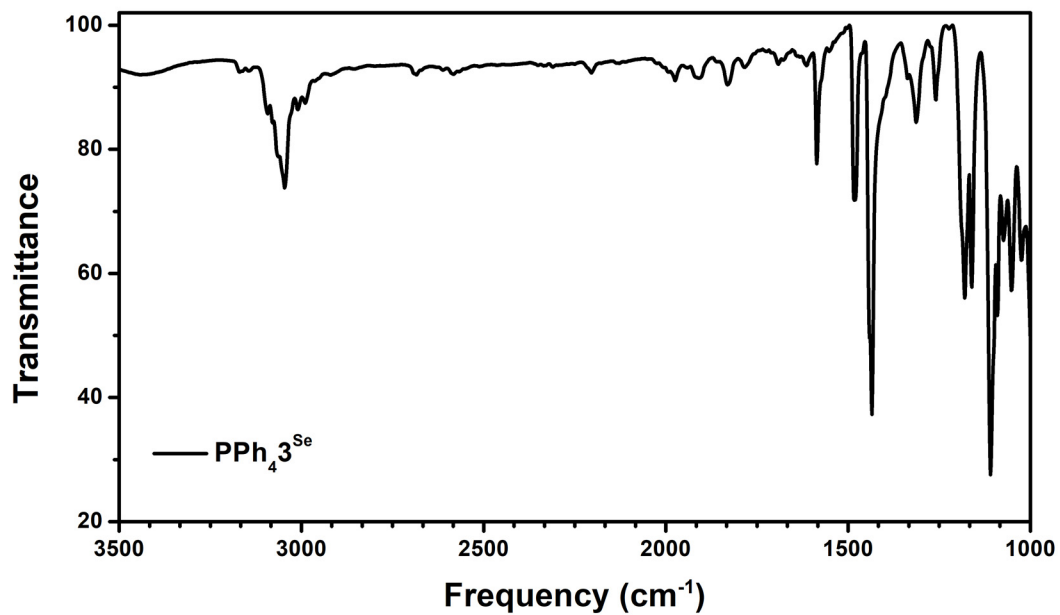


Figure S71. IR spectrum (KBr pellet) of [PPh₄][3^{Se}].

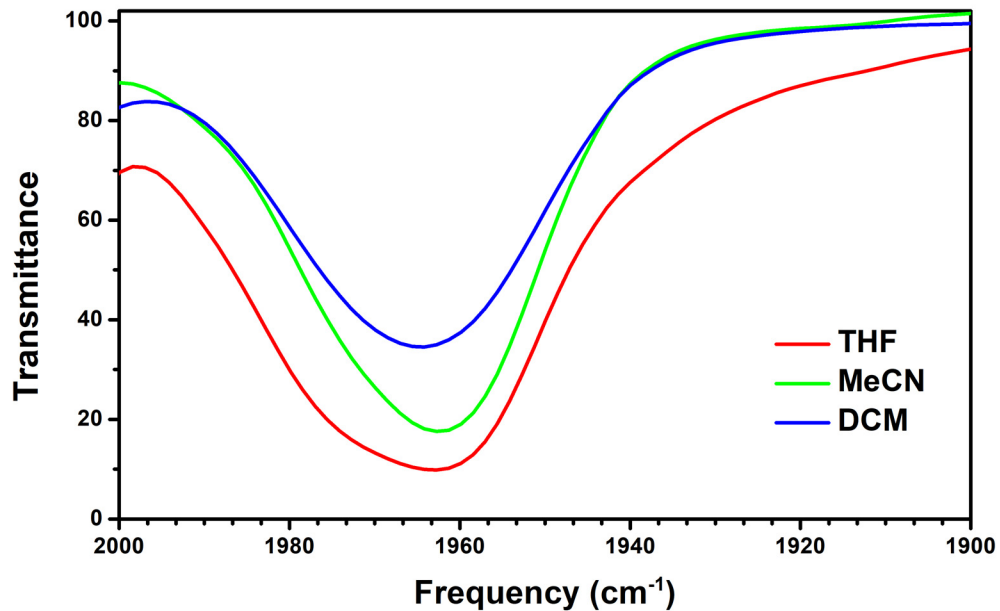


Figure S72. IR spectra of **2** in different solvents. ν_{CO} shifts by $\sim 3 \text{ cm}^{-1}$, which is within the instrument error (4 cm^{-1}).

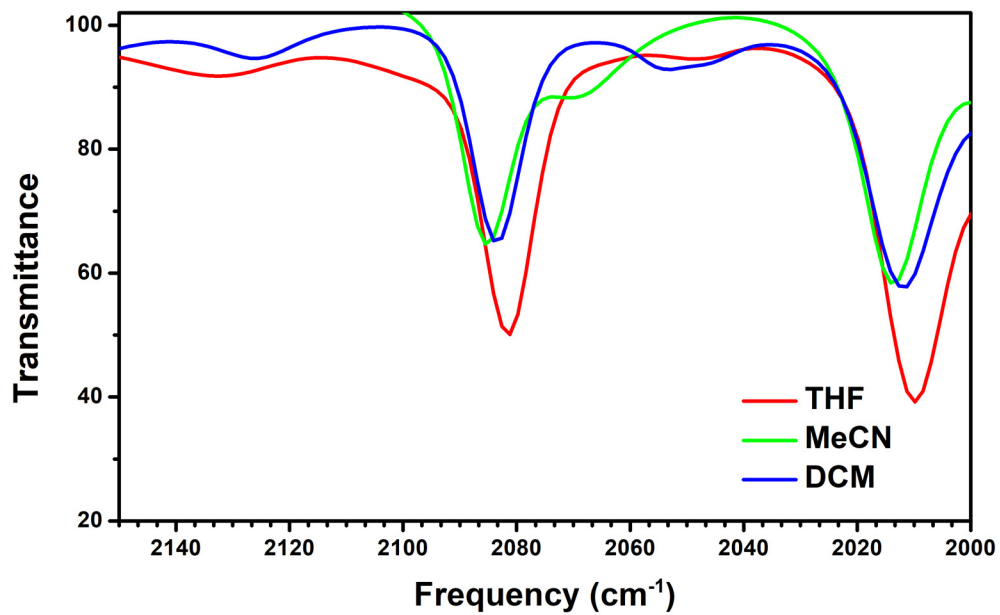


Figure S73. IR spectra of $\text{Rh}(\text{CO})_2\text{acac}$ in different solvents.

UV-visible spectra

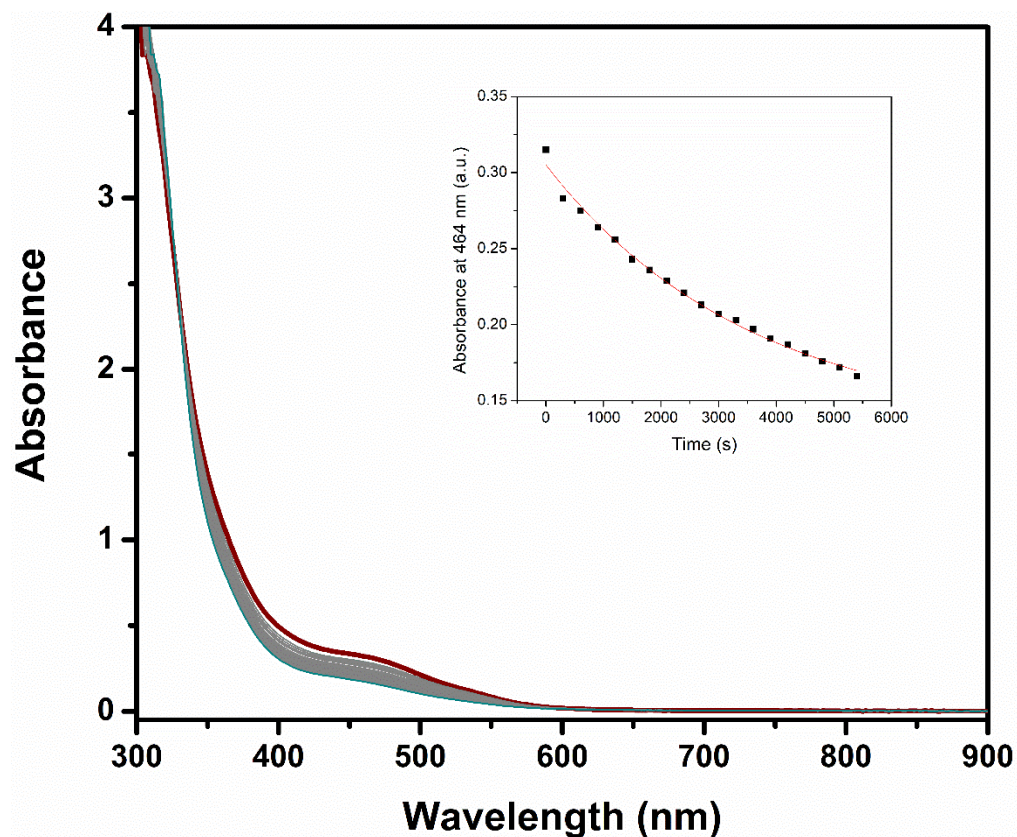


Figure S74. UV-vis traces of the reaction between $\text{Ni}(\text{COD})_2$ (0.36 mM), 1 equivalent of K1, and 21 equivalents of C_6F_6 in THF at RT, with scans taken every 5 minutes for a total of 70 minutes; the spectrum for the first scan is maroon and the spectrum for the last scan is teal. Inset: Exponential fit to the decay of the absorbance at 464 nm with the equation $y=y_0+A*\exp(R_0*x)$. The fit values are $y_0 = 0.132(9)$, $A=0.173(8)$, and $R_0 = -2.81\text{E-}4(3.05\text{E-}5)$. The k_{obs} determined from this fit is $-2.8\text{E-}4 \text{ s}^{-1}$.

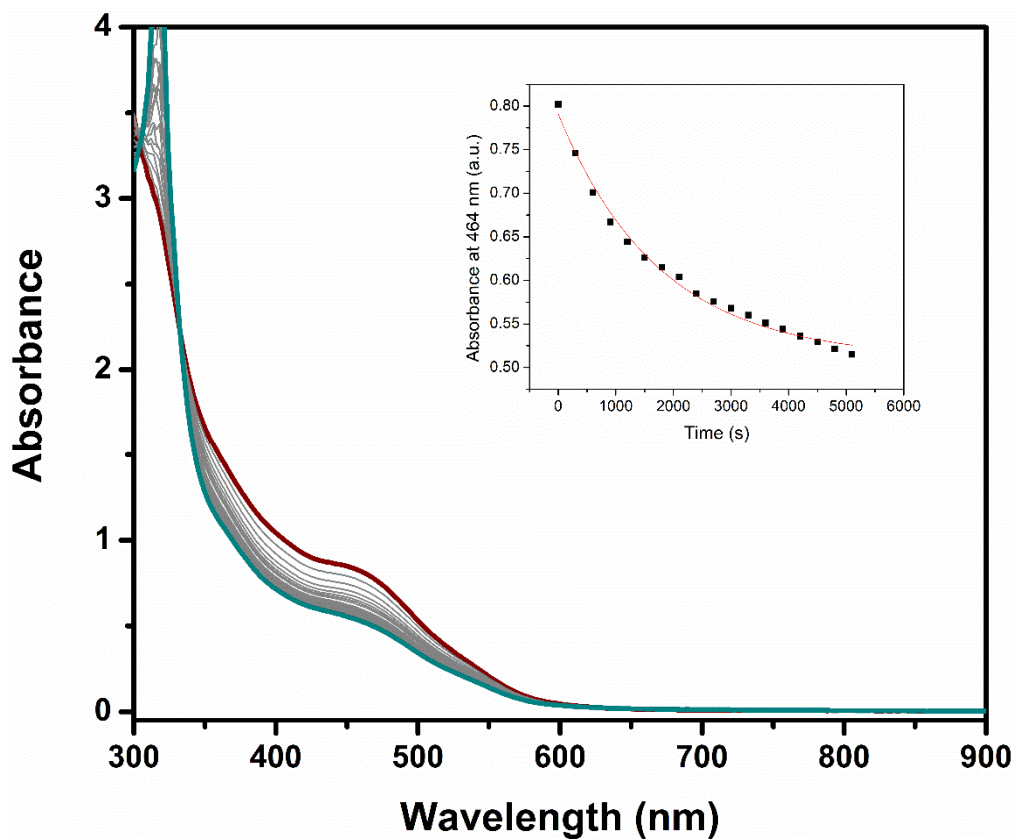


Figure S75. UV-vis traces of the reaction between $\text{Ni}(\text{COD})_2$ (0.36 mM), 2 equivalents of K1, and 21 equivalents of C_6F_6 in THF at RT, with scans taken every 5 minutes for a total of 90 minutes; the spectrum for the first scan is maroon and the spectrum for the last scan is teal. Inset: Exponential fit to the decay of the absorbance at 464 nm with the equation $y=y_0+A*\exp(R_0*x)$. The fit values are $y_0 = 0.510(6)$, $A=0.280(6)$, and $R_0 = -5.68\text{E-}4(3.98\text{E-}5)$. The k_{obs} determined from this fit is $-5.6\text{E-}4 \text{ s}^{-1}$.

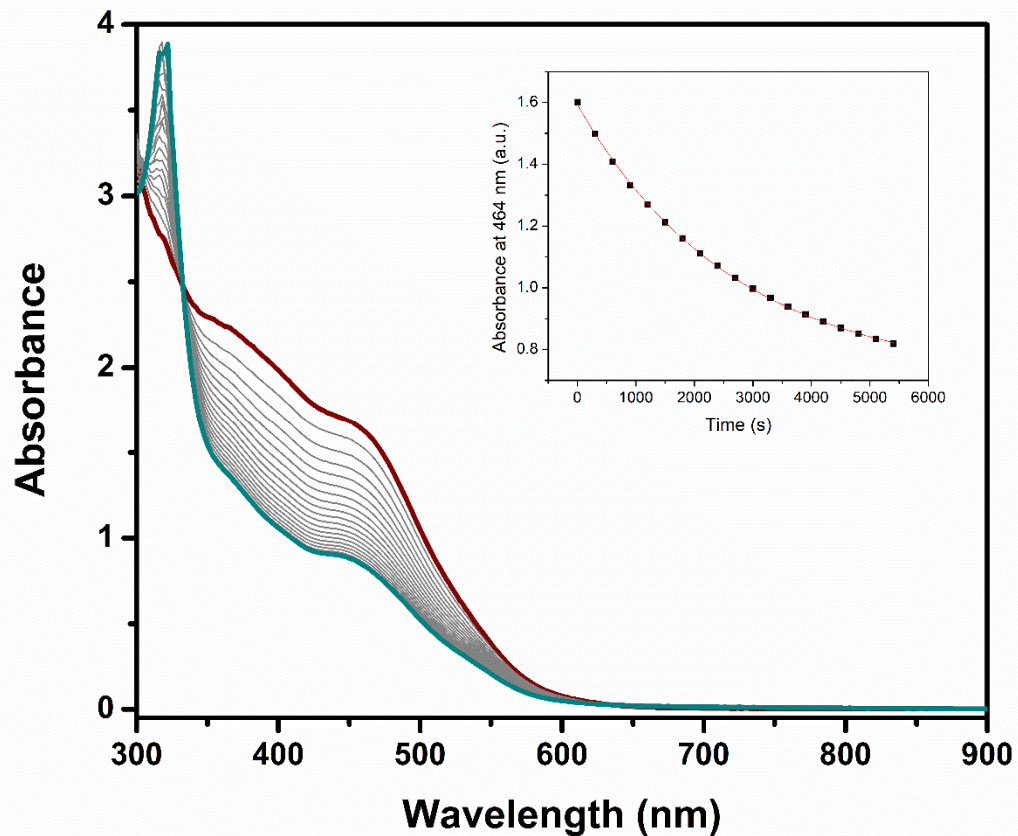


Figure S76. UV-vis traces of the reaction between Ni(COD)₂ (0.36 mM), 3 equivalents of K1, and 21 equivalents of C₆F₆ in THF at RT, with scans taken every 5 minutes for a total of 90 minutes; the spectrum for the first scan is maroon and the spectrum for the last scan is teal. Inset: Exponential fit to the decay of the absorbance at 464 nm with the equation $y=y_0+A*\exp(R_0*x)$. The fit values are $y_0 = 0.703(6)$, $A=0.890(5)$, and $R_0 = -3.71E-4(6.03E-6)$. The k_{obs} determined from this fit is $-3.7E-4 s^{-1}$.

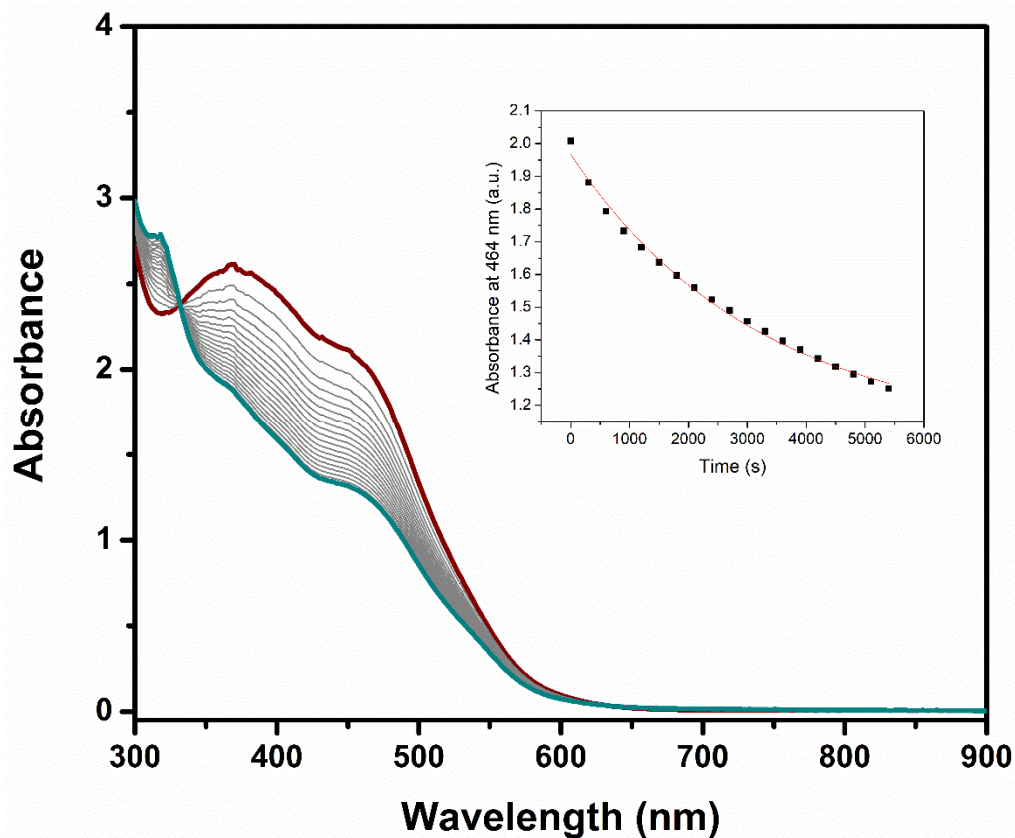


Figure S77. UV-vis traces of the reaction between $\text{Ni}(\text{COD})_2$ (0.36 mM), 4 equivalents of K1, and 21 equivalents of C_6F_6 in THF at RT, with scans taken every 5 minutes for a total of 90 minutes; the spectrum for the first scan is maroon and the spectrum for the last scan is teal. Inset: Exponential fit to the decay of the absorbance at 464 nm with the equation $y=y_0+A*\exp(R_0*x)$. The fit values are $y_0 = 1.110(35)$, $A=0.857(30)$, and $R_0 = -3.14\text{E-}4(2.69\text{E-}5)$. The k_{obs} determined from this fit is $-3.1\text{E-}4 \text{ s}^{-1}$.

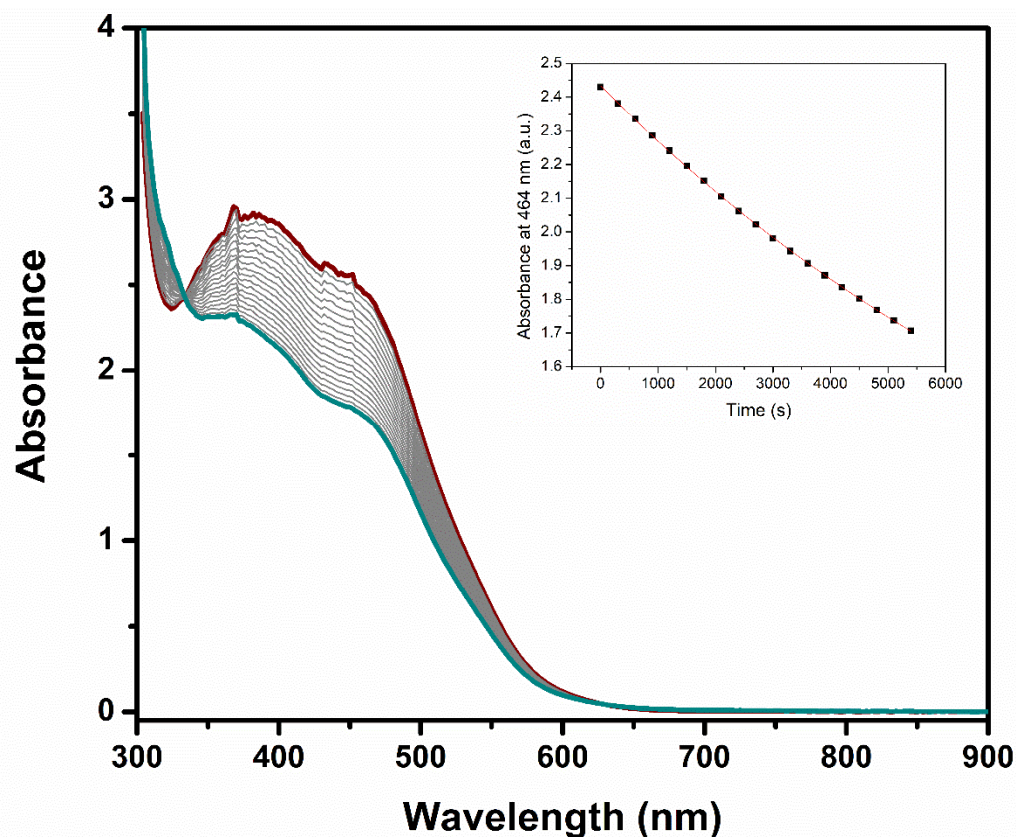


Figure S78. UV-vis traces of the reaction between $\text{Ni}(\text{COD})_2$ (0.36 mM), 8 equivalents of **K1**, and 21 equivalents of C_6F_6 in THF at RT, with scans taken every 5 minutes for a total of 90 minutes; the spectrum for the first scan is maroon and the spectrum for the last scan is teal. Inset: Exponential fit to the decay of the absorbance at 464 nm with the equation $y=y_0+A*\exp(R_0*x)$. The fit values are $y_0 = 0.609(48)$, $A=1.825(47)$, and $R_0 = -9.44\text{E}-5(3.20\text{E}-6)$. The kobs determined from this fit is $-9.4\text{E}-5 \text{ s}^{-1}$.

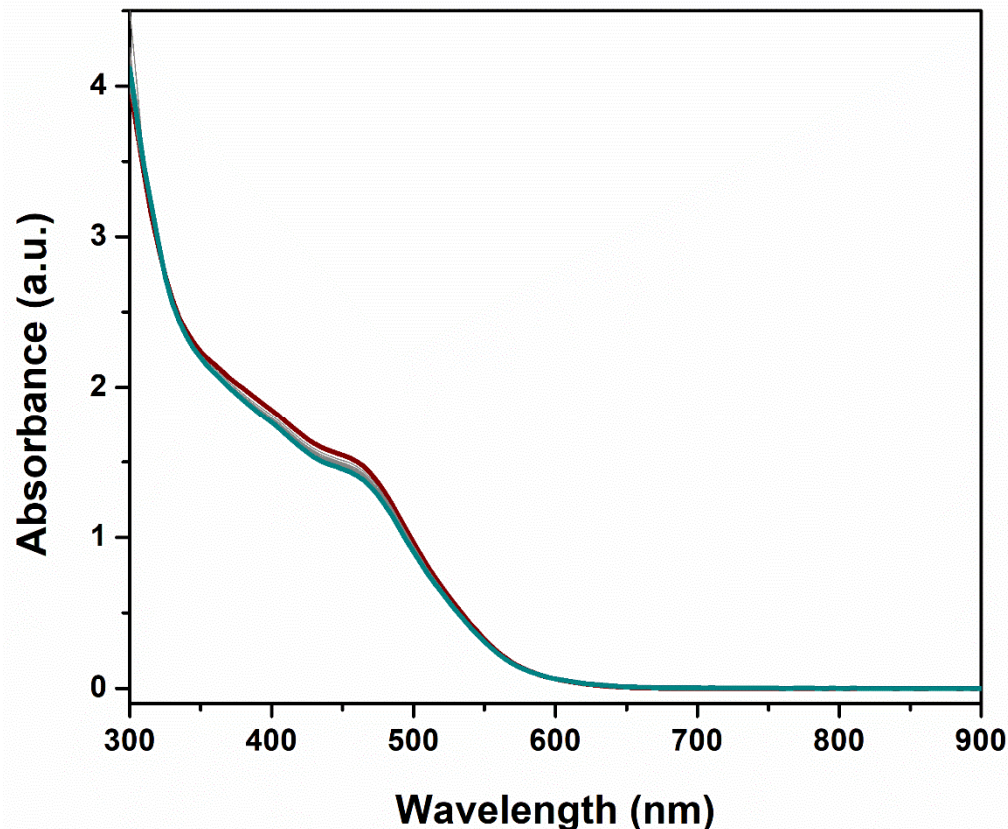


Figure S79. UV-vis traces of the reaction of Ni(COD)₂ and K1 without C₆F₆ in THF at RT, with scans taken every 5 minutes for a total of 70 minutes; the spectrum for the first scan is maroon and the spectrum for the last scan is teal.

Calculations

General considerations

The structure of **1**^{Se}, SePPh₂Et, and **2** were optimized in Orca version 4.0²⁴ using the B3P Functional, with the def2-TZVP²⁵ basis set on C, H, B, and F, and def2-TZVPP²⁵ basis set on Rh, Se, and P. Rh also had an ECP applied. Different local minima geometries of the BF₃ group were found by changing the input geometry, which resulted in optimization to two local minima in the two extremes of the BF₃ positioning. The “transoid” geometry (with a larger Se-P-C-B dihedral) was the global minimum based on comparison of energy by 3.4 kcal, but both geometries were confirmed as local minima with frequency calculations.

NMR couplings were calculated in Gaussian16²⁶ with the “Mixed” method using mPW1PW91 functional and 6-311++G(2d,2p) basis set, similar to methods used in the literature to calculate Se chemical shifts.²⁷ The average coupling was weighted for a Boltzmann population

of the cisoid and transoid isomers based on the calculated energy difference which predicts a nearly 100% population of the ground state transoid isomer at room temperature.

We also considered several solvation models to understand to rationalize the trends we observed. While implicit solvation failed to reproduce our observed trends, explicit solvation did match our observations. For these calculations, the starting geometries of **1**^{Se} were used with 10 randomly arranged solvent molecules of either MeCN, DCM, or CHCl₃. The geometry of this model was then optimized with ORCA 5.0²⁸ with the BP86 functional, with def2-QZVP basis sets on all atoms as well as the D3BJ dispersion correction. Local minima were found, but we did not perform frequency calculations both due to the size of the system, and the high likelihood of multiple minima of similar energy due to minor changes in solvent coordinates. NMR couplings were then calculated in ORCA 5.0 using the EPR/NMR module with the same basis sets but with the O3LYP functional.

The electric field exerted at phosphorus in **1**^{Se} as a result of the anionic BF₃ moiety was estimated using a variation of Coulomb's law. The electric field equation was obtained by dividing coulombs law by q_1 and explicitly separating the vector connecting the points into x, y and z components.²⁹ Doing this results in three equations describing the x, y and z components of the electric field where the z-axis vector is defined as the P-Se bond vector. The equation for the z component is shown below.

$$E_z(x_1, y_1, z_1) = \frac{q_2}{4\pi\epsilon_0} \frac{z_1 - z_2}{[(x_1 - x_2)^2 + (y_1 - y_2)^2 + (z_1 - z_2)^2]^{3/2}}$$

The charge of q_2 is in Coulombs, the constant of proportionality is in V/mC (or equivalently Nm²/C²), and the x,y,z coordinates are in meters. The resulting electric field is in units of V/m.

Two separate optimized geometries for **1**^{Se} were considered, the transoid and cisoid rotamers (see main text and Figures S76 and S77). Both geometries were considered in order to estimate the range of accessible geometries in solution. Starting with optimized geometries, the z-axis was aligned along the P=Se bond in Avogadro.³⁰ The x,y,z coordinates for the B were used as the location of a negative charge, point 2, and the coordinates for phosphorus were used as point 1. An example of the code put into Matlab to calculate the electric field in the transoid geometry (coordinates included in code) is shown below. The electric field calculated at P for this geometry in V/Å was E(x, y, z) = (0.5145, 0.9015, -1.0672). The electric field was analogously calculated at Se(x,y,z) = (0, 0, 2.14028) in V/Å and was (0.1334, 0.2338, -0.5423). The coordinates for boron and selenium in the cisoid geometry were B(x, y, z) = (0.52958, 2.85487, -0.94860) and Se(x,y,z) = (0, 0, 2.11743). The electric field calculated at P in the cisoid geometry in V/Å is E(x, y, z) = (0.2679, 1.4444, -0.4799). The electric field at Se in the cisoid geometry in V/Å was (0.1014, 0.5467, -0.5872). The same code was used to estimate the location for a point charge on the z axis below the phosphine to replicate the electric field. The x and y coordinates were set to 0 and values were entered into the z coordinate until a similar field was predicted. In this case, placing a negative point charge at (0, 0, -3.7) resulted in a predicted field at P of (0, 0, -1.0533). This negative point charge was included via the "charge" input in Gaussian.

```

%Electric field at P - defining coordinates - transoid
Px = 0;
Py = 0;
Pz = 0;
Bx = 1.07559/10^10; %enter position in Å, converts to m
By = 1.88457/10^10;
Bz = -2.23090/10^10;
CP = 9E9; %constant of proportionality, units in Vm/C
elec = -1.60218E-19; %electron charge in C

%defining distances
PB = (Px-Bx)^2 +(Py-By)^2+(Pz-Bz)^2;
rPB = PB^(3/2);

%electric field at P from transoid B1 in V/m
EBx = CP*elec*(Px-Bx)/rPB;
EBy = CP*elec*(Py-By)/rPB;
EBz = CP*elec*(Pz-Bz)/rPB;

%electric field from far B1 in V/Å
EVAx = EBx/10^10;
EVAy = EBy/10^10;
EVAz = EBz/10^10;

%electric field from far B1 in atomic units
Eaux = EVAx/51.4;
Eauy = EVAy/51.4;
Eauz = EVAz/51.4;

%summary/output
EVm = [EBx, EBy, EBz] %x,y,z components of electric field in V/m
EVA = [EVAx, EVAy, EVAz] %x,y,z components of electric field in V/Å
Eau = [Eaux, Eauy, Eauz] %x,y,z components of electric field in atomic
units

```

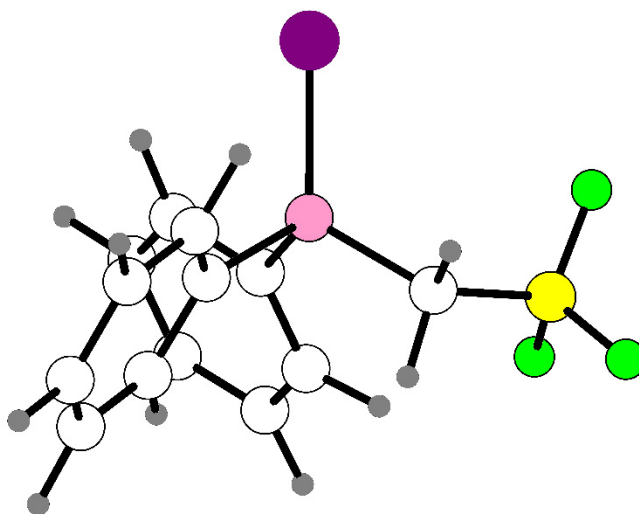


Figure S80. Calculated structure of 1^{Se} (cisoid structure).

Table S2. Coordinates of optimized structure of 1^{Se} (cisoid structure)

P	0.00000	0.00000	-0.00000
C	0.79176	-1.51897	-0.68167
C	-1.68430	-0.09969	-0.70597
C	0.95751	1.26436	-0.84601
C	-2.03216	0.57473	-1.87230
C	-3.30535	0.44636	-2.40740
C	-4.24520	-0.36639	-1.78539
C	-3.90466	-1.03762	-0.61612
C	-2.63696	-0.90181	-0.07134
C	0.34564	-2.11211	-1.86055
C	1.04760	-3.15788	-2.44199
C	2.20703	-3.64068	-1.84793
C	2.64957	-3.06779	-0.65874
C	1.94911	-2.01469	-0.08495
H	-0.54693	-1.73898	-2.35402
H	0.69672	-3.58365	-3.37695
H	2.76413	-4.44933	-2.31062
H	3.55125	-3.43509	-0.17762
H	2.29796	-1.55965	0.83836
H	-1.32880	1.27805	-2.30439
H	-3.56414	0.99679	-3.30539
H	-5.24242	-0.46288	-2.20361
H	-4.64233	-1.66290	-0.11985
H	-2.37684	-1.39091	0.86300
B	0.52958	2.85487	-0.94860

H	1.08297	0.90777	-1.87581
H	1.93004	1.18075	-0.34921
F	-0.65839	3.01138	-1.70523
F	1.56441	3.48557	-1.66849
F	0.38517	3.40672	0.32000
Se	0.00000	0.00000	2.11743

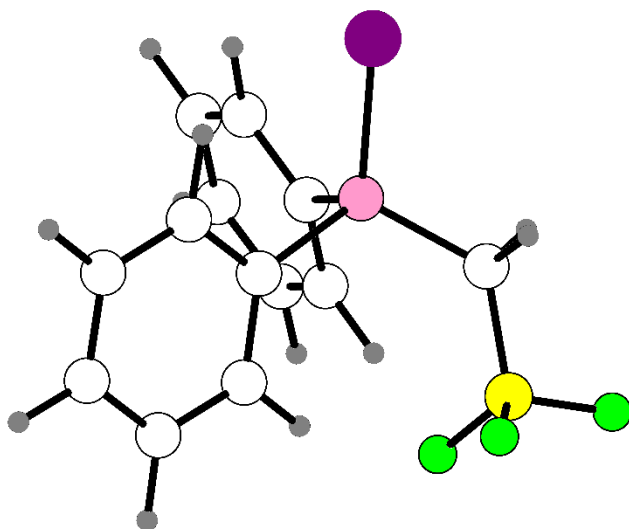


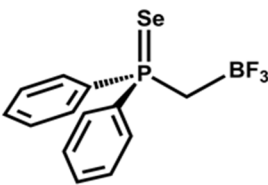
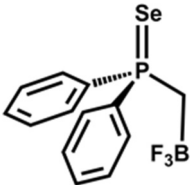
Figure S81. Calculated structure of 1^{Se} with the BF_3 group rotated down (transoid structure).

Table S3. Coordinates of calculated structure of edited 1^{Se} (transoid structure).

P	0.00000	0.00000	-0.00000
C	0.99330	-1.39843	-0.66597
C	-1.67140	-0.40144	-0.64511
C	0.47747	1.57885	-0.70985
C	-2.05904	-0.01528	-1.93709
C	-3.32542	-0.36388	-2.41501
C	-4.20617	-1.10123	-1.62104
C	-3.82135	-1.48343	-0.33348
C	-2.56304	-1.12866	0.15402
C	1.22296	-1.52383	-2.04616
C	1.83822	-2.67280	-2.54698
C	2.23379	-3.69978	-1.68536
C	2.03814	-3.56165	-0.30944
C	1.42154	-2.41535	0.19733
H	0.92192	-0.72323	-2.72719
H	2.00752	-2.76313	-3.62528
H	2.69143	-4.61047	-2.08801

H	2.36104	-4.35360	0.37473
H	1.24876	-2.29177	1.27209
H	-1.36256	0.54441	-2.57044
H	-3.62385	-0.04992	-3.42069
H	-5.20049	-1.36658	-1.99654
H	-4.51353	-2.04700	0.30141
H	-2.25464	-1.39203	1.17180
B	1.07559	1.88457	-2.23090
H	1.24869	1.94613	-0.01093
H	-0.41508	2.20718	-0.53519
F	2.43491	1.57068	-2.27037
F	0.88434	3.24873	-2.48413
F	0.40887	1.14985	-3.26352
Se	0.00000	0.00000	2.14028

Table S4. Calculated electric field and J_{P-Se} for calculated structures of 1^{Se} .

Structure	Electric Field at P from Coulomb's Law (x,y,z) (V/Å)	Electric Field at Se from Coulomb's Law (x,y,z) (V/Å)	Calculated J_{P-Se} (Hz)
 <p>Cisoid</p>	(0.2679, 1.4444, -0.4799)	(0.1014, 0.5467, -0.5872)	849
 <p>Transoid</p>	(0.5145, 0.9015, -1.0672)	(0.1334, 0.2338, -0.5423)	792

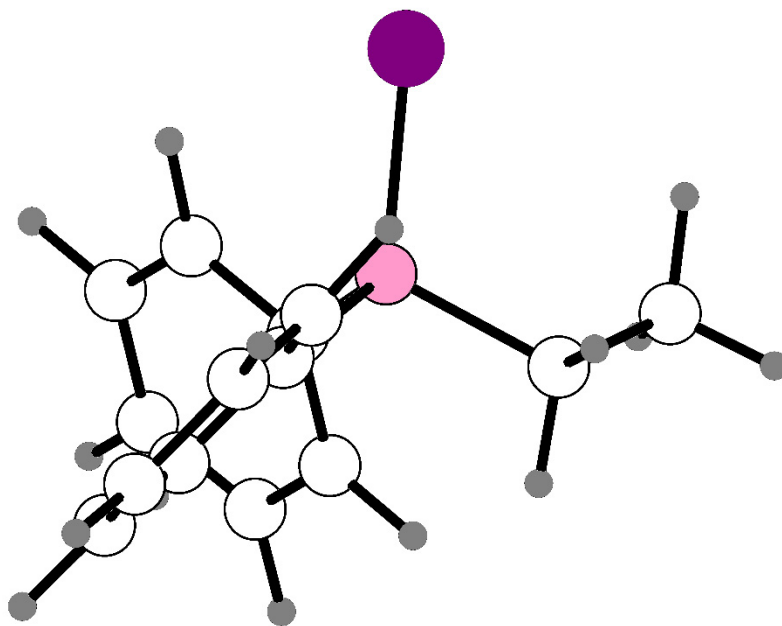


Figure S82. Optimized structure of SePPh₂Et

Table S5. Coordinates of calculated structure of SePPh₂Et

P	-1.35788240879875	-0.13006160366219	0.01411152467337
C	0.46035043089732	-0.00894111268972	-0.11297709391472
C	-1.94517319766249	1.58601434389281	-0.16172337078438
C	-1.61801775841252	-0.61050169284086	1.76310436384687
C	-2.01014632290093	2.47292110281823	0.92410985893433
C	-2.41206155900290	3.79576392924933	0.72657268228532
C	-2.74084901275680	4.24437941334151	-0.55433651062815
C	-2.68265886616421	3.36481109808462	-1.63800769868336
C	-2.29720178239310	2.03882087923351	-1.44152423911476
C	1.13167743910790	1.22211021431696	-0.09833764454327
C	2.52599984121426	1.26309941428321	-0.17498367322925
C	3.25881284879158	0.07870400585500	-0.25496759670394
C	2.59497006687365	-1.15128021566608	-0.27269699876603
C	1.20289958940165	-1.19608897060009	-0.21338937206687
H	0.56785142998232	2.15646750575397	-0.03584727525056
H	3.04127036520655	2.22861672964623	-0.17613907033801
H	4.35118313528202	0.11411607368298	-0.31698548311317
H	3.16578660570770	-2.08138803595474	-0.34956853358883
H	0.67898692040419	-2.15558358314002	-0.27123364941962
H	-1.74109270514662	2.14154866229593	1.93092698724380

H	-2.47180495620726	4.47777195354649	1.57995780443591
H	-3.05874211021555	5.28023958410241	-0.70753760639855
H	-2.95473464600281	3.71205680917404	-2.63940545838434
H	-2.27331831816806	1.33201706440374	-2.27737773784354
C	-3.07492682591919	-0.83763875445270	2.14339590507861
H	-1.12647794003861	0.14336875047400	2.40307130334858
H	-1.02905993305891	-1.53660194524061	1.87501787192442
H	-3.65864309342022	0.09485089645599	2.08972538205654
H	-3.14747222882146	-1.22835025412969	3.17174579213329
H	-3.54324381001111	-1.56577579313832	1.46318209837571
Se	-2.23970119776762	-1.48167646909590	-1.34535256156543

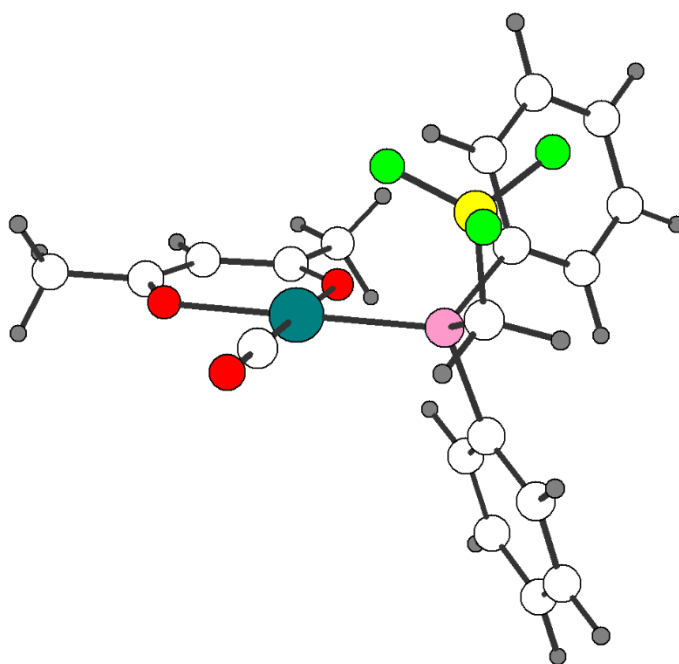


Figure S83. Optimized structure of **2**.

Table S6. Coordinates of calculated structure of **2**.

C	8.403788	17.368792	2.615641
P	9.705222	18.509041	3.115911
Rh	10.136258	18.933402	5.313363
C	11.221557	17.926186	2.268307
C	9.347099	20.115557	2.288545
O	12.057864	19.603935	4.821644
O	10.615003	19.337603	7.337524
C	8.446174	18.381288	5.731046
C	11.755851	18.531018	1.132847
C	10.200942	21.200914	2.513834

C	8.220460	20.311465	1.492247
C	12.970067	19.954472	5.623701
C	11.726087	19.727819	7.776966
O	7.383820	18.076726	6.041198
C	9.941245	22.438077	1.944732
C	7.951510	21.556867	0.932416
C	14.277143	20.329974	4.968282
C	12.872159	20.025527	7.017917
C	11.802153	19.879283	9.279178
C	8.811293	22.622504	1.153446
B	8.595388	15.744242	2.943153
F	7.324750	15.146053	2.848943
F	9.450987	15.161508	1.986774
F	9.128192	15.529631	4.230298
C	11.858493	16.802787	2.800076
C	12.910173	18.028815	0.541690
C	13.006304	16.301171	2.206666
C	13.539880	16.915029	1.079053
H	8.265032	17.454439	1.531862
H	7.484652	17.707179	3.107181
H	11.272738	19.401040	0.701904
H	11.071467	21.061570	3.147696
H	7.540607	19.486130	1.312565
H	10.616970	23.267955	2.129427
H	7.063383	21.690232	0.321928
H	14.120589	21.199587	4.322298
H	14.601816	19.508033	4.324507
H	15.059281	20.560440	5.693265
H	13.754680	20.343503	7.559616
H	11.578020	18.916231	9.746747
H	11.033490	20.584266	9.608231
H	12.779454	20.225718	9.619559
H	8.602193	23.593992	0.716399
H	11.432442	16.310556	3.667469
H	13.313992	18.511300	-0.343251
H	13.482115	15.419730	2.624111
H	14.440215	16.521415	0.617090

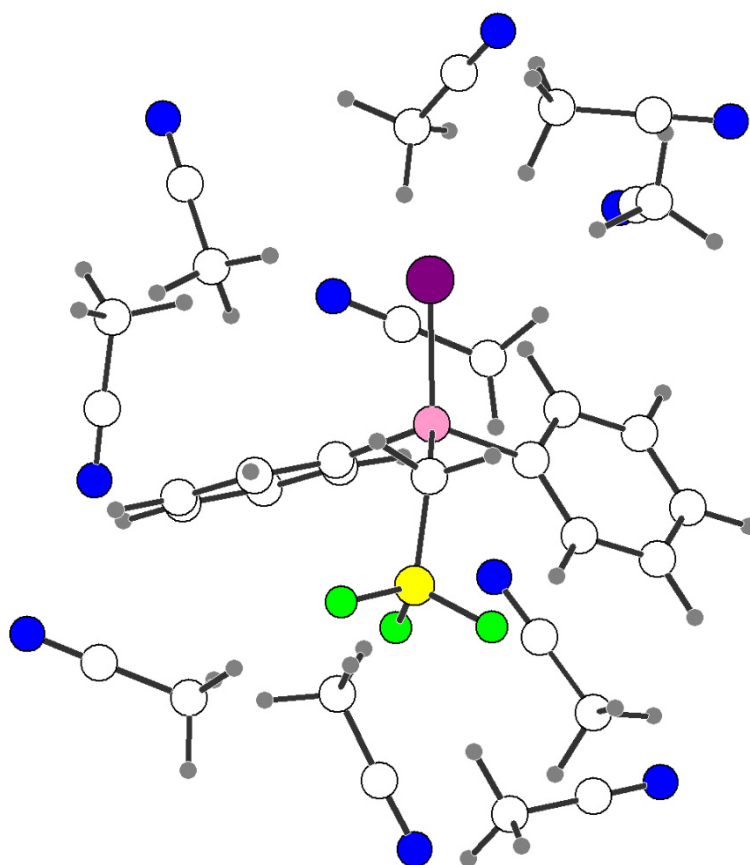


Figure S84. Optimized structure of 1^{Se} with explicit MeCN solvation.

Table S7. Coordinates of calculated structure of 1^{Se} with explicit MeCN solvation.

P	-1.215603	-0.313816	-0.472603
Se	-0.452603	0.248122	-2.411729
C	-1.721581	-2.066081	-0.495162
C	-1.493133	-2.908706	0.602266
C	-1.822447	-4.263899	0.517415
C	-2.396733	-4.778258	-0.646201
C	-2.638699	-3.938294	-1.735938
C	-2.293813	-2.591119	-1.663500
C	-2.707716	0.674159	-0.128220
C	-3.966208	0.239733	-0.561081
C	-5.087875	1.052126	-0.388416
C	-4.962674	2.299978	0.226319
C	-3.708347	2.734752	0.667955
C	-2.584152	1.927887	0.490717
C	-0.040690	-0.059408	0.866975
B	-0.510147	-0.196130	2.450299

F	-0.170423	0.992445	3.149852
F	0.129594	-1.303411	3.063515
F	-1.933628	-0.398601	2.594030
H	-1.042836	-2.524385	1.514471
H	-1.633018	-4.910069	1.373390
H	-2.649734	-5.836958	-0.706282
H	-3.078320	-4.330834	-2.651482
H	-2.432730	-1.938092	-2.524644
H	-4.078742	-0.742407	-1.013860
H	-6.062973	0.708223	-0.728742
H	-5.843932	2.925502	0.362265
H	-3.604260	3.701942	1.158719
H	-1.613228	2.268975	0.846775
H	0.364301	0.946397	0.685159
H	0.783835	-0.753565	0.647108
C	-5.442646	-2.227617	-3.477505
C	-5.336566	-0.791763	-3.639717
N	-5.237553	0.358162	-3.768755
H	-5.378838	-2.489664	-2.411015
H	-4.631030	-2.716633	-4.035989
H	-6.407195	-2.575770	-3.868225
C	-2.440901	0.309633	-5.580876
C	-1.092308	0.070320	-6.055856
N	-0.006545	-0.133433	-6.416793
H	-3.113227	-0.472801	-5.950284
H	-2.802497	1.293150	-5.904573
H	-2.436771	0.277555	-4.481624
C	2.646389	-0.449481	-4.347672
C	3.094388	-1.828017	-4.419539
N	3.431963	-2.938858	-4.480810
H	1.996284	-0.223324	-5.205310
H	3.505315	0.232815	-4.348115
H	2.058545	-0.289982	-3.429966
C	-5.153169	-4.562444	1.811660
C	-5.385003	-3.618940	0.734791
N	-5.586309	-2.856525	-0.118124
H	-5.729211	-4.268714	2.697871
H	-4.091691	-4.581615	2.088111
H	-5.451597	-5.570295	1.497872
C	-2.835791	2.383102	4.145979
C	-2.954180	3.808661	3.899754
N	-3.052301	4.947176	3.686635
H	-3.520366	1.836220	3.487325

H	-3.082280	2.154222	5.190130
H	-1.819008	2.027970	3.925770
C	-2.999744	2.934914	-2.821018
C	-3.321985	3.440134	-4.139771
N	-3.590052	3.834529	-5.200567
H	-2.853144	3.760663	-2.115272
H	-2.083266	2.320936	-2.842279
H	-3.812313	2.293239	-2.459085
C	-2.203664	-2.654008	4.974889
C	-2.314015	-3.939191	4.313247
N	-2.413328	-4.964999	3.775761
H	-1.923030	-1.883856	4.243357
H	-1.428567	-2.694293	5.749690
H	-3.169898	-2.394630	5.425166
C	-0.182729	-2.966933	-4.418177
C	-1.554122	-3.073047	-4.870747
N	-2.663566	-3.140890	-5.211907
H	0.122377	-3.883151	-3.899510
H	-0.102686	-2.114996	-3.720387
H	0.485249	-2.791158	-5.268621
C	-6.671189	3.308174	-3.147741
C	-7.588852	3.012575	-2.061968
N	-8.314697	2.767618	-1.187945
H	-6.141664	2.393897	-3.452956
H	-5.933715	4.053741	-2.827386
H	-7.214467	3.707480	-4.012696
C	-5.084714	-0.537145	2.567380
C	-5.391995	-1.470471	3.632964
N	-5.627071	-2.236146	4.475949
H	-5.420149	-0.942859	1.606192
H	-3.999278	-0.375841	2.508936
H	-5.590123	0.421405	2.734982

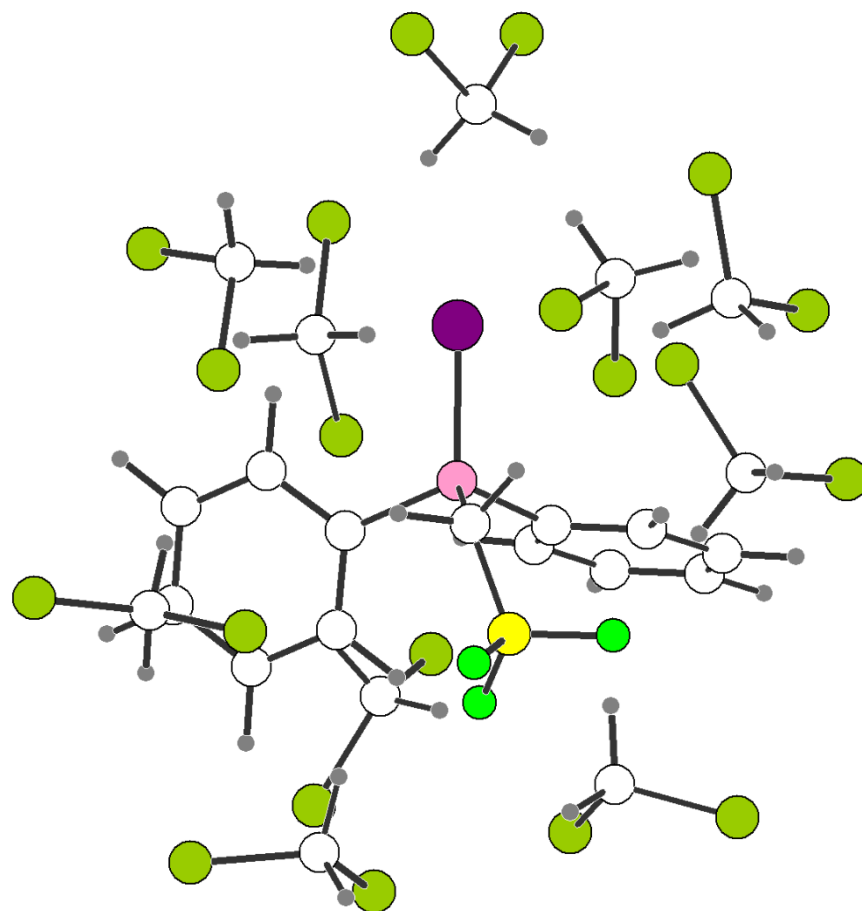


Figure S85. Optimized structure of 1^{Se} with explicit DCM solvation.

Table S8. Coordinates of calculated structure of 1^{Se} with explicit DCM solvation

P	-2.116135	0.987532	0.229504
Se	-2.954463	1.797678	-1.590603
C	-2.211619	-0.819228	0.097613
C	-1.199681	-1.512743	-0.583168
C	-1.327655	-2.880182	-0.817747
C	-2.460240	-3.566243	-0.371599
C	-3.471556	-2.879047	0.301118
C	-3.353379	-1.508392	0.528257
C	-3.142849	1.423475	1.683769
C	-2.962926	0.773611	2.914702
C	-3.764508	1.112543	4.005726
C	-4.750135	2.096078	3.879420
C	-4.918992	2.755379	2.660553
C	-4.118243	2.418084	1.568166
C	-0.429676	1.536481	0.540890
B	0.601136	0.682627	1.516994

F	1.558246	1.567516	2.053702
F	1.277625	-0.331570	0.766092
F	-0.079381	0.026111	2.595216
H	-0.306879	-0.990106	-0.912205
H	-0.532284	-3.407411	-1.340748
H	-2.554500	-4.636278	-0.549579
H	-4.363747	-3.402020	0.639362
H	-4.166033	-0.967010	1.007772
H	-2.196765	0.009247	3.017397
H	-3.618122	0.597313	4.953447
H	-5.377294	2.350763	4.733140
H	-5.669714	3.538224	2.554478
H	-4.251388	2.915878	0.609153
H	-0.562279	2.552734	0.940396
H	0.019468	1.657384	-0.454670
C	-5.969608	-2.017039	-3.073064
Cl	-4.867755	-0.797309	-2.383457
Cl	-6.509231	-3.229418	-1.870345
H	-5.428153	-2.541982	-3.861552
H	-6.852393	-1.495185	-3.445252
C	-1.776886	-1.011407	-3.917404
Cl	-2.429335	-2.640982	-4.256854
H	-0.693943	-1.096877	-3.829627
Cl	-2.131210	0.151098	-5.227299
H	-2.243408	-0.627752	-3.006934
C	-0.674152	-2.993900	2.658287
H	-1.110806	-2.532898	1.774329
Cl	0.480158	-4.239721	2.117588
H	-0.147032	-2.266031	3.273509
Cl	-2.010733	-3.687959	3.632914
C	-2.002481	4.215974	3.938690
Cl	-2.123232	5.875905	4.605239
H	-2.294820	3.520950	4.725543
Cl	-0.359674	3.787055	3.417884
H	-2.657517	4.161415	3.069320
C	-5.220897	1.983551	-4.222838
Cl	-6.401445	1.189694	-5.309250
Cl	-4.958771	3.705000	-4.621753
H	-4.269922	1.459317	-4.325257
H	-5.618409	1.927105	-3.210437
C	-3.285165	5.288915	-0.760646
Cl	-2.103211	5.341202	0.572442
H	-3.066858	6.111391	-1.442497

Cl	-4.978068	5.488211	-0.201112
H	-3.202567	4.298299	-1.227013
C	2.116176	-0.180504	-2.177546
Cl	1.838264	-1.846233	-2.786698
H	3.132958	0.102526	-2.451499
Cl	0.994007	0.996050	-2.915390
H	1.946062	-0.185241	-1.095661
C	-5.163820	-1.906251	3.544488
Cl	-5.223204	-1.991502	5.326420
H	-5.416969	-0.888916	3.244560
Cl	-6.323073	-3.016733	2.760089
H	-4.157872	-2.193600	3.233289
C	-6.564644	1.303696	-0.250783
Cl	-7.724446	1.354494	-1.613141
H	-6.718805	2.199660	0.349914
Cl	-6.811969	-0.116883	0.797554
H	-5.554132	1.253672	-0.671819
C	-0.401302	0.743559	5.533800
Cl	-1.148778	-0.870641	5.670191
H	0.644896	0.662864	5.828554
Cl	-1.181494	1.938817	6.620227
H	-0.504369	1.081119	4.501752

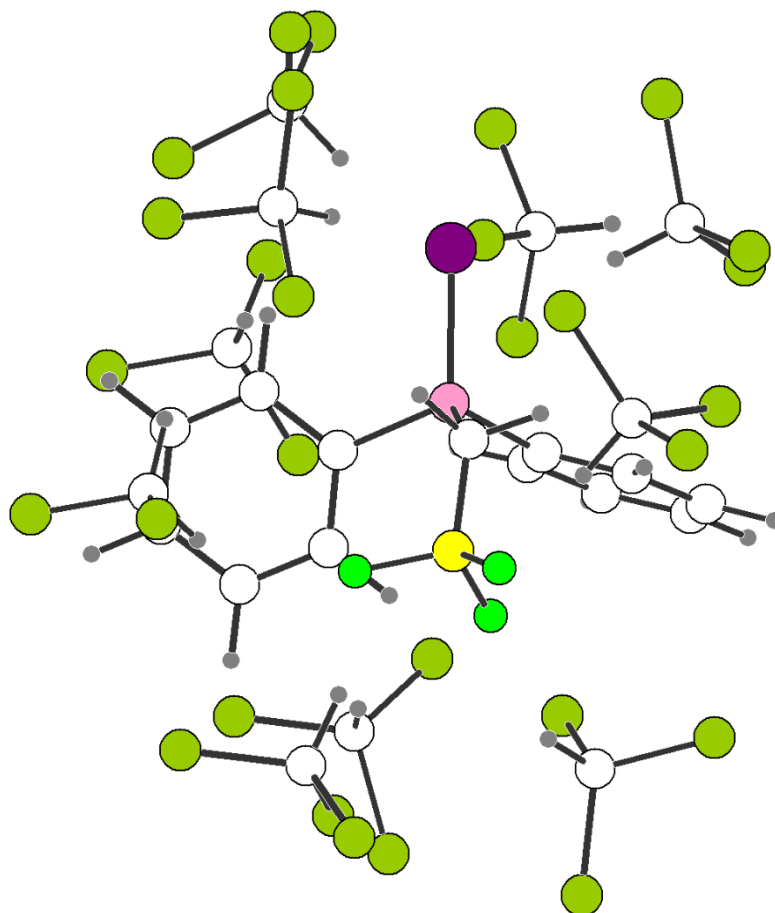


Figure S86. Optimized structure of **1^{Se}** with explicit CHCl₃ solvation.

Table S9. Coordinates of calculated structure of **1^{Se}** with explicit CHCl₃ solvation

P	-2.134019	0.681238	-0.248353
Se	-2.814572	1.554850	-2.112141
C	-2.188081	-1.128495	-0.354260
C	-1.043674	-1.846713	-0.729424
C	-1.122565	-3.222700	-0.933965
C	-2.335810	-3.889513	-0.763018
C	-3.472790	-3.179021	-0.375973
C	-3.403720	-1.802579	-0.170604
C	-3.221703	1.159688	1.130046
C	-3.146912	0.493779	2.363223
C	-3.927119	0.937330	3.429986
C	-4.778828	2.033082	3.279469
C	-4.851725	2.694992	2.054560
C	-4.079132	2.254822	0.980534
C	-0.453351	1.191386	0.118386
B	0.197734	0.865369	1.589279

F	-0.287471	1.790162	2.558936
F	1.611634	0.978494	1.513798
F	-0.125592	-0.449842	2.058268
H	-0.091052	-1.338552	-0.857215
H	-0.229145	-3.773211	-1.222296
H	-2.393730	-4.965345	-0.923716
H	-4.422327	-3.693280	-0.242051
H	-4.293626	-1.253005	0.129152
H	-2.469349	-0.350867	2.484464
H	-3.859349	0.440735	4.395198
H	-5.377578	2.374401	4.121522
H	-5.505006	3.556699	1.931689
H	-4.132532	2.757930	0.015723
H	-0.465635	2.279180	-0.034577
H	0.142362	0.775196	-0.706034
C	-6.339653	-1.842635	-3.113674
Cl	-5.313514	-0.488811	-2.563738
Cl	-6.892051	-2.852374	-1.748532
H	-5.716602	-2.467821	-3.753964
Cl	-7.724154	-1.274897	-4.088006
C	-2.328466	-1.264991	-4.156277
Cl	-2.985679	-2.931279	-4.149064
Cl	-0.555143	-1.279999	-4.239926
Cl	-3.028756	-0.321761	-5.492509
H	-2.616468	-0.765964	-3.223374
C	0.010889	-3.197076	3.079611
Cl	0.326055	-3.892480	4.692052
Cl	1.078086	-3.938600	1.856622
Cl	-1.697584	-3.385802	2.621544
H	0.229050	-2.128625	3.099328
C	-1.938819	4.351160	3.135991
Cl	-0.338063	5.063819	3.443305
Cl	-3.197716	5.032447	4.217264
H	-1.873757	3.278007	3.313988
H	-2.224834	4.582792	2.109328
C	-5.937370	3.146280	-2.733193
Cl	-7.187171	2.527185	-3.831792
Cl	-4.918970	4.366598	-3.526750
H	-5.278578	2.320006	-2.438195
Cl	-6.669463	3.805247	-1.237050
C	-1.978869	4.970948	-1.241594
Cl	-0.510767	4.928049	-0.239278
Cl	-1.718897	5.938131	-2.716411

Cl	-3.362281	5.598708	-0.299382
H	-2.220991	3.940223	-1.545776
C	2.884976	1.225234	-1.218915
Cl	2.361311	-0.275269	-2.043871
Cl	4.666396	1.330431	-1.180932
Cl	2.174394	2.653910	-2.003281
H	2.518728	1.178121	-0.187717
C	-4.706603	-2.498081	4.264596
Cl	-6.035536	-1.523564	4.932598
Cl	-5.216461	-3.342919	2.780700
Cl	-4.080618	-3.643816	5.472684
H	-3.891716	-1.824938	3.994636
C	-7.352896	0.855192	0.532008
Cl	-8.409996	0.409612	-0.822728
Cl	-8.231549	1.880809	1.704523
Cl	-6.668396	-0.575215	1.330325
H	-6.525656	1.448142	0.140035
C	-0.772219	0.489478	5.208282
Cl	-1.738479	-0.980737	5.554662
Cl	0.899158	0.267979	5.765478
Cl	-1.522395	1.927819	5.942119
H	-0.745242	0.646119	4.127642

NBO Analysis

We have considered **1**, **1^{Sc}**, and **2** with an NBO/NPA analysis to look for any donor-acceptor interactions between non-adjacent atoms. Using the second-order perturbation analysis we have been unable to find any donor-acceptor interactions >2 kcal/mol between B/F and P/Se/Rh in any of the structures we have examined.

We have also used NBO analysis to examine our simplified assumption of a “point charge” centered at B. We have used NBO analysis to look at the sum of the charges on B and the 4 atoms directly bound to it. This sum is -1.62. In the neutral congener Ph₂PEt this analogous sum is -0.69. Comparing these two net values shows that there is almost perfectly an additional -1 charge on the BF₃ substituted phosphine. Furthermore, comparison of the individual charges on each atom shows that this negative charge is fairly symmetrically distributed, albeit with a slightly larger change going from H to F (more negative) and from C to B (more positive) than is observed in the change of charge on the common methylene carbon. As the electric field at P or Se will be an average of all the charge density, the effects from each individual atom will be averaged. Overall, while there are some subtleties as to the arrangement of the charge, the NBO analysis does support that the estimation of a point charge localized at B is reasonable. This demonstrates that simple electrostatic relationships (Coulomb’s Law) and charge assumptions (approximating a BF₃ as a point charge) provide a good model for solution phase electrostatic effects.

Correlation between J_{P-Se} and TEP

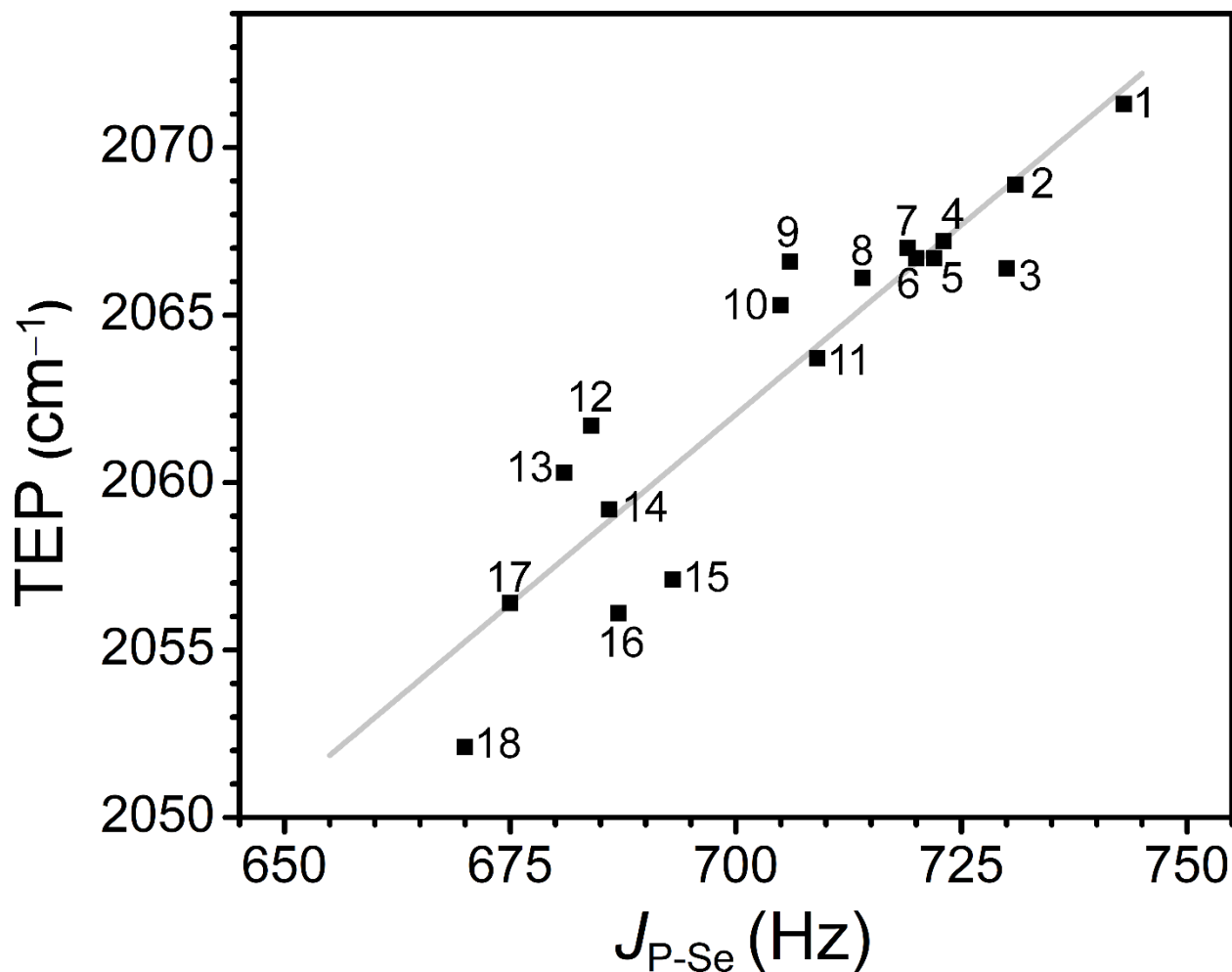


Figure S87. Plot of experimental J_{P-Se} reported in $CDCl_3$ vs. TEP determined using $Ni(CO)_3L$ in DCM or $Rh(CO)(acac)L$. Data was fit linearly using $y = mx + b$ with $m = 0.23(2)$ and $b = 1904(17)$ with $R^2 = 0.84$. Phosphines corresponding to each point are listed in the next table.

Table S10. Additional data points added to main text Figure 2. The linear fit was used to calculate the corresponding TEP or J_{P-Se} from the experimental value. Experimental TEP was determined via the linear correlation between ν_{CO} $Rh(CO)(acac)L$ and TEP.

Compound	Experimental TEP	Experimental J_{P-Se}	Calculated TEP	Calculated J_{P-Se}
2	2061.7 cm^{-1}	-	-	698 Hz
$[PPh_4][1^{Se}] CDCl_3$		657	2052.3	
$[PPh_4][1^{Se}] DMSO$		687	2059.1	
$[PPh_4][3^{Se}] CDCl_3$		677	2056.8	
$[PPh_4][3^{Se}] DMSO$		695	2060.9	

Table S11. Phosphines used in the J_{P-Se} vs. TEP fit. Data in brackets were determined using Rh(CO)(acac)L. All other TEP values were determined using Ni(CO)₃L, and all J_{P-Se} values were measured in CDCl₃. Data was collected from references 6, 23, and 31.

Number	Phosphine	J_{P-Se} (Hz)	TEP (cm ⁻¹)
1	P(<i>p</i> -FPh) ₃	743	2071.3
2	PPh ₃	731	2068.9
3	P(Bn) ₃	730	2066.4
4	P(<i>m</i> -Tol) ₃	723	2067.2
5	PPh ₂ Et	722	2066.7
6	P(<i>p</i> -Tol) ₃	720	2066.7
7	P(MePh) ₂	719	2067.0
8	P(<i>p</i> -OMeC ₆ H ₄) ₃	714	2066.1
9	P(<i>o</i> -Tol) ₃	706	2066.6
10	PMe ₂ Ph	705	2065.3
11	PEt ₂ Ph	709	2063.7
12	PEt ₃	684	2061.7
13	P(nBu) ₃	681	2060.3
14	P(^{<i>i</i>} Pr) ₃	686	2059.2
15	PAd ₂ (nBu)	693	[2057.1]
16	P(^{<i>t</i>} Bu) ₃	687	2056.1
17	PCy ₃	675	2056.4
18	PAd ₃	670	[2052.1]

Further analysis of solvent dependence

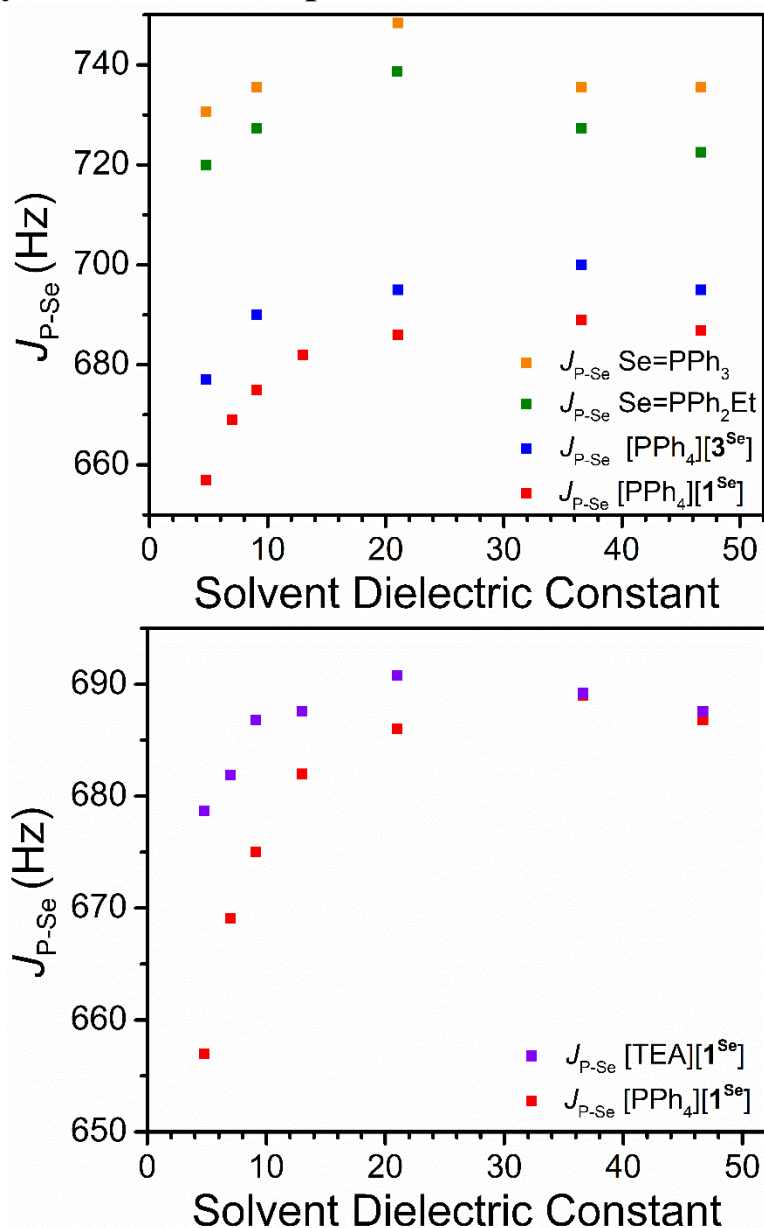


Figure S88. Plots of J_{P-Se} as a function of solvent dielectric – the PPh₄ Se compounds are compared to their neutral congeners in the top plot and the coupling of **1^{Se}** with two different counterions is compared in the bottom plot. Solvent dielectric for mixtures was estimated using a volume weighted average of the pure solvent dielectrics. We have been unable to find detailed studies of the dielectrics of these binary mixtures, but literature reports suggest that solvent mixtures of low polarity solvents scale approximately linearly with concentration and that using a volume or mole fraction weighted average of the pure solvent dielectric provides a reasonable estimate of the mixture dielectric.³² We have chosen to use volume fraction for ease but use of mole fractions results in negligible changes to the values and fits.

Table S12. J_{P-Se} (Hz) for [PPh₄][1^{Se}], [PPh₄][3^{Se}], SePPh₂Et, SePPh₃ at different dielectrics.³² To estimate the experimentally accessible electrostatic contribution to donor strength for [PPh₄][1^{Se}], the following calculation was performed: (687-657)/(722-657)*100 = 46%. The experimentally accessible electrostatic contribution for [PPh₄][3^{Se}] is (695-677)/(735-677)*100 = 31%. The coupling predicted by DFT including explicit solvent (Figures S84-S86) is included in the last column.

Solvent	Dielectric	[PPh ₄][1 ^{Se}]	[TEA][1 ^{Se}]	[PPh ₄][3 ^{Se}]	SePPh ₂ Et	SePPh ₃	1 ^{Se} DFT explicit solvent
CDCl ₃	4.8	657	679	677	720	731	-648
1:1 CDCl ₃ : CD ₂ Cl ₂	7	669	682	-	-	-	-
CD ₂ Cl ₂	9.1	675	687	690	727	735	-675
1:1 acetone- <i>d</i> ₆ : CD ₂ Cl ₂	13	682	688	-	-	-	-
acetone- <i>d</i> ₆	21	686	691	695	739	748	-
CD ₃ CN	36.6	689	689	700	727	735	-684
DMSO- <i>d</i> ₆	46.7	687	688	695	722	735	-

Table S13. Fit parameters for the linear fits of J_{P-Se} to $1/(4\pi\epsilon)$ of the form $J_{P-Se} = a + b*(1/(4\pi\epsilon))$.

Phosphine	[PPh ₄][1 ^{Se}]	[TEA][1 ^{Se}]	[PPh ₄][3 ^{Se}]	SePPh ₂ Et	SePPh ₃
a	693(1)	691(2)	700(2)	731(5)	741(5)
b	-2.12(12)*10 ³	-7(2)*10 ²	-1.4(2)*10 ³	-5(6)*10 ²	-5(5)*10 ²
R ²	0.98	0.77	0.92	0.06	0.02

Table S14. J_{P-Se} (Hz) for [PPh₄][1^{Se}] with the addition of various additional salts, the difference is relative to the coupling value for [PPh₄][1^{Se}] in the appropriate solvent. NMR spectra are shown in the NMR section.

Salt added	Solvent	Equivalents	J_{P-Se} (Hz)	Difference relative to [PPh ₄][1 ^{Se}]
PPh ₄ Br	CD ₂ Cl ₂	3	679	4
PPh ₄ Br	CD ₂ Cl ₂	20	679	4
Tetrabutylammonium chloride	CDCl ₃	20	671	14
Tetrabutylammonium chloride	CDCl ₃	1	667	9
Tetrabutylammonium PF ₆	CDCl ₃	20	671	14
Tetraethylammonium bromide	CDCl ₃	20	677	19
Tetraethylammonium bromide	CDCl ₃	1	672	14
Bis(triphenylphosphine)iminium chloride	CDCl ₃	20	656	-2

Discussion of the slopes of J_{P-Se} versus $1/(4\pi\epsilon)$ for $[PPh_4][1^{Se}]$ and $[PPh_4][3^{Se}]$

The linear fits of J_{P-Se} versus $1/(4\pi\epsilon)$ for $[PPh_4][1^{Se}]$ and $[PPh_4][3^{Se}]$ show that Coulomb's law provides a reasonable approximation for how the donor properties of these phosphine selenides vary with different solvents:

$$F = \frac{q_1 q_2}{4\pi\epsilon r^2}$$

Coulomb's law also has dependences on the charges involved in the electrostatic interaction (q_1 and q_2) as well as the distances between those charges. If we make the assumption that the charges in $[PPh_4][1^{Se}]$ and $[PPh_4][3^{Se}]$ should be identical (or at least similar), then the ratio of the slopes to the linear fits of J_{P-Se} versus $1/(4\pi\epsilon)$ should be proportional to the difference in the square of the point charge-to-test charge distances in the two phosphine selenides. If we use the B...P distance for this value, the distances are 3.029 and 3.562 Å. The ratio of the squares of these distances is 0.72. This suggests that, simplistically, we might expect that the ratio of the slopes of J_{P-Se} versus $1/(4\pi\epsilon)$ for $[PPh_4][1^{Se}]$ and $[PPh_4][3^{Se}]$ should be ~ 1.4 . The ratio from the linear fits to the data is 1.5, in good agreement to the predicted ratio from the difference charge-to-charge distance.

Single crystal X-ray crystallography

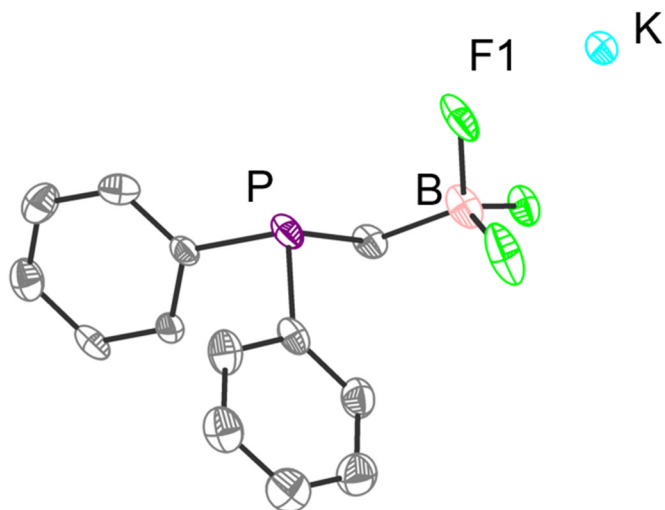


Figure S89. SXR structure of K1 with K^+ counterion shown.

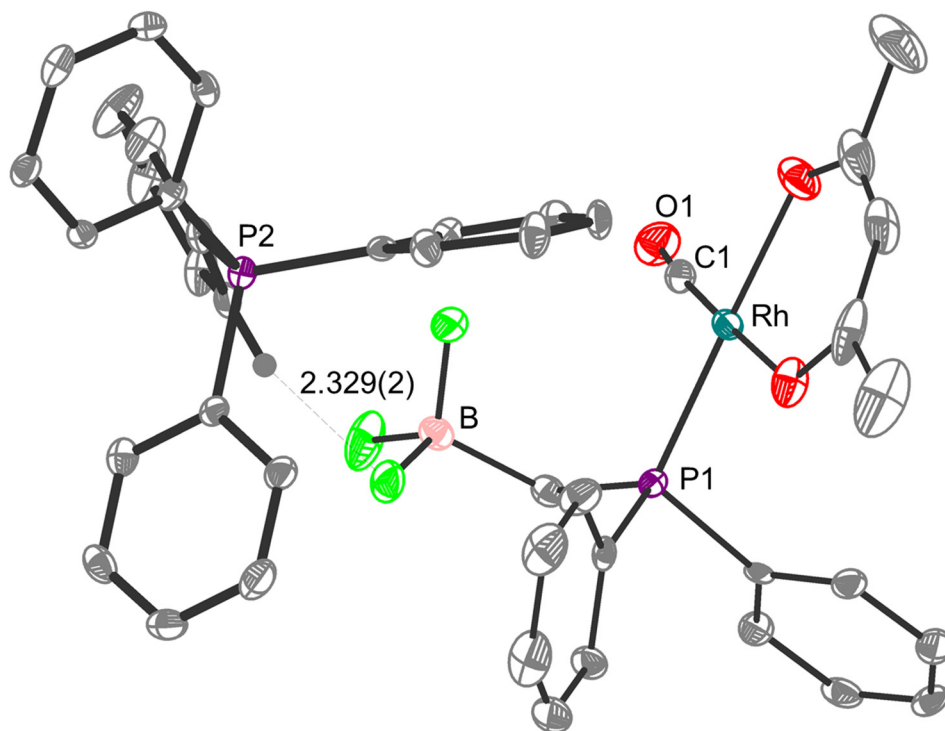


Figure S90. SXR structure of **2** with PPh_4^+ counterion shown. H-bonding interaction between BF_3 and PPh_4 indicated by a dashed line. Two independent molecules of $Rh(acac)(CO)(PPh_2(CH_2BF_3))$ are present in the asymmetric unit. The closest H-bonding interaction between the second molecule and PPh_4 is 2.303(2).

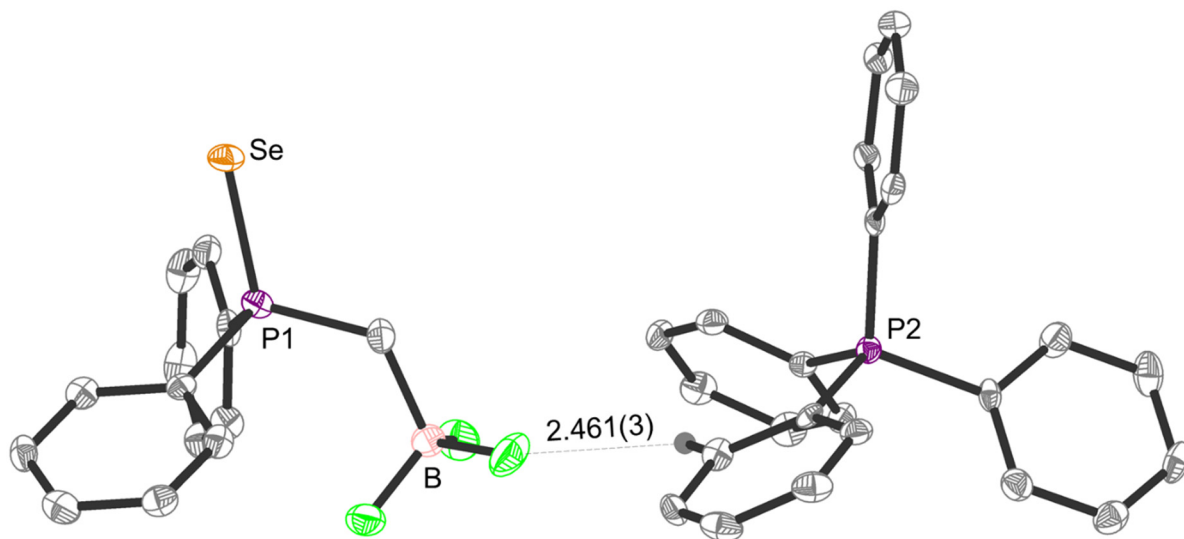


Figure S91. SXR D structure of $[\text{PPh}_4][\mathbf{1}^{\text{Se}}]$ with PPh_4^+ counterion shown. H-bonding interaction between BF_3 and PPh_4 indicated by a dashed line.

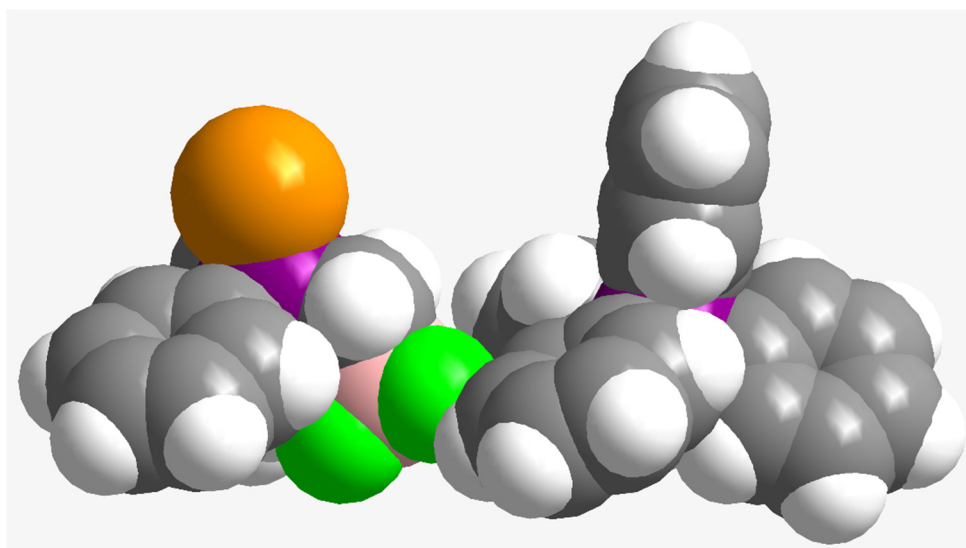


Figure S92. Space filling model of the SXR D structure of $[\text{PPh}_4][\mathbf{1}^{\text{Se}}]$ with PPh_4^+ counterion shown.

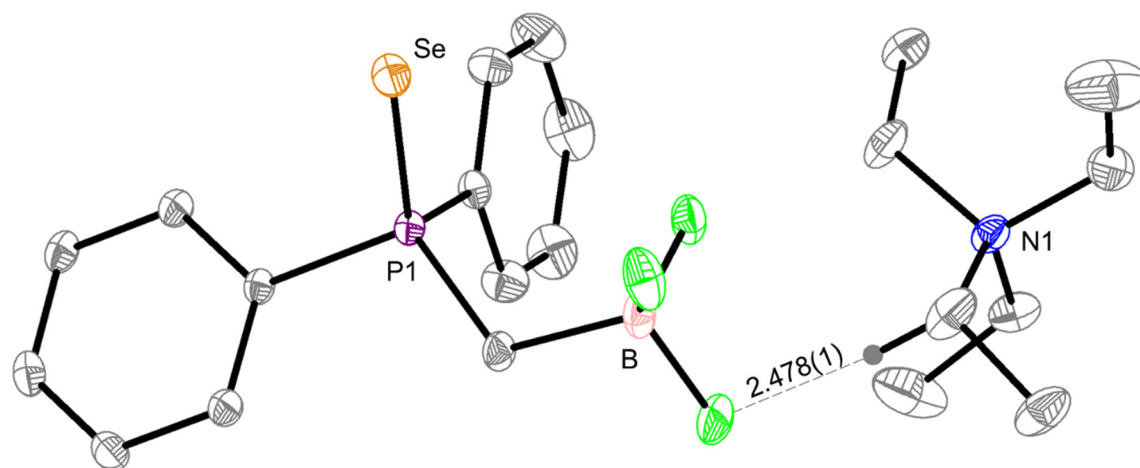


Figure S93. SXR structure of [TEA][1^{Sc}] with TEA⁺ counterion shown. H-bonding interaction between BF₃ and TEA indicated by a dashed line.

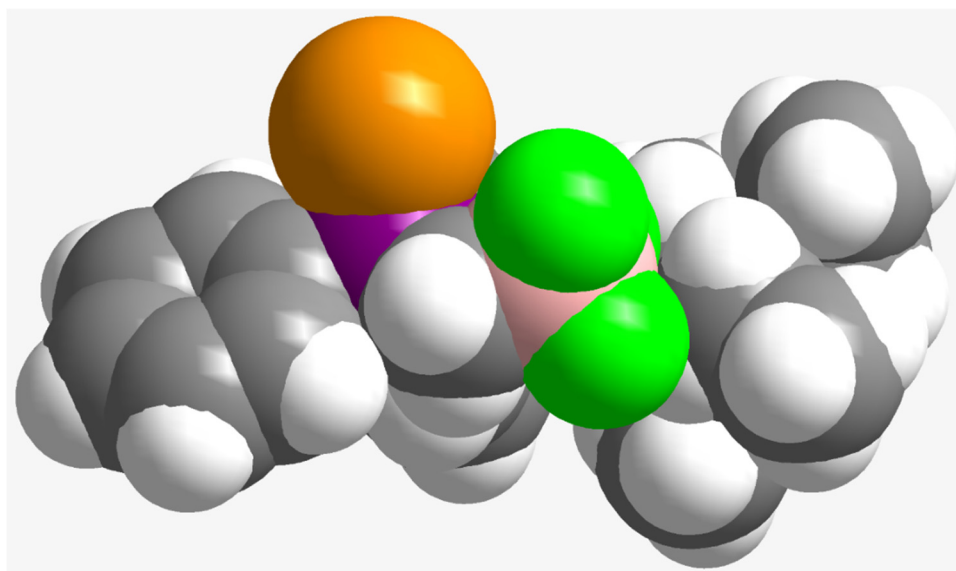


Figure S94. Space filling model of the SXR structure of [TEA][1^{Sc}] with TEA⁺ counterion shown.

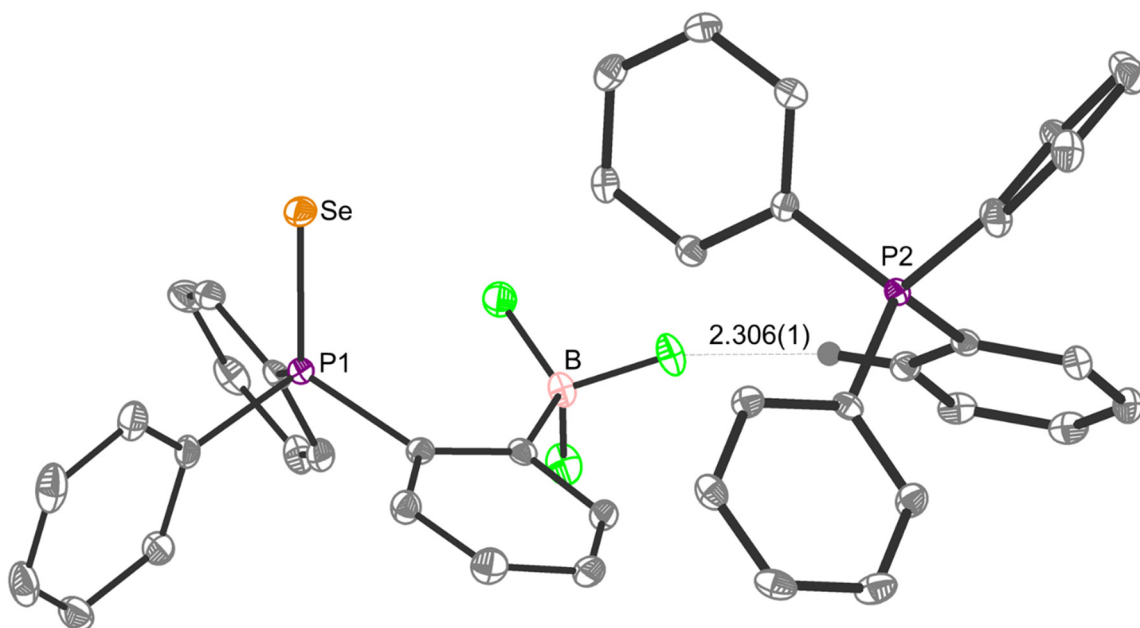


Figure S95. SXR structure of $[\text{PPh}_4][3\text{Se}]$ with PPh_4^+ counterion shown. H-bonding interaction between BF_3 and PPh_4 indicated by a dashed line.

Table S15. Selected average bond lengths for SXR structures.

	K1	2	$[\text{PPh}_4][1\text{Se}]$	$[\text{TEA}][1\text{Se}]$	$[\text{PPh}_4][3\text{Se}]$
B-P2	2.858(3)	5.685(3)	6.283(6)	-	5.895(2)
B-N1				4.766(2)	
Se-P1	-	-	2.129(1)	2.1124(4)	2.112(5)
P1-B	-	3.006(4)	3.029(6)	2.894(2)	3.562(2)
Se-B			4.848(6)	3.758(2)	4.530(2)
B-K	3.272(3)	-	-	-	-
Rh-C1	-	1.797(3)	-	-	-
B-C1	-	3.719(5)	-	-	-
B-Rh	-	4.150(4)	-	-	-
B-O	-	3.955(4)	-	-	-

Discussion of van der Waals radii in 2

Given that the van der Waals radii of B, C, O and Rh are 205, 196, 171, and 232 pm, the sum of the covalent radii for $\text{B}\cdots\text{C}$, $\text{B}\cdots\text{O}$, and $\text{B}\cdots\text{Rh}$ are 401, 376, and 437 respectively.³³ The interatomic distances for $\text{B}\cdots\text{C}$, $\text{B}\cdots\text{O}$, and $\text{B}\cdots\text{Rh}$ in the crystal structure of **2** are 371.9(4), 395.5(4) and 415.0(4) pm. Dividing the interatomic distances by the sum of the covalent radii gives 0.93, 1.05, and 0.95 for $\text{B}\cdots\text{C}$, $\text{B}\cdots\text{O}$, and $\text{B}\cdots\text{Rh}$, respectively. Although the interatomic distances between $\text{B}\cdots\text{C}$ and $\text{B}\cdots\text{O}$ are significantly shorter than that between $\text{B}\cdots\text{Rh}$, the lengths normalized for the sum of covalent radii are similar.

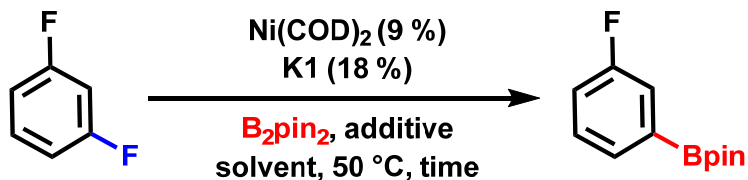
Table S16. Refinement data for crystal structures of **K1**, **2**, [PPh₄][**1**^{Se}], [TEA][**1**^{Se}], and [PPh₄][**3**^{Se}].

Identification code	K1	2	[PPh ₄][1 ^{Se}]
Empirical formula	C ₁₅ H ₁₆ BF ₃ KO _{0.5} P	C ₄₃ H ₃₉ BF ₃ O ₃ P ₂ Rh	C _{36.96} H _{31.91} B _{0.95} F _{2.87} I _{0.05} P ₂ Se _{0.95}
Formula weight	342.21	836.40	683.86
Temperature/K	100(2)	100(2)	100(2)
Crystal system	triclinic	Triclinic	Orthorhombic
Space group	P-1	P-1	Pna2 ₁
a/Å	5.6907(4)	9.1533(6)	14.5444(7)
b/Å	21.5917(16)	13.0253(9)	19.8328(10)
c/Å	26.847(2)	33.273(2)	11.0256(6)
α/°	78.847(2)	83.172(2)	90
β/°	89.976(2)	88.634(2)	90
γ/°	89.948(2)	79.181(2)	90
Volume/Å ³	3231.9(4)	3868.8(4)	3180.4(3)
Z	8	4	4
ρ _{calc} /cm ³	1.407	1.436	1.428
μ/mm ⁻¹	0.450	0.578	1.316
F(000)	1408.0	1712.0	1396
Crystal size/mm ³	0.35 × 0.25 × 0.09	0.47 × 0.26 × 0.17	0.42 × 0.14 × 0.138
Radiation	MoKα (λ = 0.71073)	MoKα (λ = 0.71073)	MoKα (λ = 0.71073)
2θ range for data collection/°	3.96 to 46.752	4.53 to 48.298	4.226 to 52.934
Index ranges	-6 ≤ h ≤ 6, -24 ≤ k ≤ 24, -29 ≤ l ≤ 29	-10 ≤ h ≤ 9, -14 ≤ k ≤ 14, -37 ≤ l ≤ 38	-18 ≤ h ≤ 18, -24 ≤ k ≤ 24, -13 ≤ l ≤ 13
Reflections collected	54508	43102	82448
Independent reflections	9397 [R _{int} = 0.0722, R _{sigma} = 0.0549]	12044 [R _{int} = 0.0802, R _{sigma} = 0.0838]	6480 [R _{int} = 0.0748, R _{sigma} = 0.0434]
Data/restraints/parameters	9397/2441/1070	12044/0/959	6480/13/407
Goodness-of-fit on F ²	1.016	1.014	1.071
Final R indexes [I ≥ 2σ (I)]	R ₁ = 0.0430, wR ₂ = 0.0798	R ₁ = 0.0424, wR ₂ = 0.0703	R ₁ = 0.0401, wR ₂ = 0.0744
Final R indexes [all data]	R ₁ = 0.0748, wR ₂ = 0.0897	R ₁ = 0.0840, wR ₂ = 0.0802	R ₁ = 0.0545, wR ₂ = 0.0788
Largest diff. peak/hole / e Å ⁻³	0.0/-0.26	0.72/-0.53	1.13/-0.32
Flack parameter	-	-	0.015(4)

Identification code	[TEA][1 ^{Se}]	[PPh ₄][3 ^{Se}]
Empirical formula	C ₂₁ H ₃₂ BF ₃ NPSe	C ₄₂ H ₃₄ BF ₃ P ₂ Se
Formula weight	476.2	747.40
Temperature/K	100(2)	100(2)
Crystal system	orthorhombic	triclinic
Space group	Pca21	P-1
a/Å	18.1513(9)	9.6724(5)
b/Å	10.6673(5)	12.8821(6)
c/Å	11.7071(6)	14.5407(7)
α/°	90	84.9610(10)
β/°	90	77.687(2)
γ/°	90	74.085(2)
Volume/Å ³	2266.8(2)	1701.43(15)
Z	4	2
ρ _{calc} /g/cm ³	1.390	1.459
μ/mm ⁻¹	1.722	1.245
F(000)	981	764.0
Crystal size/mm ³	0.433 × 0.259 × 0.165	0.303 × 0.218 × 0.13
Radiation	MoKα (λ = 0.71073)	MoKα (λ = 0.71073)
2θ range for data collection/°	4.428-62.256	4.466 to 56.758
Index ranges	-26 ≤ h ≤ 26, -15 ≤ k ≤ 15, -16 ≤ l ≤ 17	-12 ≤ h ≤ 12, -17 ≤ k ≤ 17, -19 ≤ l ≤ 19
Reflections collected	59551	62543
Independent reflections	7176 [R _{int} = 0.0245, R _{sigma} = 0.026]	8501 [R _{int} = 0.0322, R _{sigma} = 0.0207]
Data/restraints/parameters	7176/1/258	8501/0/442
Goodness-of-fit on F ²	1.082	1.074
Final R indexes [I >= 2σ (I)]	R ₁ = 0.0204, wR ₂ = 0.0518	R ₁ = 0.0293, wR ₂ = 0.0701
Final R indexes [all data]	R ₁ = 0.0219, wR ₂ = 0.0523	R ₁ = 0.0353, wR ₂ = 0.0727
Largest diff. peak/hole / e Å ⁻³	0.64/-0.15	0.55/-0.32
Flack parameter		

Catalytic C-F borylation trial reactions

Table S17. Initial scan of additives for C-F borylation of 1,3 difluorobenzene.



Other Conditions explored		
Variation	Time (h)	Yield borylated product
CsOH·xH ₂ O (15-20% H ₂ O) (8-8.5 equiv.) + MeOH (20 equiv.) in 2 mL THF	6	53%
CsOH·xH ₂ O (15-20% H ₂ O) (8-8.5 equiv.) + H ₂ O (20 equiv.) + Zn dust (1 equiv.)	16	29%
Ba(OH) ₂	13	17%
CsOH·xH ₂ O (15-20% H ₂ O) (16-17 equiv.)	7	0%
CsOH·xH ₂ O (15-20% H ₂ O) (8-8.5 equiv.)	24	32%
CsOH·xH ₂ O (15-20% H ₂ O) (2-2.1 equiv.)	7	29%
CsOH·xH ₂ O (15-20% H ₂ O) (4-4.3 equiv.) + CsF (5 equiv.)	24	35%
TMSOAc	7	0%
TMAF + LiOH	24	6%
LiOH	24	17%

Reaction conditions unless otherwise stated – 1,3 C₆F₂H₄ (40 μL, 0.4 mmol, 11 equiv.), Ni(COD)₂ (10 mg, 0.036 mmol), K1 (22 mg, 0.072 mmol), B₂pin₂ (92 mg, 0.36 mmol, 10 equiv.), additive (0.36 mmol, 10 equiv.) and CF₃Ph (20 μL, 0.16 mmol, 4.5 equiv.) were dissolved in 1 mL of THF and heated with stirring at 50 °C for the specified time. Yields determined by integration of ¹⁹F NMR peak of 1-Bpin-3-C₆FH₄ and comparison to the internal standard CF₃Ph. Yields are relative to the theoretical yield (0.4 mmol) determined using 1,3 C₆F₂H₄.

Table S18. Variation of reaction conditions with H₂O as an additive.

Variation of reaction conditions with H ₂ O		
Additive/Variation	Time (h)	Yield borylated product
No additive	7	11%
TMAF • 4H ₂ O	7	0%
TMAOH • 5H ₂ O	7	0%
Ba(OH) ₂	16	42%
Ca(OH) ₂	16	25%
LiOH	13	20%
CsF	7	20%
CsOH•xH ₂ O (15-20% H ₂ O) (8-8.5 equiv.)	7	36%
CsOH•xH ₂ O (15-20% H ₂ O) (4-4.25 equiv.)	13	34%
CsOH•xH ₂ O (15-20% H ₂ O) (8-8.5 equiv.) + H ₂ O (40 equiv.)	13	36%
CsOH•xH ₂ O (15-20% H ₂ O) (8-8.5 equiv.) + H ₂ O (10 equiv.)	13	34%

Reaction conditions unless otherwise stated – 1,3 C₆F₂H₄ (40 μL, 0.4 mmol, 11 equiv.), Ni(COD)₂ (10 mg, 0.036 mmol), K1 (22 mg, 0.072 mmol), B₂pin₂ (92 mg, 0.36 mmol, 10 equiv.), additive (0.36 mmol, 10 equiv.), CF₃Ph (20 μL, 0.16 mmol, 4.5 equiv) and H₂O (10 μL, 0.72 mmol, 20 equiv.) were dissolved in 1 mL of THF and heated with stirring at 50 °C for the specified time. Yields determined by integration of ¹⁹F NMR peak of 1-Bpin-3-C₆FH₄ and comparison to the internal standard CF₃Ph. Yields are relative to the theoretical yield (0.4 mmol) determined using 1,3 C₆F₂H₄.

Table S19. Variation of reaction conditions with alcohols as additives

Variation of reaction conditions with alcohols		
Alcohol	Time (h)	Yield borylated product
MeOH (50 equiv.)	16	36%
<i>i</i> PrOH	16	31%
<i>t</i> BuOH	16	34%
PhOH	16	0
C ₆ F ₅ OH	16	0
EtOH	16	35%
Et(CH ₂ OH) ₃	16	25%

Reaction conditions unless otherwise stated – 1,3 C₆F₂H₄ (40 μL, 0.4 mmol, 11 equiv.), Ni(COD)₂ (10 mg, 0.036 mmol), K1 (22 mg, 0.072 mmol), B₂pin₂ (92 mg, 0.36 mmol, 10 equiv.), CsOH·xH₂O (15-20% H₂O) (54 mg, 0.29-0.31 mmol, 8-8.5 equiv.), CF₃Ph (20 μL, 0.16 mmol, 4.5 equiv.) and alcohol (0.72 mmol, 20 equiv.) were dissolved in 1 mL of THF and heated with stirring at 50 °C for the specified time. Yields determined by integration of ¹⁹F NMR peak of 1-Bpin-3-C₆FH₄ and comparison to the internal standard CF₃Ph. Yields are relative to the theoretical yield (0.4 mmol) determined using 1,3 C₆F₂H₄.

Table S20. Variation of reaction conditions with MeOH as an additive

Variation of reaction conditions with MeOH		
Additive/Variation	Time (h)	Yield borylated product
Ba(OH) ₂	16	23%
CsOH·xH ₂ O (15-20% H ₂ O) (8-8.5 equiv.)	13	43%
CsOH·xH ₂ O (15-20% H ₂ O) (8-8.5 equiv.) + B ₂ pin ₂ (20 equiv.)	16	59%
CsOH·xH ₂ O (15-20% H ₂ O) (8-8.5 equiv.) + CsF (2 equiv.) + B ₂ pin ₂ (20 equiv.)	16	53%
CsOH·xH ₂ O (15-20% H ₂ O) (8-8.5 equiv.) + B ₂ pin ₂ (30 equiv.)	16	63%
Reaction conditions unless otherwise stated – 1,3 C ₆ F ₂ H ₄ (40 μL, 0.4 mmol, 11 equiv.), Ni(COD) ₂ (10 mg, 0.036 mmol), K1 (22 mg, 0.072 mmol), B ₂ pin ₂ (92 mg, 0.36 mmol, 10 equiv.), additive (0.36 mmol, 10 equiv.), CF ₃ Ph (20 μL, 0.16 mmol, 4.5 equiv) and MeOH (30 μL, 0.72 mmol, 20 equiv.) were dissolved in 1 mL of THF and heated with stirring at 50 °C for the specified time. Yields determined by integration of ¹⁹ F NMR peak of 1-Bpin-3-C ₆ FH ₄ and comparison to the internal standard CF ₃ Ph. Yields are relative to the theoretical yield (0.4 mmol) determined using 1,3 C ₆ F ₂ H ₄ .		

Table S21. Variation of reaction time with MeOH and CsOH additives and control reactions

Variable times and controls		
Variation	Time (h)	Yield borylated product
None	1	47%
None	2	55%
None	4	54%
None	6	55%
PEt ₃ (2 equiv.) no K1	4	0%
PPh ₂ Et (2 equiv.) no K1	4	0%
PCy ₃ (2 equiv.), no K1	4	0%
Reaction conditions unless otherwise stated– 1,3 C ₆ F ₂ H ₄ (40 μL, 0.4 mmol, 11 equiv.), Ni(COD) ₂ (10 mg, 0.036 mmol), K1 (22 mg, 0.072 mmol), B ₂ pin ₂ (184 mg, 0.72 mmol, 20 equiv.), CsOH·xH ₂ O (15-20% H ₂ O) (54 mg, 0.29-0.31 mmol, 8-8.5 equiv.), CF ₃ Ph (20 μL, 0.16 mmol, 4.5 equiv) and MeOH (30 μL, 0.72 mmol, 20 equiv.) were dissolved in 1 mL of THF and heated with stirring at 50 °C for the specified time. Yields determined by integration of ¹⁹ F NMR peak of 1-Bpin-3-C ₆ FH ₄ and comparison to the internal standard CF ₃ Ph. Yields are relative to the theoretical yield (0.4 mmol) determined using 1,3 C ₆ F ₂ H ₄ .		

Table S22. Variation of addition order and additives

Other Conditions explored		
Variation	Time (h)	Yield borylated product
None	4	55
LiOH (10 equiv.), no CsOH·xH ₂ O (15-20% H ₂ O)	4	35
Addition order*: combine MeOH and CsOH·xH ₂ O (15-20% H ₂ O) in THF, add B ₂ pin ₂ , fluoroarenes, then Ni complex	4	56
Addition order*: combine MeOH and CsOH·xH ₂ O (15-20% H ₂ O) in THF, then add Ni complex, then B ₂ Pin ₂ and fluoroarenes	4	53
Addition order*: combine MeOH and LiOH (20 equiv.) in THF, add B ₂ pin ₂ , fluoroarenes, then Ni complex, no CsOH·xH ₂ O	4	34
B ₂ neop ₂ (20 equiv.), no B ₂ pin ₂	4	32
B ₂ cat ₂	2	0
LiOMe (10 equiv.), no CsOH·xH ₂ O	4	29
LiOMe (10 equiv.), no CsOH·xH ₂ O, no MeOH	4	10
No CsOH·xH ₂ O	2	8
No CsOH·xH ₂ O, no MeOH	2	6
RT	22	44
100 °C	2	48
<p>Reaction conditions unless otherwise stated – 1,3 C₆F₂H₄ (40 μL, 0.4 mmol, 11 equiv.), Ni(COD)₂ (10 mg, 0.036 mmol), K1 (22 mg, 0.072 mmol), B₂pin₂ (184 mg, 0.72 mmol, 20 equiv.), CsOH·xH₂O (15-20% H₂O) (54 mg, 0.29-0.31 mmol, 8-8.5 equiv.) and CF₃Ph (20 μL, 0.16 mmol, 4.5 equiv) were dissolved in 1 mL of THF and heated with stirring at 50 °C for the specified time. Yields determined by integration of ¹⁹F NMR peak of 1-Bpin-3-C₆FH₄ and comparison to the internal standard CF₃Ph. Yields are relative to the theoretical yield (0.4 mmol) determined using 1,3 C₆F₂H₄.</p> <p>*Standard order of addition: combine Ni(COD)₂, K1, and B₂pin₂ in 1 mL THF. Add CF₃Ph, then 1,3 C₆F₂H₄, then CsOH·xH₂O (15-20% H₂O) and finally MeOH before placing on hot plate.</p>		

Table S23. Variation of cations.

Alternative cations		
Variation	Time (h)	Yield borylated product
Combine K1 and PPh ₄ Br (2 equiv.) in THF, filter and dry to isolate crude PPh ₄ 1, use instead of K1	2	8
Combine K1 and TBACl (2 equiv.) in THF, filter and dry to isolate crude TBA1, use instead of K1	2	46
Combine K1 and TEABr (2 equiv.) in THF, filter and dry to isolate crude TEA1, use instead of K1	2	35
Add 18-crown-6 (2 equiv.)	2	43
<p>Reaction conditions unless otherwise stated – 1,3 C₆F₂H₄ (40 μL, 0.4 mmol, 11 equiv.), Ni(COD)₂ (10 mg, 0.036 mmol), K1 (22 mg, 0.072 mmol), B₂pin₂ (184 mg, 0.72 mmol, 20 equiv.), CsOH·xH₂O (15-20% H₂O) (54 mg, 0.29-0.31 mmol, 8-8.5 equiv.) and CF₃Ph (20 μL, 0.16 mmol, 4.5 equiv) were dissolved in 1 mL of THF and heated with stirring at 50 °C for the specified time. Yields determined by integration of ¹⁹F NMR peak of 1-Bpin-3-C₆FH₄ and comparison to the internal standard CF₃Ph. Yields are relative to the theoretical yield (0.4 mmol) determined using 1,3 C₆F₂H₄.</p> <p>*Standard order of addition: combine Ni(COD)₂, K1, and B₂pin₂ in 1 mL THF. Add CF₃Ph, then 1,3 C₆F₂H₄, then CsOH·xH₂O (15-20% H₂O) and finally MeOH before placing on hot plate.</p>		

Table S24. Variation of reaction solvent.

Solvent variation		
Variation	Time (h)	Yield borylated product
Dioxane ($\epsilon = 2.25$) instead of THF ($\epsilon = 7.58$)	2	43
Toluene ($\epsilon = 2.38$) instead of THF ($\epsilon = 7.58$)	2	20
Diethyl ether ($\epsilon = 4.33$) instead of THF ($\epsilon = 7.58$)	2	10
Methyl tert-butyl ether ($\epsilon = 4.5$) instead of THF ($\epsilon = 7.58$)	2	13
Cyclopentyl methyl ether ($\epsilon = 4.76$) instead of THF ($\epsilon = 7.58$)	2	24
4-Methyl tetrahydropyran ($\epsilon = 4.8$) instead of THF ($\epsilon = 7.58$)	2	49
Tetrahydropyran ($\epsilon = 5.7$) instead of THF ($\epsilon = 7.58$)	2	59
MeTHF ($\epsilon = 6.97$) instead of THF ($\epsilon = 7.58$)	2	52
Dimethoxyethane ($\epsilon = 7.2$) instead of THF ($\epsilon = 7.58$)	2	47
1,4 C ₆ F ₂ H ₄ instead of 1,3 C ₆ F ₂ H ₄ Tetrahydropyran ($\epsilon = 5.7$) instead of THF ($\epsilon = 7.58$)	2	26

Reaction conditions unless otherwise stated – 1,3 C₆F₂H₄ (40 μ L, 0.4 mmol, 11 equiv.), Ni(COD)₂ (10 mg, 0.036 mmol), K1 (22 mg, 0.072 mmol), B₂pin₂ (184 mg, 0.72 mmol, 20 equiv.), CsOH·xH₂O (15-20% H₂O) (54 mg, 0.29-0.31 mmol, 8-8.5 equiv.) and CF₃Ph (20 μ L, 0.16 mmol, 4.5 equiv) were dissolved in 1 mL of THF and heated with stirring at 50 °C for the specified time. Yields determined by integration of ¹⁹F NMR peak of 1-Bpin-3-C₆FH₄ and comparison to the internal standard CF₃Ph. Yields are relative to the theoretical yield (0.4 mmol) determined using 1,3 C₆F₂H₄.

References

1. Molander, G. A.; Ham, J. Synthesis of Functionalized Organotrifluoroborates via Halomethyltrifluoroborates. *Org. Lett.* **2006**, *8* (10), 2031-2034.
2. Gott, A. L.; Piers, W. E.; Dutton, J. L. McDonald, R.; Parvez, M., Dimerization of Ethylene by Palladium Complexes Containing Bidentate Trifluoroborate-Functionalized Phosphine Ligands. *Organometallics* **2011**, *30* (16), 4236-4249.
3. Kim, Y.; Jordan, R. F.; Synthesis, Structures, and Ethylene Dimerization Reactivity of Palladium Alkyl Complexes that Contain a Chelating Phosphine Trifluoroborate Ligand. *Organometallics* **2011**, *30*, 4250-4256.
4. J-W.; Wang, L-N.; Li, M.; Tang, P-T.; Luo, X-P.; Jurmoo, M.; Liu, Y-J.; Zeng, M-H. Ruthenium-Catalyzed Gram-Scale Preferential C-H Arylation of Tertiary Phosphine. *Org. Lett.* **2019**, *21* (8), 2885-2889.
5. Allen, D. W.; Taylor B. F. The chemistry of heteroarylphosphorus compounds. Part 15. Phosphorus-31 nuclear magnetic resonance studies of the donor properties of heteroarylphosphines towards selenium and platinum(II). *J. Chem. Soc., Dalton Trans.* **1982**, 51-54.
6. Niemayer, Z. L.; Milo A.; Hickey, D. P.; Sigman, M. S. Parameterization of phosphine ligands reveals mechanistic pathways and predicts reaction outcomes. *Nat. Chem.* **2016**, *8*(6), 610-617.
7. Shen, Y.; Pan, Y.; Liu, J.; Sattasathuchana, T.; Baldrige, K. K.; Duttwyler, S. Synthesis and full characterization of an iridium B-H activation intermediate of the monocarba-*closo*-dodecaborate anion. *Chem. Commun.* **2017**, *53*, 176-179.
8. Chen, S.; Manoury, E.; Poli, R. Slow Exchange of Bidentate Ligands between Rhodium(I) Complexes: Evidence of Both Neutral and Anionic Ligand Exchange. *Eur. J. Inorg. Chem.* **2014**, *34*, 5820-5826.
9. Bresler, L. S.; Buzina, N. A.; Varshavsky, Y. S.; Kiseleva, N. V.; Cherkasova, T. G. Carbon-13 nuclear magnetic resonance spectra of rhodium carbonyl complexes. *J. Organomet. Chem.*, **1979**, *171*, 229-235.
10. Bootle-Wilbraham, A.; Head, S.; Longstaff, J.; Wyatt, P Alane – A chemoselective way to reduce phosphine oxides. *Tetrahedron Lett.*, **1999**, *40*, 5267-5270.
11. Sheldrick, G. M. SHELXT- Integrated space-group and crystal-structure determination. *Acta Cryst.* **2015**, *A71*, 3- 9.
12. Dolomanov, O.V.; Bourhis, L. J.; Gildea, R. J.; Howard, A. K.; and Puschmann, H.,. Olex2, a complete structure solution, refinement, and analysis program. *J. Appl. Cryst.* **2009**, *42*, 339

13. (a) Sheldrick, G. M. A Short History of SHELX. *Acta Cryst.* **2008**, *A64*, 112-122. (b) Sheldrick, G. M. Crystal structure refinement with SHELX. *Acta Cryst.* **2015**, *C71*, 3-8.
14. (a) Diaz, A. A.; Buster, B.; Schomish, D.; Khan, M. A.; Baum, C. J.; Wehmschulte, R. J. Size Matters: Room Temperature P-C Bond Formation Through C-F Activation in *m*-Terphenyldiiodophosphine. *Inorg. Chem.* **2008**, *47* (7), 2858-2863. (b) Kreienbrink, A.; Sarosi, M. B.; Rys, E. G.; Lonneck, P.; Hey-Hawkins, E. Carborane-substituted 1,2-Diphosphetanes. *Angew. Chem. Int. Ed.* **2011**, *50* (20), 4701-4703.
15. Cronin, L.; Higgitt, C. L.; Karch, R.; Perutz, R. N. Rapid Intermolecular Carbon-Fluorine Bond Activation of Pentafluoropyridine at Ni(0): Comparative Reactivity of Fluorinated Arenes and Fluorinated Pyridine Derivatives. *Organometallics* **1997**, *16*(22), 4920-4928.
16. Amin, N.; Claridge, T. Quantitative NMR Spectroscopy. 2017. <http://nmrweb.chem.ox.ac.uk/Data/Sites/70/userfiles/pdfs/quantitative-nmr.pdf>
17. Zhou, J.; Kuntze-Fechner, M. W.; Bertermann, R.; Paul, U. S. D.; Berthel, J. H. J.; Friedrich, A.; Du, Z.; Marder, T. B.; Radius, U. Preparing (Multi)Fluoroarenes as Building Blocks for Synthesis: Nickel-Catalyzed Borylation of Polyfluoroarenes via C-F Bond Cleavage. *J. Am. Chem. Soc.* **2016**, *138*, 5250-5253.
18. Bao, F.; Liu, Z.; Bai, H.; Zhang, H.; Liu, P.; Zhang, Q.; Chai, G. Palladium/Sensory Component-Catalyzed Homocoupling Reactions of Aryl Halides. *Synlett.* **2020**, *31*, 1501-1506.
19. Zick, M. E.; Lee, J.-H.; Gonzalez, M. I.; Velasquez, E. O.; Uliana, A. A.; Kim, J.; Long, J. R.; Milner, P. J. Fluoroarene Separations in Metal-Organic Frameworks with Two Proximal Mg²⁺ Coordination Sites. *J. Am. Chem. Soc.* **2021**, *143*, 1948-1958.
20. Firth, J. D.; Hammarback, L. A.; Burden, T. J.; Eastwood, J. B.; Donald, J. R.; Horbaczewskyj, C. S.; McRobie, M. T.; Tramaseur, A.; Clark, I. P.; Towrie, M.; Robinson, R.; Krieger, J.-P.; Lynam, J. M.; Fairlamb, I. J. S. Light- and Manganese-Initiated Borylation of Aryl Diazonium Salts: Mechanistic Insight on the Ultrafast Time-Scale Revealed by Time-Resolved Spectroscopic Analysis. *Chem.-Eur. J.* **2021**, *27*, 3979-3985.
21. Feofanov, M.; Akhmetov, V.; Takayama, R.; Amsharov, K. Catalyst-Free Synthesis of O-Heteroacenes by Ladderization of Fluorinated Oligophenylenes. *Angew. Chem. Int. Ed.* **2020**, *60*, 5199-5203.
22. (a) Sigvartsen, T.; Gestblom, B.; Noreland, E.; Songstad J. Conductometric and Dielectric Behaviour of Solutions of Tetrabutylammonium Perchlorate in Solvents of Low and Medium Permittivity. *Acta Chemica Scandinavica* **1989**, *43*, 103-115. (b) Gestblom, B.; Songstad, J. Solvent Properties of Dichloromethane. VI. Dielectric Properties of Electrolytes in Dichloromethane. *Acta Chemica Scandinavica* **1987**, *41B*, 396-409.

23. Chen, L.; Ren, P.; Carrow, B. P. Tri(1-adamantyl)phosphine: Expanding the Boundary of Electron-Releasing Character Available to Organophosphorus Compounds. *J. Am. Chem. Soc.* **2016**, *138*, 6392-6395.
24. Neese, F. "The ORCA program system" *Wiley interdisciplinary Reviews - Computational Molecular Science*, **2012**, *2*, 73–78.
25. Weigend F.; Ahlrichs, R. Balanced basis sets of split valence, triple zeta valence and quadruple zeta valence quality for H to Rn: Design and assessment of accuracy. *Phys. Chem. Chem. Phys.* **2005**, *7*, 3297.
26. Gaussian 16, Revision C.01, Frisch, M. J.; Trucks, G. W.; Schlegel, H. B.; Scuseria, G. E.; Robb, M. A.; Cheeseman, J. R.; Scalmani, G.; Barone, V.; Petersson, G. A.; Nakatsuji, H.; Li, X.; Caricato, M.; Marenich, A. V.; Bloino, J.; Janesko, B. G.; Gomperts, R.; Mennucci, B.; Hratchian, H. P.; Ortiz, J. V.; Izmaylov, A. F.; Sonnenberg, J. L.; Williams-Young, D.; Ding, F.; Lipparini, F.; Egidi, F.; Goings, J.; Peng, B.; Petrone, A.; Henderson, T.; Ranasinghe, D.; Zakrzewski, V. G.; Gao, J.; Rega, N.; Zheng, G.; Liang, W.; Hada, M.; Ehara, M.; Toyota, K.; Fukuda, R.; Hasegawa, J.; Ishida, M.; Nakajima, T.; Honda, Y.; Kitao, O.; Nakai, H.; Vreven, T.; Throssell, K.; Montgomery, J. A., Jr.; Peralta, J. E.; Ogliaro, F.; Bearpark, M. J.; Heyd, J. J.; Brothers, E. N.; Kudin, K. N.; Staroverov, V. N.; Keith, T. A.; Kobayashi, R.; Normand, J.; Raghavachari, K.; Rendell, A. P.; Burant, J. C.; Iyengar, S. S.; Tomasi, J.; Cossi, M.; Millam, J. M.; Klene, M.; Adamo, C.; Cammi, R.; Ochterski, J. W.; Martin, R. L.; Morokuma, K.; Farkas, O.; Foresman, J. B.; Fox, D. J. Gaussian, Inc., Wallingford CT, **2016**.
27. Struppe, J.; Zhang, Y.; Rozovsky, S. ⁷⁷Se Chemical Shift Tensor of L-selenocystine: Experimental NMR Measurements and Quantum Chemical Investigations of Structural Effects. *J. Phys. Chem. B.* **2015**, *119* (9), 3643-3650.
- 28 Neese, F.; Wennmohs, F.; Becker, U.; Riplinger, C., The ORCA quantum chemistry program package. *J. Chem. Phys.* **2020**, *152* (22).
29. Feynman, R.P.; Leighton, R. B.; Sands, M. L. Chapter 4: Electrostatics. In *The Feynman Lectures on Physics: Mainly Electromagnetism and Matter* [Online]; Gottlieb, M. A., Pfeiffer, R., Eds.; Basic Books, USA, **2011**. <https://www.feynmanlectures.caltech.edu/info/> (accessed October 2020).
30. Avogadro: an open-source molecular builder and visualization tool. Version 1.2.0 <http://avogadro.cc/>, Marcus D Hanwell, Donald E Curtis, David C Lonie, Tim Vandermeersch, Eva Zurek and Geoffrey R Hutchison; "Avogadro: An advanced semantic chemical editor, visualization, and analysis platform" *Journal of Cheminformatics* **2012**, *4*, 17.
31. Tolman, C. A. Steric Effects of Phosphorus Ligands in Organometallic Chemistry and Homogeneous Catalysis. *Chem. Rev.* **1977**, *77*, 313-348.

32. (a) See Figure 2 in Wang, P. Anderko, A. Computation of dielectric constants of solvent mixtures and electrolyte solutions. *Fluid Phase Equilib.* **2001**, *186* (1-2), 103-122. (b) Jouyban, A.; Soltanpour, S.; Chan, H.-K. A Simple Relationship between Dielectric Constant of Mixed Solvents with Solvent Composition and Temperature *Int. J. Pharm.* **2004**, *269*, 353-360. (c) Jouyban, A.; Soltanpour, S. Prediction of Dielectric Constants of Binary Solvents at Various Temperatures *J. Chem. Eng. Data* **2010**, *55*, 2951-2963.
33. Batsanov, S. S. Van der Waals Radii of Elements *Inorganic Materials* **2001**, *37*, 871-885.